POLITECNICO DI MILANO

SCUOLA DI INGEGNERIA CIVILE, AMBIENTALE E TERRITORIALE

CORSO DI LAUREA MAGISTRALE IN INGEGNERIA CIVILE – CIVIL ENGINEERING – INFRASTRUTTURE DI TRASPORTO

STUDY OF AN EXPERIMENTAL ANCHOR SYSTEM – "STAPLE ANCHORS" – FOR EXTERNALLY BONDED FRP LAMINATES USED FOR THE CONSOLIDATION AND RETROFITTING OF REINFORCED CONCRETE STRUCTURES, THROUGH AN INNOVATIVE DOUBLE SHEAR TEST METHOD

Relatore: Prof. Carlo Poggi
Co-Relatore: Prof. Antonio Nanni

Elaborato di:

Thomas Cadenazzi, matr. 823552

Academic Year: 2015/2016

To my parents,
for their love, their precious support
and for gave me the best education.

To my family,
My stronghold.

AKNOWLEDGEMENT

I would like to thank all the people who made this thesis possible and those who contributed to my personal growth and gave me inspiration and support:

- Dr. Carlo Poggi, my Italian advisor, for his great kindness and for gave me the opportunity to take part in this wonderful experience.
- Dr. Antonio Nanni, my American advisor, for his wonderful advice and teachings, for his great enthusiasm and his important inspirations that made me improve every day, for his availability at every request.
- Dr. Francisco De Caso, for his kindness and for making me feel an important part of this group, for his help and advice, and for always pushing me with enthusiasm towards my works.
- Ed Wheatley, the producer of my anchors, for his availability, his enthusiasm, his great help and interest for my projects.
- My brothers Matteo and Marco that always supported me all through my entire university career, pushing me towards my goals, and an affectionate thought to my sisters Chiara, Elena and Monica.
- Büşra, for being always present and being a big part of my Miami experience, for her help, kindness and support in every situation, for her help in make me grow as a person.
- Marco, my companion of adventure, for sharing with me this incredible experience, for his help and good suggestions.
- Houman, Nicolas and Pietro, for being true friends in the Miami experience.
- Omid and Zahra, for being my desk mates and for sharing with me all the secrets of the laboratory, for their help during classes, and for their good suggestions.
- Saverio, for helping me since the very first day and for giving me the initial opportunity to take active part in one of the most innovative and wonderful project in the University of Miami: the "Innovation Bridge".
- Guillermo, Phil, Keith and Christian for all the help they provided me in the laboratory, for the good time spent together while working on our projects.
- Gabriel, my internship Brazilian student assigned, for his help in the laboratory during my successful tests.

TABLE OF CONTENTS

LIST OF TABLES

LIST OF FIGURES

ABSTRACT

The thesis investigates a new type of anchorage system, called "staple" anchor as a mean of anchoring externally bonded fiber-reinforced polymers (FRP) sheets into concrete. The investigation will employ experimental work, which includes concrete blocks strengthened with FRP sheets connected to the concrete blocks footings via these innovative types of carbon anchors set up in different configurations.

The staples anchors are designed in two different types: flat staples and round staples. Both the types of anchors are provided as prefabricated elements formed by strands of carbon fibers that are inserted into epoxy filled holes in the concrete, and an external part that is also impregnated and connected externally to the bonded FRP laminate. They appear in different shapes and sizes and they also have different processes of installation but they share the same aim: enhance the bond of externally bonded FRP laminates into concrete.

The experimental campaign is composed by a double shear test through which it is investigated the resistance of the anchors under tension load in different anchor configurations, in order to find the best configuration that is sufficient to enhance the bond of the FRP sheets. In particular, two series of double shear tests are performed: the first one is conducted with a past method already used in the University of Miami laboratory to investigate the performance of the spikes' anchors. Since this past method revealed some difficulties in the set-up procedure of the test and mostly inaccurate results, a second test is performed with an innovative installation procedure and set-up of the test, which gives successful and consistency results through a more reliable set-up of the test.

The purpose of this study is to test the effectiveness of the staple anchors through an innovative set-up of the double shear test. Currently, no specific criteria or guidelines exist to help the designer to understand the improvement in terms of strengthening of the existing concrete structure after the installation of FRP anchors. This thesis helps to create new specific design guidelines, providing to engineers, in this way, the necessary information to make design decisions when incorporating a staple anchor system to enhance the bond of externally bonded FRP laminates. Finally, also a comparison between the performance of the staple and the spike anchors is provided.

ABSTRACT (Italian)

La presente tesi investiga una nuova tipologia di sistema di ancoraggi, denominato "ancoraggi a staple", che rappresentano un sistema di ancoraggi esterni in compositi FRP (materiali compositi fibrorinforzati a matrice polimerica). Queste tipologie di ancoraggio permettono alla lamina di raggiungere deformazioni ben oltre quelle di "debonding", creando così i presupposti per una miglior efficienza del rinforzo strutturale. La presente ricerca include una campagna sperimentale, mediante test con blocchi di calcestruzzo rinforzati con lamine in FRP, collegate agli stessi blocchi mediante tipologie di ancoraggio in carbonio, installati secondo diverse configurazioni.

Gli ancoraggi "a staple" si dividono in due diverse categorie: gli ancoraggi "flat" e gli ancoraggi "round". Entrambe le tipologie vengono forniti come elementi prefabbricati formati da un fascio di fibre in carbonio. Di queste una parte viene inserita nella cavità del substrato di calcestruzzo, precedentemente riempito di resina epossidica e un'altra rimane esternamente ancorata alla lamina in FRP. Essi appaiono secondo diverse forme e dimensioni e vengono installati secondo diversi processi, ma condividono lo stesso scopo: migliorare l'adesione tra le lamine di FRP applicate sulla superficie del calcestruzzo.

La campagna sperimentale è composta da due double shear test attraverso il quale si investiga la resistenza degli ancoraggi sotto un certo carico di tensione, con gli ancoraggi disposti secondo diverse configurazioni, al fine di trovare la migliore configurazione che risulta sufficiente per migliorare l'adesione della lamina di FRP. In particolare, due serie di double shear test sono state condotte: la prima è stata eseguita mediante una metodologia già condotta presso il laboratorio di materiali dell'università di Miami, al fine di investigare la performance degli ancoraggi a "spike". Dal momento che questa metodologia di utilizzo ha rivelato diverse difficoltà non solo nel set-up della prova, ma anche riguardo i risultati del test, il secondo test è stato realizzato mediante una procedura di installazione innovativa, che si è rivelata una metodologia affidabile che ha portato a risultati di esito molto positivo.

Lo scopo di questa ricerca è testare l'efficienza degli ancoraggi "a staple" attraverso questa metodologia di installazione innovativa. Attualmente non esistono criteri progettuali o linee guida che aiutino il progettista a quantificare il miglioramento, in termini di resistenza, della struttura esistente, previa installazione degli ancoraggi a "staple". Questa tesi aiuta a creare nuove line guida per disporre agli ingegneri e progettisti le informazioni necessarie per operare correttamente nel momento in cui si voglia utilizzare gli ancoraggi a "staple" come metodo di rinforzo dei sistemi di lamine in

FRP. Infine, viene presentato un confronto tra la performance degli ancoraggi a "staple" e quelli a "spike".

1. INTRODUCTION

In this chapter, a brief overview of the historic perspective of the FRP materials is provided. This section is an introduction to composite materials and in particular, it investigates the FRP composite systems by presenting the properties of the fibers and the resins used to combine a fiber-reinforced polymer (FRP) material.

1.1 HISTORIC PERSPECTIVE

The practical knowledge for the design, fabrication, and construction of FRP was passed over generations. In the 1970's it has started building some of the first important practical application of fiber-reinforced polymers such as giant grain silos and tubes for water pipelines and aggressive wastewater. In those years, it has been used the merely practical knowledge for design and fabrication process, since this knowledge was considered top secret and no written documents were available; but this trend changed in the upcoming years. In the 1980 and in the following decade, the research about such topics increased manifold and thousands of publications related to FRP for civil purposes appeared. In late 1990's launch of new design codes such as ACI, ICBO (ACI Committee 440, 1996; ICBO 1997) were made, allowing the risen of this material from state-of-the-art to mainstream technology. During the twenty-first century, more defined standards and precise codes were published (ACI 440, 2006 - CNR, 2008 and followings) bringing to light specific and validate landmarks of designing that nowadays are used by engineers.

1.2 INTRODUCTION TO COMPOSITE MATERIALS

In the very long history of civil construction, the idea of combining two or more different materials resulting in a new material with improved properties has fascinated mankind. A composite material, in fact, is a combination of two or more materials that results in better properties than those of the individual components used alone. Apart from the metallic alloys, which are generally not considered as composites, each material retains its separate chemical, physical, and mechanical properties. The main advantages of composite materials are their high strength, stiffness, corrosion resistance and a greater fatigue resistance, combined with low density and a weight reduction when compared with bulk materials. Obviously, all of those advantages are accompanied by the elevated costs, especially of the same materials (the raw material) and the manufacturing process (fabrication and assembly).

A composite material is formed by a matrix and a reinforcement. The matrix is the element into which the reinforcement is embedded, and it is the continuous part. The

matrix can be polymers (PMCs, e.g. thermosetting resins, polyester and epoxy resins), metals (MMCs, e.g. aluminum, magnesium or titanium, which provide a compliant support for the reinforcement), or ceramics (CMCs e.g. carbon, special silicon carbide, alumina and mullite). Usually, polymers have low strength and stiffness, metals have intermediate strength and stiffness but high ductility, and ceramics have high strength and stiffness but are brittle. Concerning the PMCs, as before mentioned there are the epoxy resins, also known as polyepoxides, which are a class of reactive pre-polymers and polymers that contain epoxide groups. The applications for epoxy-based materials are extensive and include coatings, adhesives, and composite materials indeed, such as those using carbon fiber and fiberglass reinforcements (although polyester, vinyl ester, and other thermosetting resins are also used for glass-reinforced plastic). The chemistry of epoxies and the range of commercially available variations allow cure polymers to be produced with a very broad range of properties. In general, epoxies are known for their excellent adhesion, chemical and heat resistance, good-to-excellent mechanical properties and very good electrical insulating properties. The good fact of the epoxies is also that many properties of them can be modified, for example, silver-filled epoxies with good electrical conductivity are available, although epoxies are typically electrically insulating. Variations offering high thermal insulation, or thermal conductivity combined with high electrical resistance for electronics applications, are available.

Instead, the continuous reinforcement is given to the fibers (or a particulate) which are responsible for their high strength and stiffness. It is provided as a general rule that the thinner the fiber, the more the material can be resistant to a unidirectional force (supposed directed along the main axis of the fibers, see figure 1.1).
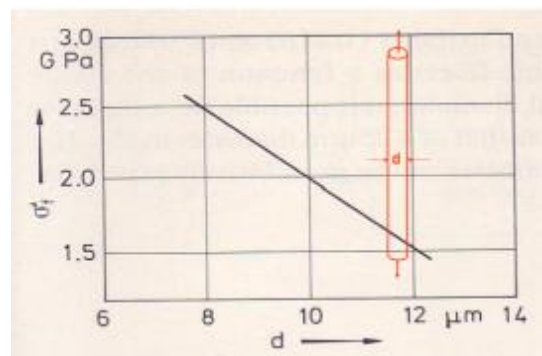
Figure 1.1 - Decrease in strenght (σf) of a carbon fiber with increase of diameter

In fact, the smaller the diameter of the fiber, the higher its strength, but often the cost increases as the diameter becomes smaller (remember the manufacturing's costs explained at the beginning). In addition, a smaller diameter and high strength fibers have greater flexibility and are more favorable fabrication's processes. Fibers provide the

mechanical strength of the assembly, while the matrix keeps them fixed in position and direction, fully coating them and protecting them from the external environment, giving, thus, to a composite, its shape, surface appearance and environmental tolerance. The matrix thus transmits the external loads to the fibers through the surface of the interface, which must have sufficient adhesion in order to not occur in any relative sliding. Moreover, the matrix redistributes the load to surroundings fibers when an individual fiber fractures and laterally supports the fibers to prevent buckling in compression.
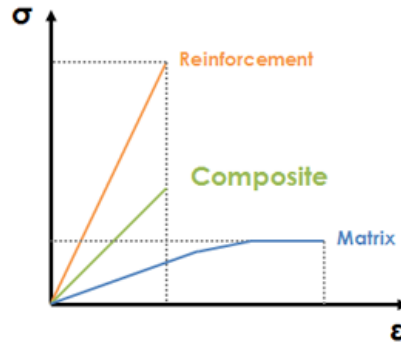
Figure 1.2 - Application's field of the composites

The graph in Figure 1.2 illustrates the relationship between the stress and the strain of the reinforcement. Clearly, the reinforcement has a much greater mechanical strength than the matrix so that the bond between them generates a material, called composite, of intermediate mechanical properties. It is important to notice that the fibers must be located in the directions in which are more effective, anticipating all the stresses that can occur in different circumstances, to make the most of the mechanical properties of the composite.

Typical fibers include glass, boron, aramid and carbon, which may be continuous or discontinuous. Continuous fibers have long aspect ratios, while discontinuous fibers have short aspect ratios. Continuous-fiber composites normally have a preferred orientation, while discontinuous fibers generally have a random orientation. Examples of continuous reinforcements include unidirectional, woven cloth, and helical winding, while examples of discontinuous reinforcements are chopped fibers and random mat (see Figure 1.3).
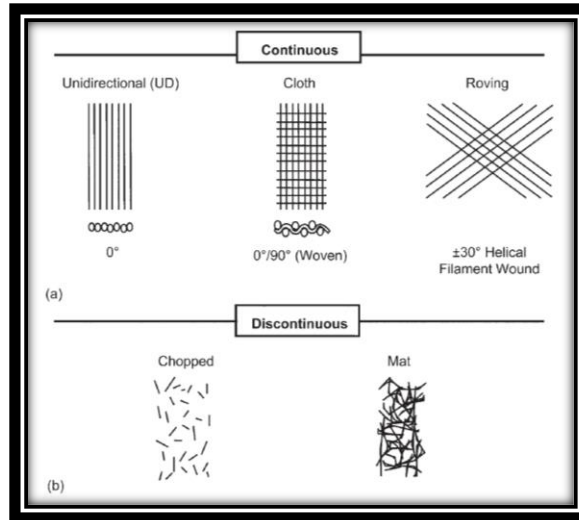
Figure 1.3 - Typical reinforcement types

Typically in aerospace, civil engineering, military, and motorsports, there is a great usage of the carbon fibers (graphite fibers), which properties such as high stiffness, high tensile strength, low weight, high chemical resistance, high-temperature tolerance and low thermal expansion play an important role in these applications' design (despite these kinds of fibers are very susceptible to oxidization in hot air). However, they are relatively expensive when compared to similar fibers, such as glass fibers or plastic fibers. In fact, glass fibers although are not as strong or as rigid as carbon fiber, they are much cheaper and significantly less brittle when used in composites. Glass fibers are used as a reinforcing agent for many polymer products; there is a very strong and relatively lightweight fiber-reinforced polymer (FRP) composite material called glass-reinforced plastic (GRP), also popularly known as "fiberglass". This structural material product contains little air, is denser than glass wool, and they are a very useful thermal insulators because of their high ratio of surface area to weight.

Also, Boron is a very important element for the usage as a composite, especially for the aerospace structures, because the boron fibers manifest a combination of high strength and high modulus, even though these fibers are very lightweight. The chemical vapor deposition on a high melting temperature core material (usually tungsten) during the fabrication process imprint to boron fibers the high strength at a very high temperature (about 2000 °C) and the capacity to retain high stiffness.

Composites can be categorized using the processing and manufacturing methods used to fabricate them. Discontinuous-fiber composites are normally somewhat random in alignment, which dramatically reduces their strength and modulus. However, discontinuous-fiber composites are generally much less costly than continuous-fiber composites. Therefore, continuous-fiber composites are used where higher strength and

20

stiffness are required (but at a higher cost), and discontinuous-fiber composites are used where cost is the main driver and strength and stiffness are less important.

High stiffness and strength usually require a high proportion of fibers in the composite. This is achieved by aligning a set of long fibers in a thin sheet (a lamina or ply). However, such material is highly anisotropic, generally being weak and compliant (having a low stiffness) in the transverse direction. Commonly, high strength and stiffness are required in various directions within a plane. The solution is to stack and weld together a number of sheets, each having the fibers oriented in different directions. Such a stack is termed a laminate.

The materials that constitute a composite include, as just previously mentioned, at least the matrix and the reinforcement. However, oftentimes the matrix is not homogeneous but mixed with inert fillers, performance-enhancing additives, etc. Likewise, the reinforcement is normally surface treated or coated with some substance to improve properties. For instance, with sandwich components (which is a technique that consists of attaching two thin skins bonded to a unique plastic core), the core and the face-core adhesive are additional constituents that improve the entire final element in terms of mechanical properties.

At the beginning, it has been introduced some of the main advantages of using composite materials. Now the purpose of this section is to enter into the detail of these. Firstly, it is important to say that what makes the real difference is that composite materials are tunable: this means that, on making a composite, we actually give it the properties and characteristic we prefer (evidently as a result of a proper design of all the components). Then, is also the specific strength (strength/density) and specific modulus (modulus/density) of high strength fibers (especially carbon) that are higher than those of other comparable aerospace metallic alloys, aluminum alloys or steels. This translates into greater weight savings resulting in improved performance, greater payloads, longer range, and fuel savings. The chief engineer of aircraft structures for the U.S. Navy once told that he liked composites because "they don't rot (corrode) and they don't get tired (fatigue)." In fact, corrosion of aluminum alloys is a major cost and a constant maintenance problem for both commercial and military aircraft. The corrosion resistance of composites can result in major savings in supportability costs. Carbon fiber composites cause galvanic corrosion of aluminum if the fibers are placed in direct contact with the metal surface, but bonding a glass fabric electrical insulation layer on all interfaces that contact aluminum eliminates this problem. Other important properties are the thermal ones, since composite structures act as very good insulators, whilst retaining their shape while not becoming brittle in cold temperatures, and the strength, since it is comparable

to aluminium and steel, strength characteristics of many materials can be reproduced through research and development with reinforcements, eg. Glass.

The graph in Figure 1.4 wants to clearly represent the advantages of using a composite material instead of a simple structural metal.
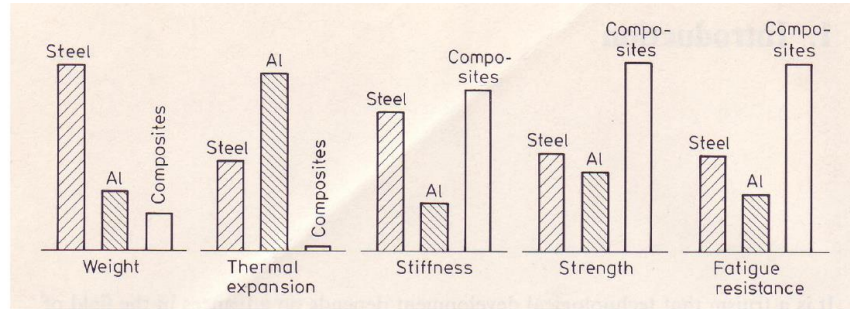
Figure 1.4 - Main advantages of the composite materials compare with steel and aluminum alloys

1.2.1 Fiber Reinforced Polymer

A fiber-reinforced polymer (FRP) is a specific type of composite material which consist of high-strength fibers surrounded in a resin matrix. The matrix combines the fibers together and also it distributes forces through them, providing protection against wear and deterioration. Frequent types of FRPs include CFRP, GFRP, and AFRP, composed of carbon fibers, glass fibers, and aramid fibers respectively. Rarely but not unusual, there is also the usage of paper, wood or asbestos as fibers.

In selecting the type of fiber to be used for civil application, there are a few things to consider. GFRP is excellent for seismic upgrades where the seismic loads only temporarily engage the FRP. In cases where stresses are sustained in the FRP (such as in bending and shear strengthening), GFRP should be avoided (or service stresses maintained at a minimum level) because of creep rupture effects (this phenomenon results in the eventual failure of the material under sustained loads higher than a fraction of the instantaneous ultimate load). Carbon is much more suitable for these applications. Similarly, in exterior applications, CFRP will be much more durable.

Typically, carbon fibers used in the construction industry have strengths that reach 10 times that of the typical steel used for reinforcement and over twice as strong as steel used for pre-stressing. The stiffness is similar to that of steel. Carbon is also quite resistant to most environmental conditions and can withstand high sustained and fatigue loading conditions. Carbon is, however, is a conductive fiber material; and while carbon itself will not corrode, when it gets in contact with steel, instead, it will accelerate corrosion of the steel.

22

The growing trend in using FRP materials as internal reinforcement to strength traditional structures is a result of reasons such as short installation time, incredible improvements to strength and longer material lifetime, due to their high corrosion resistance. In Figure 1.5 the structure of a typical FRP composite material is shown.
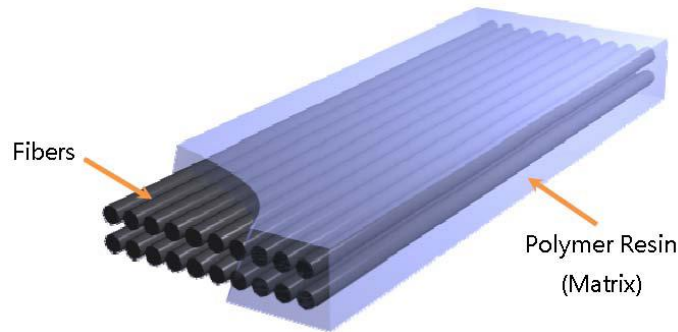
Figure 1.5 - FRP Composite (photo credit by Dingyi Yang)

1.3 EXTERNALLY BONDED FIBER REINFORCED POLYMER

FRP systems in the concrete repair industry are used to strengthen existing structures, that are affected by deterioration, design/construction errors or seismic problems. Externally bonded FRP can essentially be applied as reinforcement in concrete providing strength where concrete is weakest (in tension). In this way, typical applications of externally bonded FRP are on beam or slab soffits to provide additional flexural strength, on the sides of beams to provide additional shear strength, or wrapped around columns to provide confinement and additional ductility. Among many other applications, concrete and masonry walls may be strengthened to better resist seismic and wind loads, concrete pipes may be lined with externally bonded FRP to resist higher internal pressures, and silos and tanks may be strengthened to resist higher pressures. The following Figure 1.6 shows some of these typical applications of externally bonded CFRP.

Figure 1.6 - Typical applications of externally bonded CFRP

1.4 FRP ANCHORAGE SYSTEM PURPOSES

1.4.1 Influence of anchorage

Anchorage systems have been introduced to prevent or delay the premature failure of the FRP that occurs with the initial process of the FRP laminate's debonding and ends with the delamination. Past studies indicated that the potential use of anchors may change the failure mode of FRP strengthened elements. It is, therefore, reasonable to assume that: An anchor must be designed and effectively functioning not to fail before FRP fracture. Also, before the debonding process starts, the tensile force in the FRP will decay exponentially toward the anchored end (Chen et al. [2001]), once the FRP starts to peel off, this debonding trend propagates quickly (Chen et al. [2001]) and results in a more even strain distribution in FRP laminates.

Typically, an anchorage system for externally bonded FRP fulfills three main aims: firstly, an anchorage system is needed to prevent or delay the interfacial crack opening at the starting of debonding or failure of the concrete substrate, due to tensile normal forces associated with the certain debonding failure modes. This goal is most commonly reached by install the anchorage system at the termination of FRP laminates, and sometimes throughout their entire length. An example application of anchorage preventing this problematic is shown in Figure 1.7, in which the FRP on an RC beam is anchored at the laminate end in order to prevent concrete cover separation and "plate-end" interfacial debonding.

Plate End
Debonding/Cover Separation Occurs

Type I Anchor
Prevents Failure
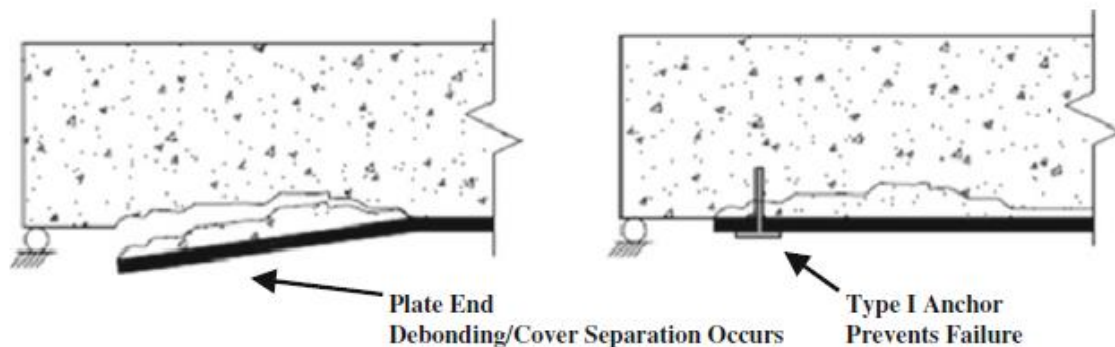
Figure 1.7 - Anchorage system installed at the FRP laminate end

Secondly, an anchorage system increases the total available interfacial shear stress transfer. This is usually achieved by increasing the area over which the shear stress is transferred, or reducing the length of FRP used by increasing the interfacial stress transfer.

24

Thirdly an anchor provides a load transfer mechanism at critical locations of structural members (such as at the location of an interface between two orthogonal structural members) where no bond length is available beyond the critical section. This special case leads a difficult challenge on the designing since the FRP strengthening system can be considered to have no contribution to the strength without their inclusion. In Figure 1.8, it is shown an example of this particular case.
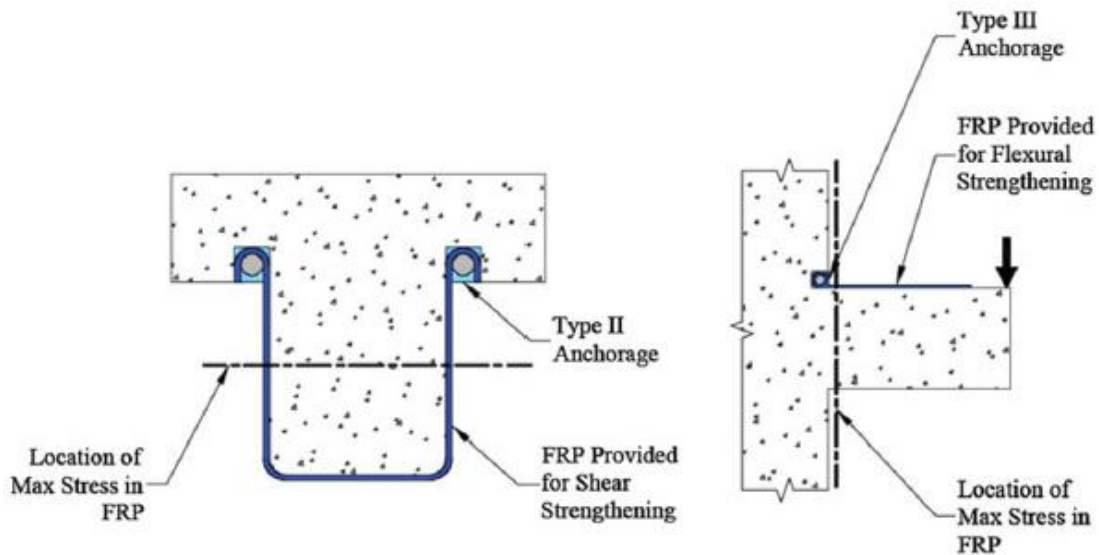
Figure 1.8 - Anchorage system installed at critical locations of structural members

1.4.2 Existing types of FRP anchorage systems

In this section a brief description of existing FRP anchorage systems is reported:

1.4.2.1 Anchor Spikes

The most used anchor system is the "anchor spikes" type. This consists of strands of bundle fibers with one end embedded in the concrete substrate and the other one embedded over the FRP sheet, with different configurations and orientations of fans. Figure 1.9 illustrates a typical anchor spike configuration at 90°. Figure 1.10 shows some of the orientations adopted for the anchor spikes shear test.
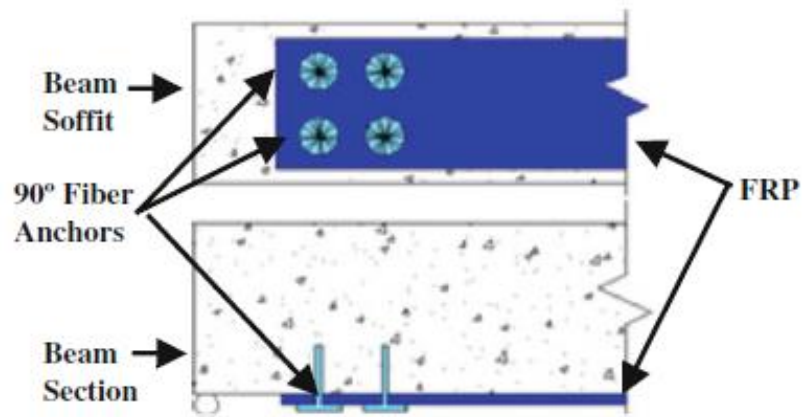
Figure 1.9 - 90° anchor spikes
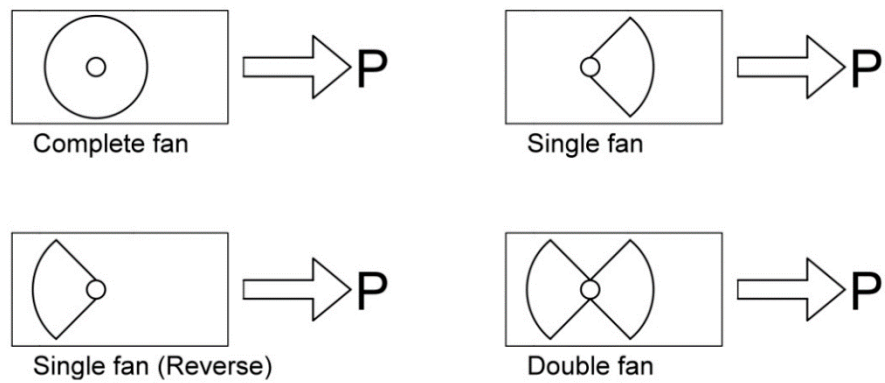
Figure 1.10 - Orientations anchor spikes

There is also another configuration adopted for the spike anchors, which is the 180° configuration, in which the anchor is installed in-plane with the anchored FRP so that the fibers in the anchor can transfer the tensile force in the anchored FRP to the anchor. In Figure 1.11 is shown the 180° configuration.
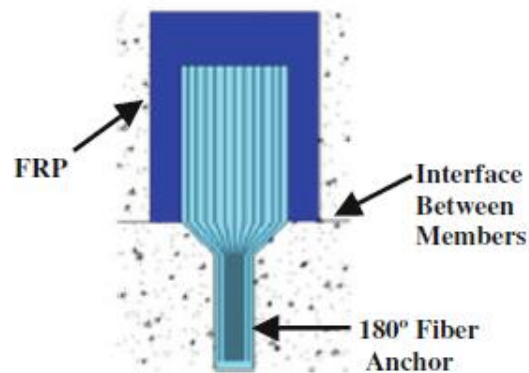
Figure 1.11 - 180° anchor spikes

The most important advantage that brings to success the anchor spikes type is their possibility to be fabricated in the field with the same FRP material used as the externally bonded fabric (which facilitates the construction and eliminates potential corrosion hazards from the different material, making the whole anchorage system homogenous).

1.4.2.2 Transverse Wrapping

Transverse wrapping is usually in the form of discrete strips situated along the laminate length or at its end. The fiber orientation can be perpendicular to the longitudinal axis or inclined whit a certain angle. Using a wrap bonded to FRP with another FRP sheet provides a clamping effect in the wrapped FRP and thus, it can be seen as a form of anchorage.

Usually, as in the case of spikes anchors system, the wrapping material can be the same of the strengthening reinforcement, avoiding the potential corrosion hazards that can result from using dissimilar materials.
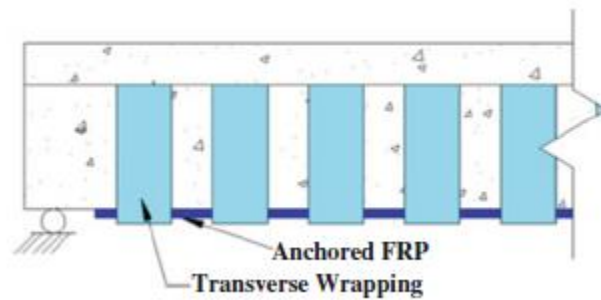
Figure 1.12 - Transverse Wrapping

In Figure 1.12 it is illustrated an example of transverse wrapping anchorage on a T-beam

The wrapping installation can be challenging, due to the member geometry and the eventual access to its adjacent sides. Furthermore, the transverse wrapping is not totally effective until a certain level of tensile stress is reached in the wrap itself and unless the transverse wraps are stressed in tension.

1.4.2.3 U-Anchors

A U-Anchor is installed in a groove made in the concrete surface onto which or adjacent to where the strengthening FRP sheets are placed.

The FRP sheets are then pressed into the groove that is filled with epoxy, sometimes in combination with steel bars. A scheme of a typical U-Anchor is shown in Figure 1.13.
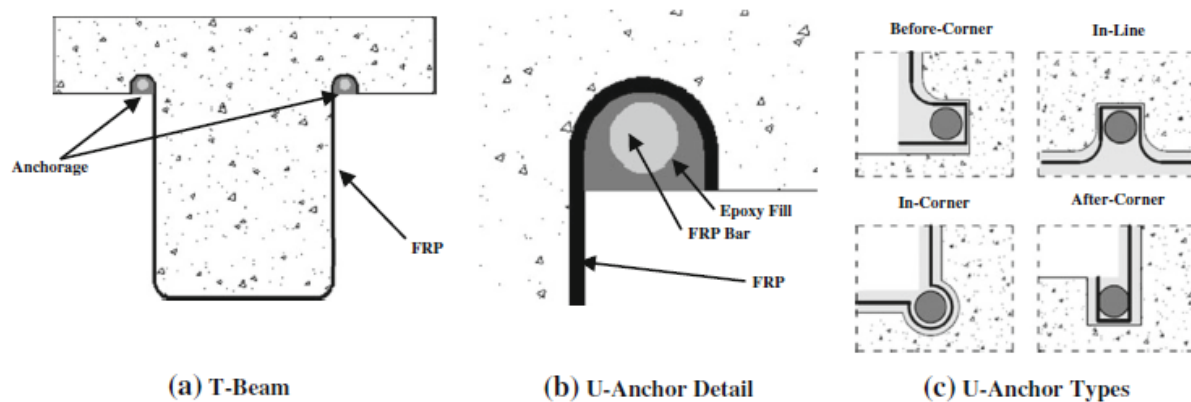
Figure 1.13 - U-Anchors

The U-anchor system works by increasing the bonded area of FRP to concrete; this bonded area is the area of the FRP bonded to concrete in the walls of the groove. Many studies have demonstrated that this type of anchor improves the interfacial stress transfer between the FRP and the concrete.

1.4.2.4 FRP Strips

Fiber reinforced polymer strips are a very simple type of anchorage, compared to the other anchorage devices, installed on the top of the FRP sheet used to strengthen the reinforced concrete member. They are typically installed perpendicular to the direction of the force of the strengthening FRP sheets and for this reason they have limited efficiency. Although they may seem similar to the transverse wrapping, it can be distinguished because the strips do not provide a confining effect to the FRP sheet. Because of this reason, the FRP strip anchorages must be loaded out-of-plane; this means that they should be loaded in a direction that does not stress the fibers in pure tension, leading to an inefficient force transfer mechanism. As the previous cases, in order to avoid the potential problem of corrosion resulted by using different materials, the material must the same used to anchor the FRP sheet. In the following Figure 1.14, there is an example of FRP strip anchorage.
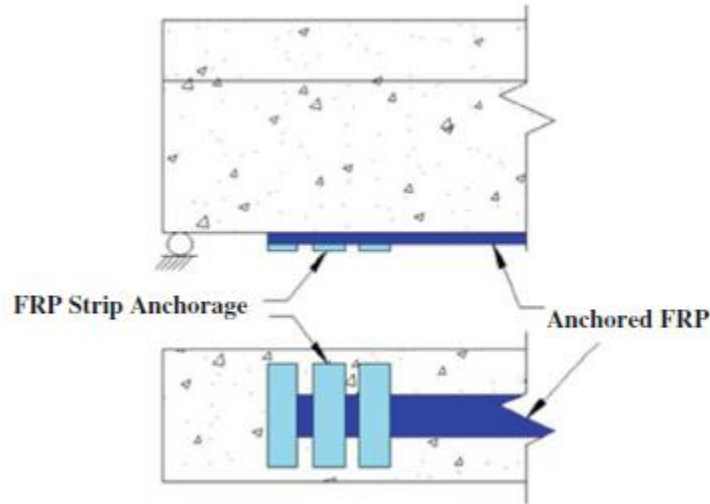
Figure 1.14 - FRP strips

1.4.2.5 Longitudinal Chase

The longitudinal chase is a particular type of anchorage system created by cutting a groove in the concrete parallel to the surface of the FRP. The groove is filled in with epoxy resin and, in some cases, a steel or FRP bar is embedded (some studies developed by Kalfat and Al-Mahaidi in 2010 found that exclusion of the bar from the groove should not affect the strength of the anchorage system). Finally, the FRP sheet is bonded to the concrete and over the top of the groove. This anchorage system is based on the concept that the interfacial shear stresses are better distributed to a larger area of concrete through the mechanical properties of the epoxy resin poured into the groove. The additional bonded area is equal to the width and twice the depth of the groove, times its length. The Figure 1.15 shows a longitudinal chase anchorage system.
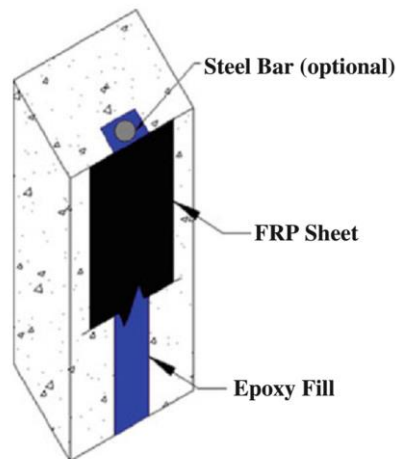
Figure 1.15 - Longitudinal chase anchorage (Grelle and Sneed, 2013)

1.4.2.6 Plate Anchors

This anchorage system is made up of FRP sheets anchored to the plates (metallic or composite plates), which are either bolted or bonded to the concrete substrate. This configuration allows transferring the shear stress to the FRP–plate interface. Then, the plate transfers the stress to the concrete substrate via its connection, which consists of bolts through the plate into the concrete. The Figure 1.16 shows a typical plate anchorage system.
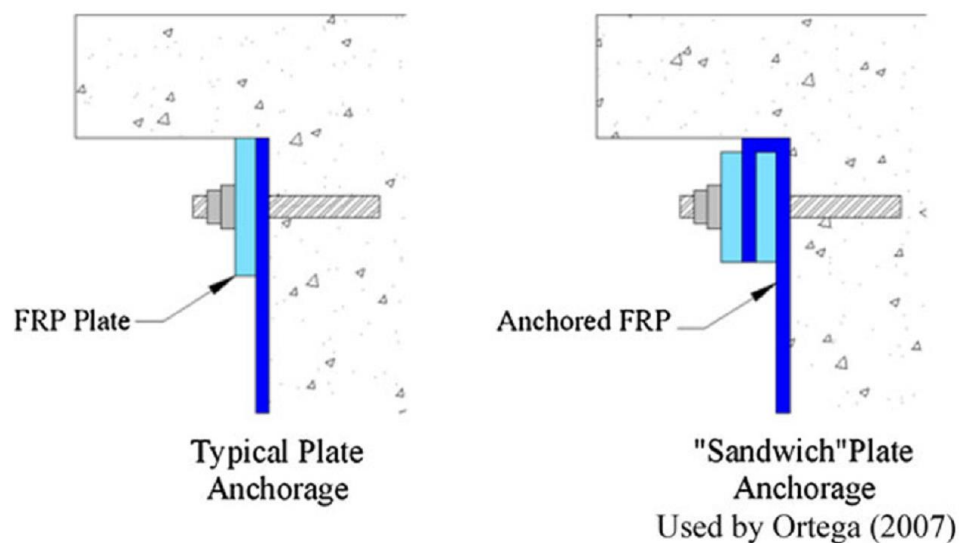
Figure 1.16 - Plate anchors (Grelle and Sneed, 2013)

From various tests performed on steel and FRP plate anchors by Ceroni et al. (2008) indicated that the plates generally offer a better performance over U-Anchors and unanchored FRP on otherwise identical specimens. This type of anchor can be also presented in the ''sandwich'' configuration (Ortega, 2009) as shown in the Figure 1.16 (on the right), which obviously performs better than similar single plate systems.

1.4.2.7 Bolted Angles

Bolted angles made of steel or aluminum are a type of FRP anchorage devices, that are installed in 90° joints. Usually, the FRP is laid around the joint, the angle is bonded to the FRP in the joint and bolted to the concrete either through or around the FRP sheet. Even if bolted angles have several limitations, as the problem of corrosion (they are made of steel) or the problem of stress concentration in the FRP (due to the 90° corner), which lead to a premature failure, they are frequently used because steel angle shapes are easy

30

to obtain and require little fabrication. Figure 1.17 shows two different applications of bolted angles.
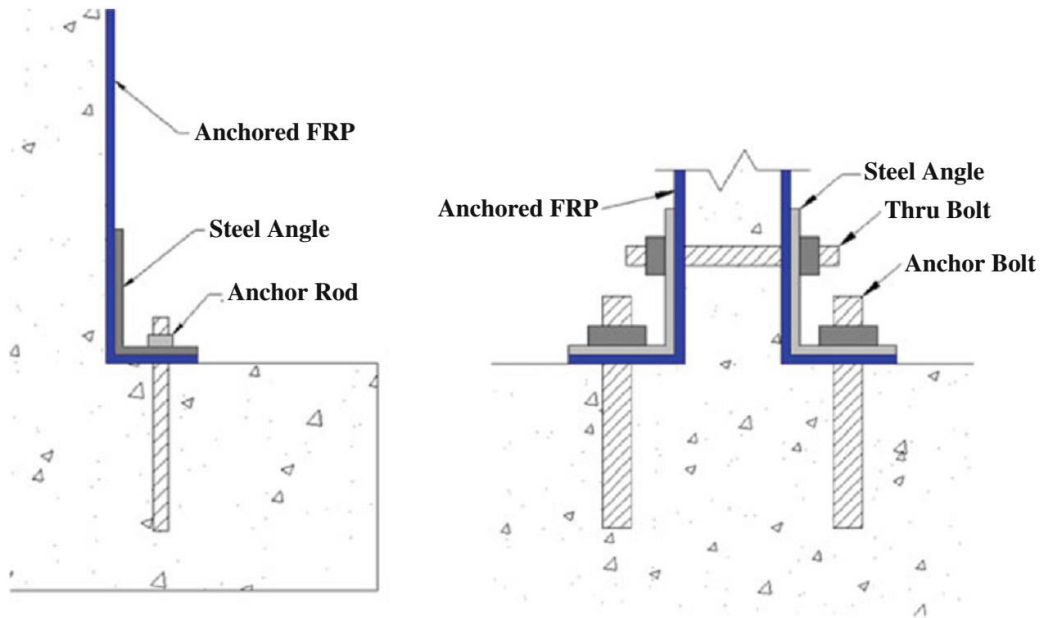
Figure 1.17 - Bolted Angles

1.4.2.8 Cylindrical Hollow Section

Designed for 90° joints applications, this type of anchorage is composed a steel pipe is bolted through the FRP at a 45 angle in order to eliminate the potential for local stress concentrations at the 90° corner. An example of the cylindrical hollow section is shown in Figure 1.18.
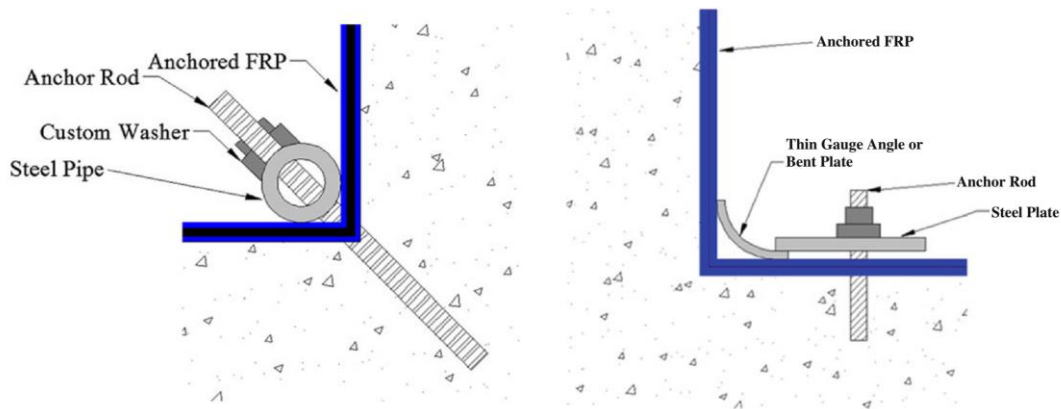
Figure 1.18 - Cylindrical Hollow Section

1.4.3 Staples Anchorage system

In this section, we will not go much in too deep the process of the anchors' making and assembling. This section, though, describes, in general, the principal anchors' characteristics and the main differences between them, respecting in this way the will of the producer.

1.4.3.1 Flat staple
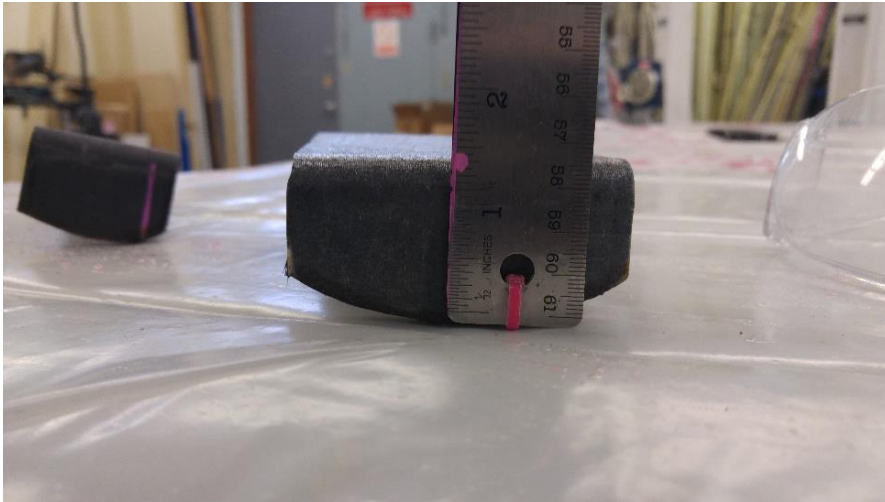
Figure 1.19 – Leg view of a flat staple anchorage system

The flat staple anchors are called so thanks to their shape that literally recall the shape of a staple. Figure 1.19 shows the leg's detail of a flat staple, remarking its 1-inch depth.

With the uni-directional fibers of the anchor aligned in a longitudinal way to the flexural FRP sheet, the flat staple anchor is made by carbon fibers pre-impregnated with a particular synthetic resin. In Figure 1.12 it is reported a 3D view of a flat staple with the indication of the fibers direction.
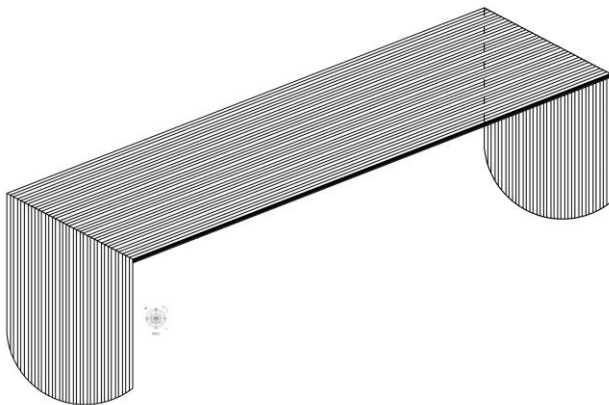
Figure 1.20 – 3D view of a flat staple with the fibers direction perspective

Also, the flat staple anchors are very competitive thanks to their low material cost of fabrication. The vertical length of the leg – measured with the ruler in the figure - represents the depth of the anchor, while the horizontal length – longitudinal to the position of the ruler in the figure – represents the width of the anchor.

Table 1.1 – Carbon fibers' characteristics

Vf = 60%

TYPICAL PROPERTIES	SI	US
Tensile Strength	1,850 MPa	268 ksi
Tensile Modulus	130 GPa	18.9 msi
Compressive Strength	1,320 MPa	191 ksi
Compressive Modulus	125 GPa	18.1 msi
Interlaminer Shear Strength	70 MPa	10 ksi
Glass Translation Temperature (Tg,G")	120°C	248°F

Table 1.1 describes the carbon fibers' characteristics, which the flat staple (but also the round staple) anchors are made of.

1.4.3.2 Round staple

Figure 1.21 – Plan view of a round staple, remarking its 6,5-inch length

The round staple anchors (shown in Figure 1.21) are called so thanks to their rounded shape.

Again, the uni-directional fibers of the anchor are aligned in a longitudinal way to the flexural FRP sheet, covered by an epoxy layer that keeps the fibers together.

The following sketch in Figure 1.22 represents the shape of a round staple anchor, without the indication of the fibers direction.

3D View   Cross-section
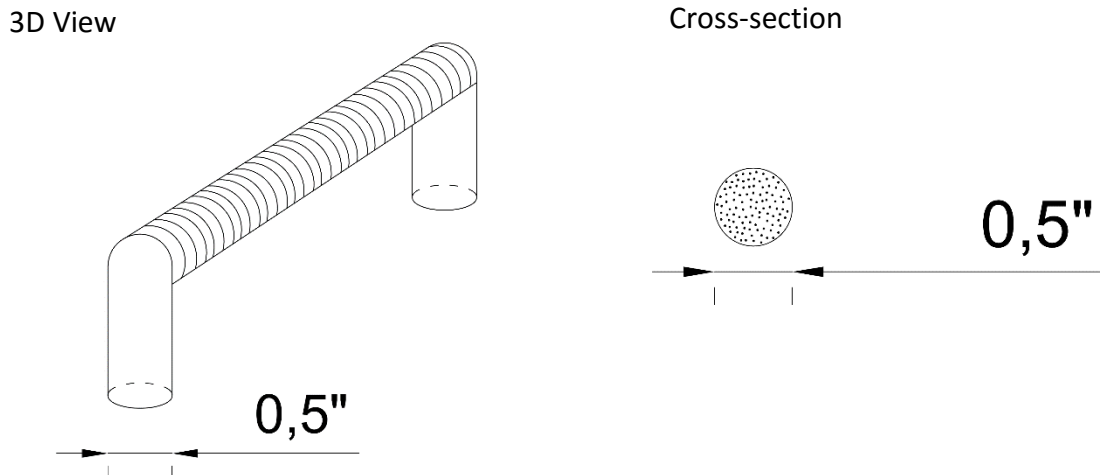
Figure 1.22 – 3D view and cross section of the prototype version of the round staples

After a couple of specimens run with the round staple in the old shape configuration (sketch above in Figure 1.22), the round staples were improved. They were arranged in a new shape with 3 main important differences:

Firstly, the under part of the anchor is flat, increasing the area in contact with the FRP laminate

Secondly, the upper part of the anchor is no more rounded but elliptical, in order to prevent the formation of air bubbles in between the folded part of the flexural FRP sheet over the anchor and the anchor itself. Also, this shape allows the squeezed epoxy in excess to come out laterally, by the legs sides of the anchor.

Thirdly, many fibers were concentrated on the bend radius, improving the resistance in this location, where the stresses are more concentrated.
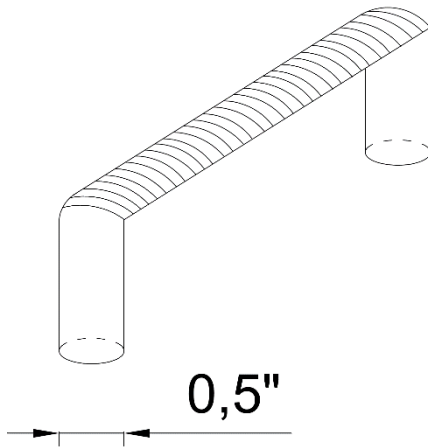
3D View   Cross-section
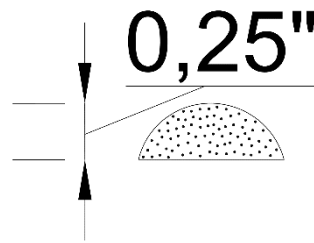
Figure 1.23 - 3D view and cross section of the new version of the round staples

The pictures in Figure 1.23 and 1.24 represent respectively the 3D view, cross section, under view and profile view of the new round staple anchors shape.

Figure 1.24 – Under-view and profile view of the new round staples

2. EXPERIMENTAL PROGRAM

2.1 SHEAR TEST PROGRAM

The force transfer between FRP plate and concrete substrate takes place primarily through shear stresses and thus, shear tests are commonly adopted to determine the maximum debonding force. Despite that, comparisons of different set-ups show that, in general, shear tests offer lower bond strength than bending tests. Also, their simplicity makes them popular for laboratory investigations of FRP to concrete bond behavior. It is important to remark that the double-shear test is generally preferred over the single shear test, due to symmetry and for better control of induced normal stresses. However, it should be kept in mind that in flexural elements, peeling stresses (see Figure 2.1) also develop along the FRP-concrete interface and their interaction with shear stresses can lead to a reduction in the bond strength of the strengthening system. To better understand, a sketch with all the different type of stresses is shown in Figure 2.2
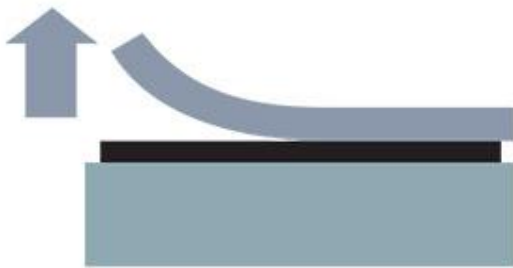
Figure 2.1 - Peel stress (westsystem.com)
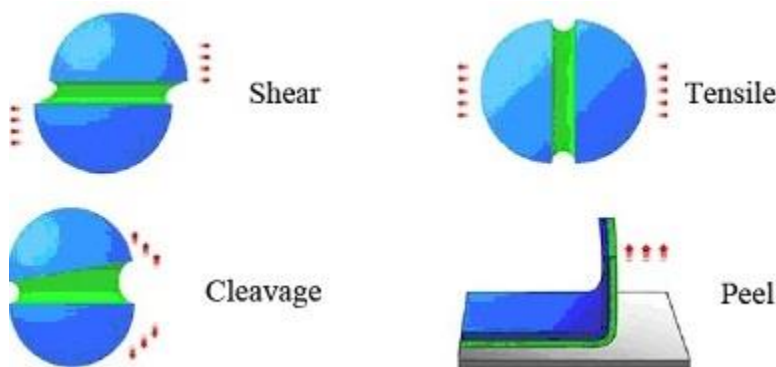
Figure 2.2 - Types of stress between two surfaces (adhesives.org)

While the direct tension pull-out test is generally adopted for in-situ quality control of bond and determination of the pure tension load capacity of the anchors (to resist to the peel stresses), the double-shear tests utilize a symmetrical system so that load application

presents fewer challenges than a single shear test. Because of the specimen's symmetry, the load can be applied to an object such as a concrete block to which the FRP is attached, which is generally simpler than devising a system to apply a load directly and evenly to the FRP.

CNR DT200, 2013 identifies other 3 failures due to the debonding:

1. The plate end debonding
2. Debonding by flexural cracks in the beam
3. Debonding by diagonal shear cracks
4. Debonding by irregularities and roughness of the concrete surface

The plate end debonding (shown is Figure 2.3) is the failure mode in which the end portions of the FRP system are subjected to high interfacial shear stresses for a length of approximately 100-200 mm. Since the double shear test aim is to generate an interfacial shear stress between the surface of concrete and the FRP sheets, this test only refers to the plate debonding failure mode (the first failure mode). In this way, when strengthening is done with FRP laminates, tensile stress perpendicular to the interface between FRP and support (normal stress) may arise due to the significant stiffness of FRP laminate (see Figure 2.4). Normal stresses may reduce the value of interfacial shear stress as shown in Figure 2.5. Failure mode by end debonding is characterized by brittle behavior.
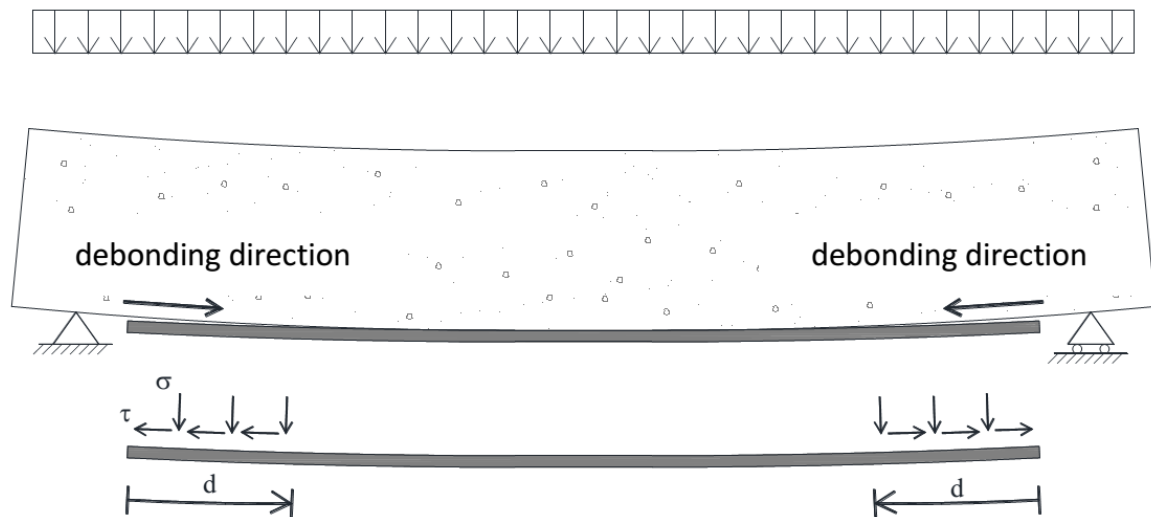
Figure 2.3 - Plate end debonding (CNR DT200, 2013)
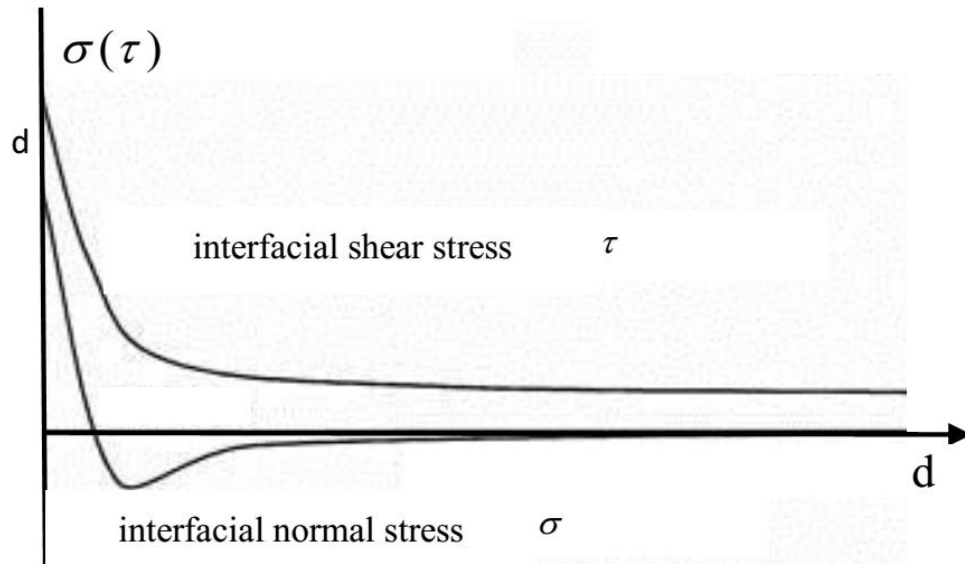
Figure 2.4 - Interfacial shear and normal stress along the length of a bonded FRP laminate (CNR DT200, 2013)
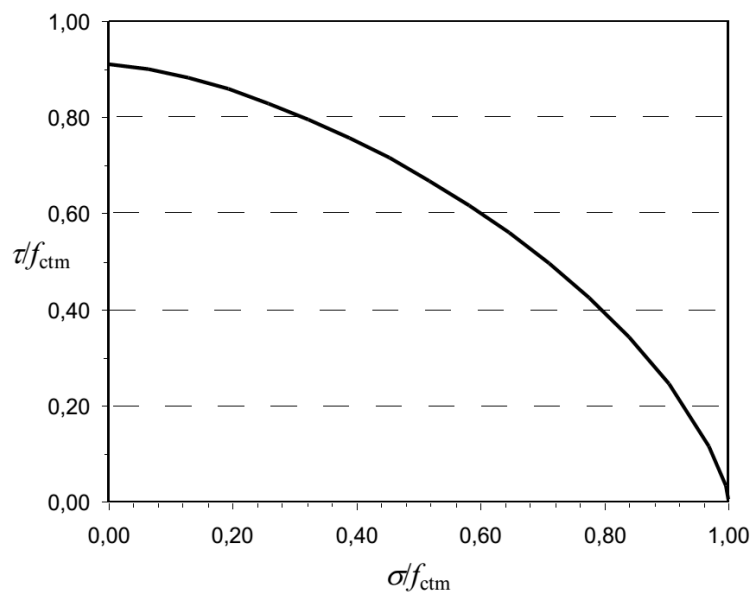
Figure 2.5 - Strength domain represented by interfacial shear and normal stresses (CNR DT200, 2013)

2.1.1 Design strength for laminate/sheet end debonding

The bond system is fundamental because is responsible transferring the load from the concrete to the FRP flexural element. The bond behavior between FRP and concrete is associated with the interfacial stress diffusion, which is correlated to mechanical characteristics, such as the geometry or the properties of the materials. The bond behavior is usually represented by a shear stress relationship $\tau - s$ (with s = slip). There are many examples of stress-slip relationship present in literature but the most largely

adopted due to its good correspondence with the experimental results is the bi-linear behavior, which is shown in Figure 2.6
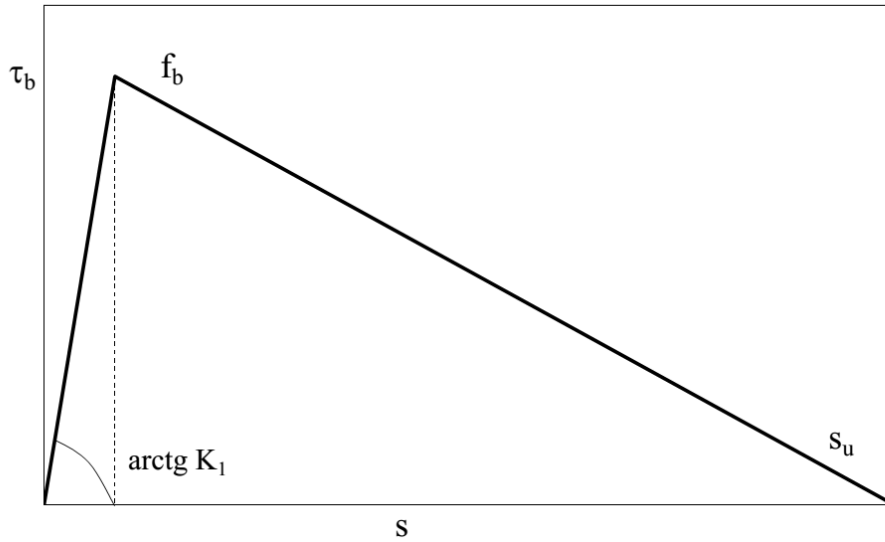
Figure 2.6 - Bilinear constitutive law (CNR DT200, 2013)

The ultimate value of the force transferred from FRP reinforcement to the support prior to FRP debonding depends on the length, l_b, of the bonded area. This value grows with l_b up to a maximum corresponding length, l_e: further increase of the bond area does not increase the force that it is possible to transfer. The length l_e is called optimal bond length and corresponds to the minimal bond length able to carry the maximum anchorage force.
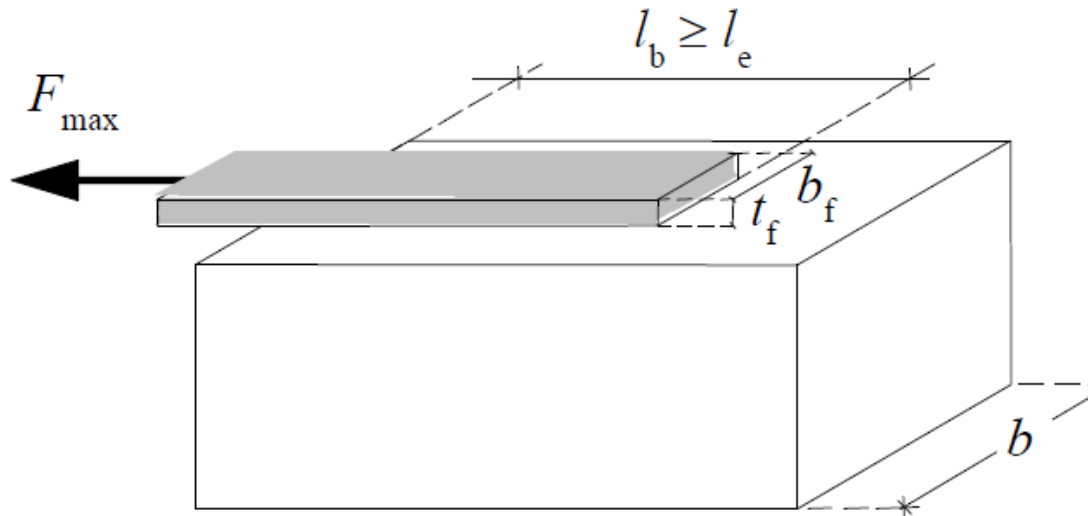
Figure 2.7 - Maximum force transferred between FRP and concrete (CNR DT200, 2013)

The optimal bond length, l_{ed}, shall be estimated as follows:

$$l_{ed} = \max \left\{ \frac{1}{\gamma_{Rd} \cdot f_{bd}} \sqrt{\frac{\pi^2 \cdot E_f \cdot t_f \cdot \Gamma_{Fd}}{2}}; 150 \text{ mm} \right\}.$$

Where

- E_f and t_f are the Young modulus of elasticity of FRP reinforcement and the FRP thickness, respectively.
- γ_{Rd} is a corrective factor agreed upon a value of 1.25.
- $f_{bd} = \frac{2\Gamma_{Fd}}{s_u}$, with $s_u = 0{,}25mm$ is the design bond strength between FRP reinforcement and concrete.
- Γ_{Fd} is the design value of specific fracture energy, which is a corrective factor calculated as:

$$\Gamma_{Fd} = \frac{k_b \cdot k_G}{FC} \cdot \sqrt{f_{cm} \cdot f_{ctm}}$$

   Where:

   - f_{cm} e f_{ctm} are the mean values of the concrete compressive and tensile strengths, respectively, evaluated on-site.
   - FC is the confidence factor.
   - k_b is the geometrical corrective factor and function of the ratio between the FRP width (b_f) and concrete width (b), b_f/b. k_b is defined with the following equation:

$$k_b = \sqrt{\frac{2 - b_f/b}{1 + b_f/b}} \geq 1$$

   with a value of $b_f/b \geq 0.25$ (if $b_f/\beta \geq 0.25$, k_b is equal to 1.18).

   - k_G is an additional corrective factor calibrated from experimental results and equal to $0{,}023\ mm$ or $0{,}037\ mm$ for pre-cured and wet lay-up systems, respectively.

In table 2.1 we introduce all the materials data calculated as above explained:

Table 2.1 - Materials data

Data			
Ef	Elastic Modulus FRP	77040,00	Mpa
tf	thickness of FRP	1,02	mm
FC	Confidence factor	1,00	
bf	width	152,40	mm
b	length	254,00	mm
Kb	geometrical corrective factor	0,94	-
KG	additional corrective factor for wet lay-up systems	0,04	mm
fctm	concrete tensile strength	4,13	Mpa
fcm	concrete compressive strength	59,00	Mpa
Γfd	Design fracture energy	0,41	Mpamm
su	design bond strength between FRP and concrete	0,25	-
YRd	Corrective factor (standard)	1,25	-
fbd	factor fbd	3,27	Mpa

Finally, we can compute the optimal bond length as equal to:

$$L_{ed} = 97{,}25\ mm\ (= 3{,}83\ in.)$$

2.2. MATERIAL PROPERTIES

2.2.1 Concrete properties

In order to characterize the concrete, a total of 20 cylinders were casted into plastic molds with a cylindrical shape, in accordance with ASTM C39 (2014); the test, in fact, aims to find out the compressive strength of cylindrical concrete specimens. This method consists of applying a compressive axial load to molded cylinders at a rate which is within a prescribed range until failure occurs. The compressive strength of the specimen (f'_c) is calculated by dividing the maximum load reached during the test by the cross-sectional area of the specimen.

Figure 2.8 illustrates the casting of the cylinders.

Figure 2.8 – Casting of the cylinders

The cylinders casted were 20 but only 9 of them were tested, because during the curing period and the during the set up of the machine 11 specimens were lost.

Figure 2.9 illustrates the machine used for the compression test, while in Figure 2.10 a comparison between the specimen before and after the test is shown.

Figure 2.9 – Compression test machine
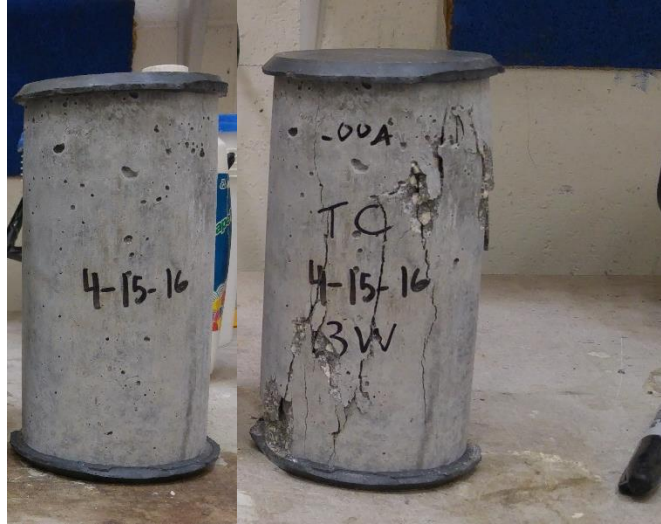
Figure 2.10 – Specimen before and after the compression test

As a long term observation, 3 different tests were run. After 14 days (half curing period) the first 3 specimens were tested. Then, other 3 specimens were tested after 21 days and finally after 28 days, the period through which the concrete should have reached an almost stationary plafond.

Table 2.2 summarizes the results obtained from each test: here, the diameter is presented in inches calculated at the midspan, top and bottom of the cylinder. Then, an average between those values has been calculated.

The area is the average cross-sectional area, based on the diameter's average. The peak load represents the maximum axial load reached by the machine during the test and f'$_c$ is the compressive strength.

All of the specimens show a failure mode 3. As described in ASTM C39, failure mode 3 represent the rupture type in which columnar vertical cracking through both the ends and no well-formed cones are presented (see Figure 2.10).

Finally, the standard deviation and the coefficient of variation (C.V) were calculated for each sequence of the test.

Table 2.2 – Compressive strength test results

Cylindrical concrete specimen test results

	Specimen ID	Date cast	Date tested	Diameter [inches] Midspan	Top	Bottom	Area [inches²]	Diameter Average	Diameter [mm]	Area [mm²]	Peak load [lbs]	Peak load [KN]	f'c [Mpa]	Failure mode
14 days after	_001	04.15.2016	04.29.2016	4,014	4,009	4,004	12,65449	4,009	101,8286	8143,842	104510	464,8836	57,08407	Type 3
	_002	04.15.2016	04.29.2016	4,046	4,032	4,019	12,85706	4,032333	102,4213	8238,916	103320	459,5903	55,78285	Type 3
	_003	04.15.2016	04.29.2016	4,051	4,052	4,033	12,88885	4,045333	102,7515	8292,125	109250	485,9682	58,60599	Type 3
	Average										105693,33	470,15	57,16	
	St deviation										2561,44	11,39	1,15	
	Coefficient of variation (C.V) ((%)*										2,42	2,42	2,02	

Cylindrical concrete specimen test results

	Specimen ID	Date cast	Date tested	Diameter [inches] Midspan	Top	Bottom	Area [inches²]	Diameter Average	Diameter [mm]	Area [mm²]	Peak load [lbs]	Peak load [KN]	f'c [Mpa]	Failure mode
21 days after	_001	04.15.2016	05.06.2016	4,013	4,038	4,009	12,64818	4,02	102,108	8188,594	114960	511,3676	62,44876	Type 3
	_002	04.15.2016	05.06.2017	4,012	4,056	4,044	12,64188	4,037333	102,5483	8259,361	114240	508,1648	61,52593	Type 3
	_003	04.15.2016	05.06.2018	4,032	4,057	4,045	12,76823	4,044667	102,7345	8289,392	98340	437,4381	52,77083	Type 3
	Average										109180,00	485,66	58,92	
	St deviation										7670,67	34,12	4,36	
	Coefficient of variation (C.V) ((%)*										7,03	7,03	7,40	

Cylindrical concrete specimen test results

	Specimen ID	Date cast	Date tested	Diameter [inches] Midspan	Top	Bottom	Area [inches²]	Diameter Average	Diameter [mm]	Area [mm²]	Peak load [lbs]	Peak load [KN]	f'c [Mpa]	Failure mode
28 days after	_001	04.15.2016	05.06.2016	3,998	4,058	4,029	12,5538	4,028333	102,3197	8222,578	116830	519,6857	63,20228	Type 3
	_002	04.15.2016	05.06.2017	4,011	4,054	4,027	12,63558	4,030667	102,3789	8232,107	116520	518,3068	62,96162	Type 3
	_003	04.15.2016	05.06.2018	4,011	4,051	4,008	12,63558	4,023333	102,1927	8202,179	98380	437,616	53,35363	Type 1
	Average										110576,67	491,87	59,84	
	St deviation										8625,27	38,37	4,59	
	Coefficient of variation (C.V) ((%)*										7,80	7,80	7,67	
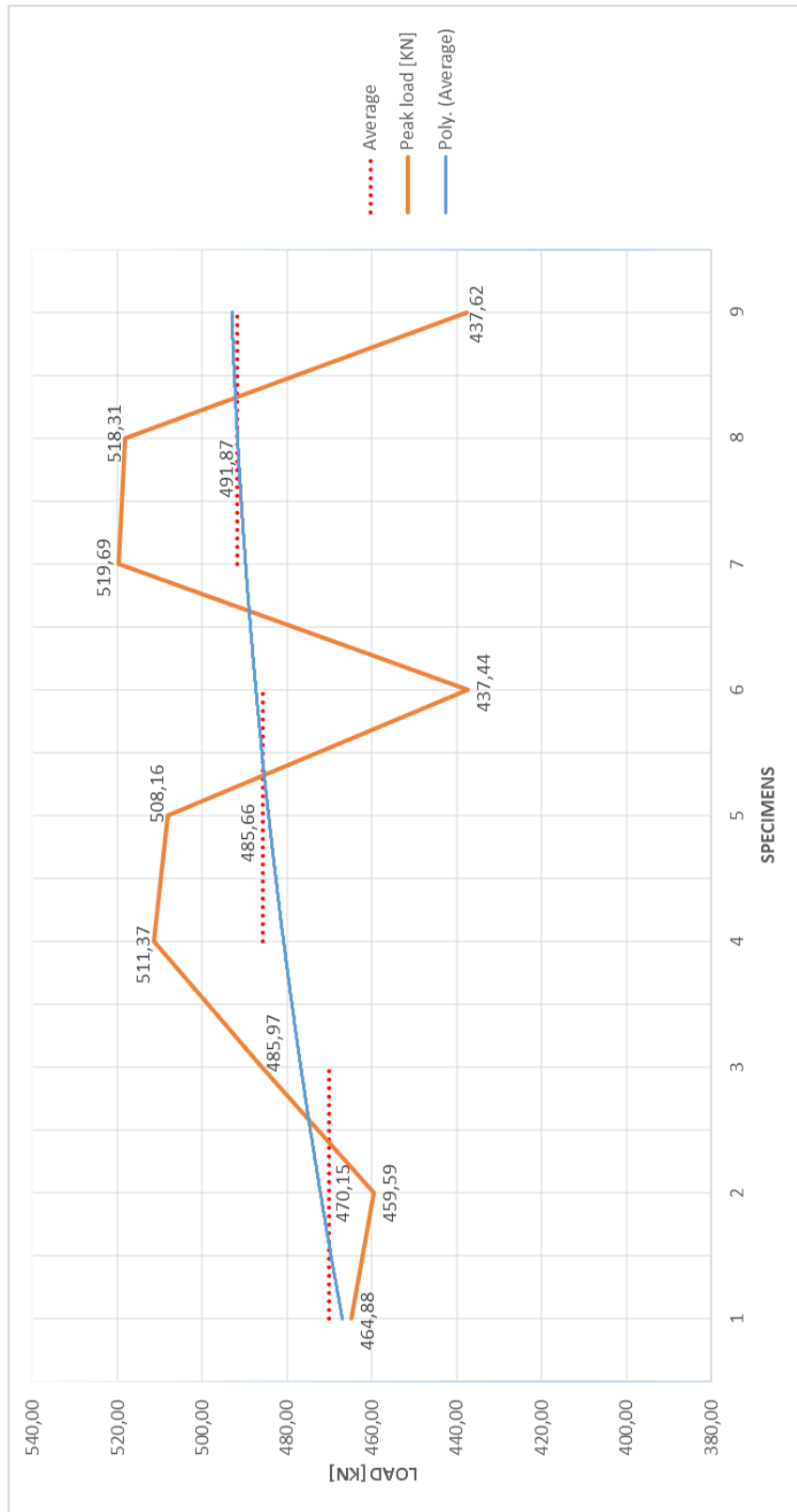
Figure 2.11 - Cylindrical concrete specimen test results comparison 14-21-28 days

The graph in Figure 2.11 shows the trend and progress of the concrete curing after 14, 21 and 28 days.

This graph is based in term of the average of 3 points' peak loads taken from each test. The blue line represents the logarithmic curve based on the average of all the specimens. This curve represents the plotted progress based on all the 9 specimens.

In the end, the theoretical concrete tensile strength (f_{ctm}) and the elastic modulus were calculated.

A number of empirical formulae connecting f_{ctm} and f_c' have been suggested, many of them of the following type:

$$f_t = k(f'_c)^n$$

where k and n are co-efficients. Values of n between ½ and ¾ have been suggested. The former value is used by the American Concrete Institute, but Gardner and Poon found a value near the later, cylinders being used in both cases. Probably the best fit overall is given by the expression recommended by Neville (2000):

$$f_t = 0,27(f'_c)^{\frac{2}{3}} = 0,27(59,84)^{\frac{2}{3}} = 4,13 \; Mpa$$

For normal weight concrete the elastic modulus is given by ACI 318-14 Concrete (2014) by the following formula:

$$E_c = 57000(f'_c)^{\frac{1}{2}} \; (in \; psi)$$

This relation can be simplified into MPa in SI units:

$$E_c = 4700(f'_c)^{\frac{1}{2}} \; (in \; MPa) = 4700(59,84)^{\frac{1}{2}} = 36357,47 \; MPa$$

Following the D.M. 14 Gennaio 2008, the formula for the Elastic modulus is

$$E_c = 22000\left(\frac{(f'_c + 8)}{10}\right)^{0,3} = 22000\left(\frac{(59,84 + 8)}{10}\right)^{0,3} = 39072,25 \; MPa$$

Finally, for the concrete, the shear modulus is given by the following relation:

$$G = \frac{E}{2(1 + v)}$$

Where v is the Poisson's ratio, usually equal to 0,2 and E is the elastic modulus.

$$G = \frac{39072,25}{2(1 + 0,2)} = 16280,1 \; MPa$$

In the following Figure 2.12, the strength curve of a typical concrete is shown:
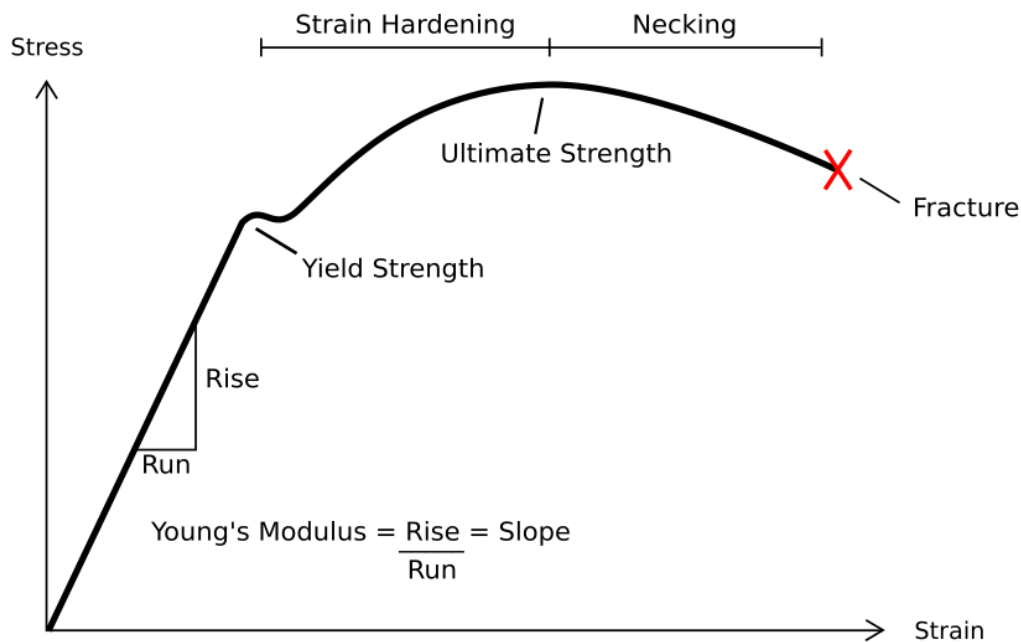
Figure 2.12 – Concrete strength curve

In addition, during the casting of the concrete, the Abrams Cone Slump Test was performed, following the guidelines provided from the ASTM C143-12. The concrete slump test is an empirical test that measures workability of fresh concrete. In fact, this test is performed to check the consistency of freshly made concrete. Consistency refers to the ease with which concrete flows. It is used to indicate the degree of wetness.

48

Consistency affects workability of concrete. That is, wetter mixes are more workable than drier mixes, but concrete of the same consistency may vary in workability. The test is also used to determine consistency between individual batches. (Wikipedia)

The ASTM C143-12 attests that for this test the slumps range should be from 2 to 8 inches to have a good workability of the fresh concrete. As shown in Figure 2.13, the obtained slump of the provided concrete was about 6 inches, which is clearly in this accepted range.

Figure 2.13 - Abrams Cone Slump Test

2.2.1.1 Concrete blocks

The blocks size was decided taking into account the diameter of the steel support that was about 14 inches, in order to have the FRP sheet in tension perfectly aligned during the test. While for the first test the blocks size was 8'' X 10'' X 14'', for the second test it has been preferred blocks sizes of 10'' X 10'' X 14'' (see Figure 2.14), for two main reasons. Firstly, paying attention at the result obtained from the first test run, it has been noticed that 8'' was a too restrictive side, in other words, it was practically difficult to grind the concrete on the sides where the anchors should have been positioned later. Secondly, increasing the resistant section of the concrete, this was able to withstand more to the tensile stresses imposed during the test.
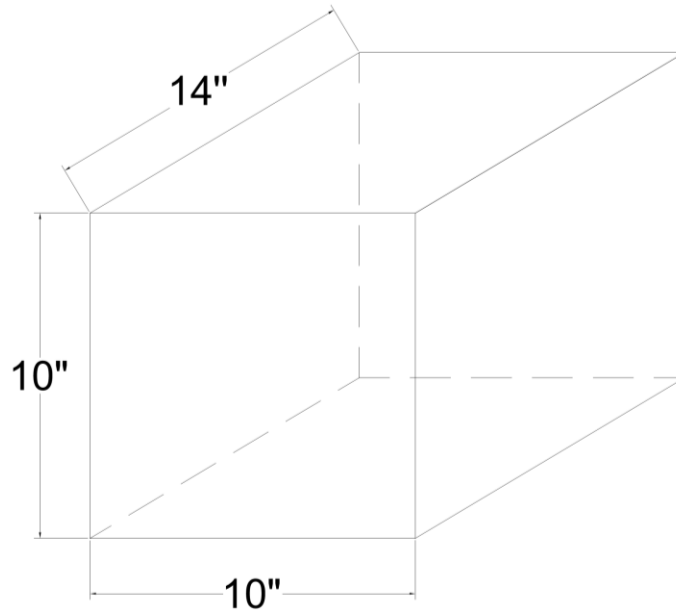
Figure 2.14 – Concrete block sizes for the test 2

From the chosen concrete section, it is possible to calculate the operative tensile strength of the concrete as:

$$f'_t = 0,7 \ \frac{0,27(f'_c)^{2/3}}{1,5} = 0,7 \ \frac{0,27(59,84)^{2/3}}{1,5} = 1,93 \ MPa$$

Being 0,70 and 1,50 two concrete corrective factors.

The section of the concrete used for the main test of this research (test 2) is:

$$A = 10 \ in \ \cdot 10 \ in = \ 254 \ mm \ \cdot \ 254 \ mm \ = 64,516 \ mm^2$$

Finally, it is possible to calculate the theoretical maximum peak load (applied by the hydraulic jack) that these concrete blocks can support, for the specific test case:

$$P_{max,th} = \frac{f'_t}{1000} \ [KPa] \cdot A = \frac{1,93}{1000} \cdot 64,516 = 124,36 \ KN$$

2.2.2 CFRP properties

The CFRP material used to bond FRP materials to the test specimens, according to specifications from the manufacturer, was V-Wrap C200 H. Generally, CFRP materials are famous for their high stiffer and great strength. The Figure 2.15 presents a stress-strain curve, with the data of the V-Wrap C200 H material plotted as the blue curve. Clearly, carbon fiber material present a brittle behavior with a very high ultimate strength, while by way of comparison, in the same figure is also plotted in violet the typical behavior of a ductile material: steel (type AISI 1020 HR).
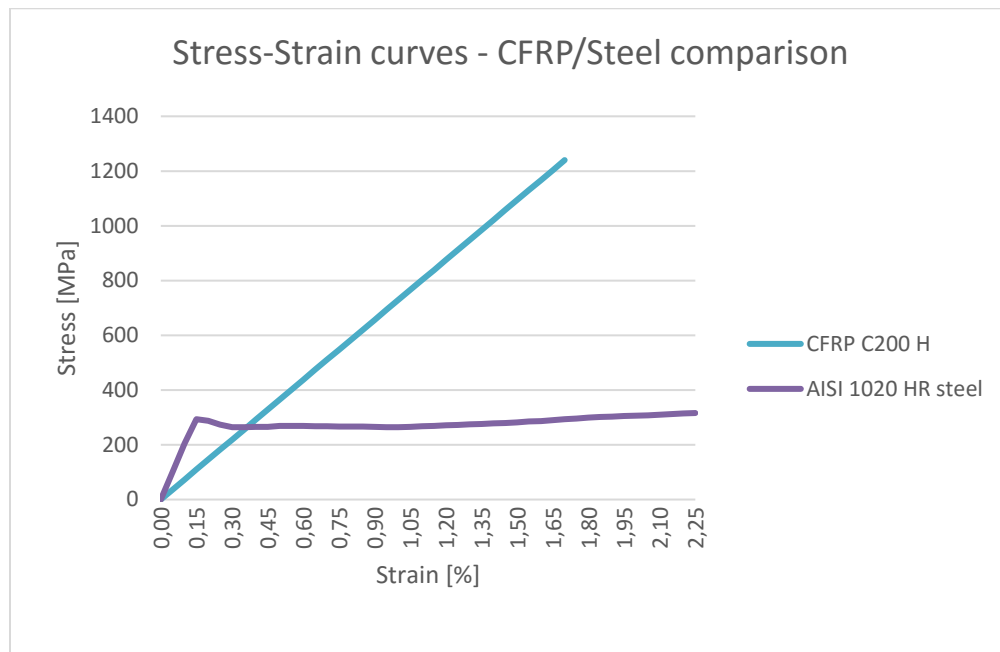
Figure 2.15 - Stress-Strain curves - CFRP/Steel comparison

The V-Wrap C200 H CFRP sheet, used in this research, has the following properties:

Dry fibers

- ➤ Average thickness: 1.016 mm
- ➤ Average ultimate strain: 1.7 %
- ➤ Modulus of elasticity: 73.77 GPa
- ➤ Ultimate strength: 1240 MPa

Wet fibers

- ➤ Average thickness: 1.016 mm
- ➤ Average ultimate strain: 1.8 %
- ➤ Modulus of elasticity: 74.59 GPa
- ➤ Ultimate strength: 1339,4 MPa

The properties reached with the wet fibers refer to the case in which the fibers of the C200 H CFRP material are impregnated with the epoxy resin (V-Wrap 770 epoxy resin).

It is important to underline that the materials are one directional and, in both cases of dry and wet configuration, it has very small tensile capacity in the transverse fiber direction.
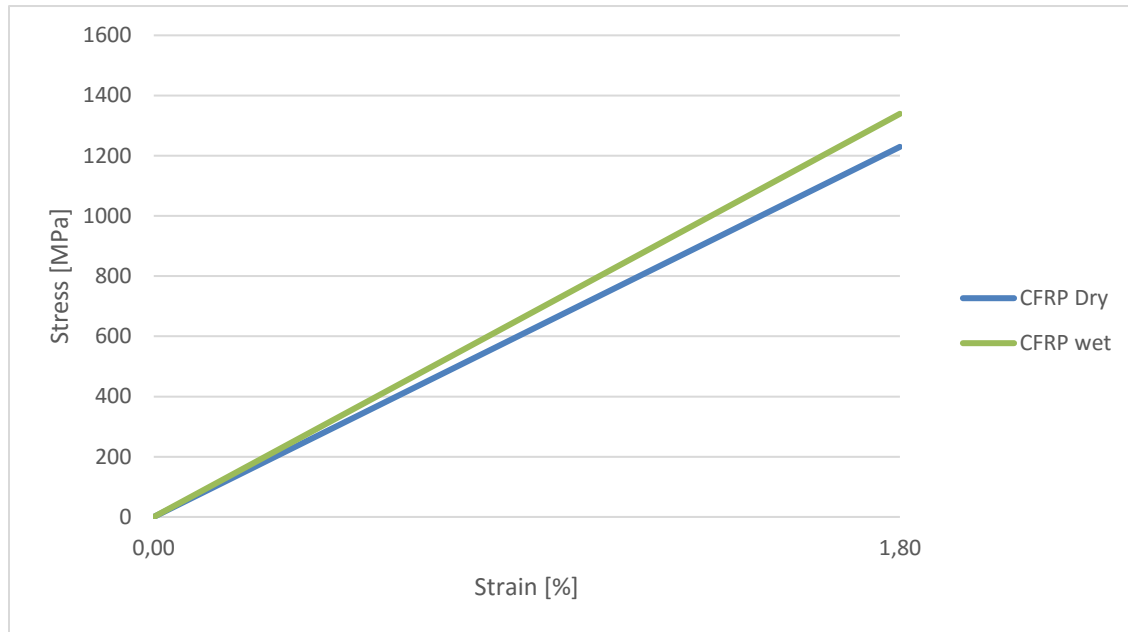
Figure 2.16 - Stress-Strain curves - CFRP Dry/Wet

The Figure 2.16 shows the difference in terms of stress-strain between the dry and wet fibers configuration. The wet configuration presents firstly higher values of ultimate strength and modulus of elasticity. Also, the wet fibers avoid intensifications or different stresses distribution along the CFRP sheet.

2.2.3 Epoxy resin

The history of the chemistry of epoxy dates back to early 1900's, while commercialization attempts began in late 1930's. The first commercial products (epoxy adhesives and casting resins) of epoxy resin was in the coating field, due to its high resistance to chemicals, durability, and toughness. Later, epoxy started to be used to encapsulate electrical and electronic component, due to its high resistance to chemicals and outstanding adhesion, durability and toughness. Nowadays epoxy resins can be used as a strong adhesive in metal and construction material; they are strong enough to be used in place of rivets and welds in certain applications. Also, the epoxy resins are useful for encapsulating electrical and electronic devices, thanks to the high electrical resistance, durability at high and low temperatures, and ease with which they can be poured or cast without forming bubbles. Currently, this material has been used in industrial tooling applications to produce molds, master models, laminates, casting, fixtures, and other industrial production aids. This "plastic tooling" replaces metal, wood, and other traditional materials improving the efficiency.

It is interesting how over 20% of global epoxy resin production goes into the applications of fiber-reinforced composites. In fact, one of the main advantages of epoxy resins is that they have excellent adhesion to a broad range of substrates and reinforcements.

Generally, epoxy resins are low molecular weight prepolymers that can be characterized by the presence of one or more epoxy (oxirane) groups per molecule. The epoxy group ring contains two carbon atoms and one oxygen atom. The generalized structure of an epoxy resin is given in Figure 2.17.
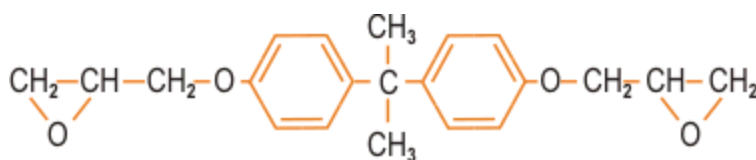
Figure 2.17 - Chemical structure of a typical epoxy

Epoxies are different from polyester resins since they are cured by a 'hardener' rather than a catalyst. The hardener, often an amine, is added in order to cure the epoxy. Both the materials take place in the chemical reaction. The chemistry of this reaction means that there are usually two epoxy sites binding to each amine site. This forms a complex three-dimensional molecular structure.

In order to have a complete reaction it is important to pay attention to the mixing ratio; if amine and epoxy are not mixed together in the correct ratio, unreacted epoxy or

hardener will remain inside the matrix. This affects the final properties of the material after the curing period. That is why every company that produces epoxy resins provides the precise mixing ratio (by weight or by volume).

For this research, two epoxy resins were used:

The epoxy resin used to apply the CFRP sheet on the concrete surface was the V-Wrap 770 Epoxy Adhesive (a liquid epoxy), while the one used to apply the anchors over the CFRP sheet into the concrete holes was the Fortress 4000 Hi-Temp Toughened Structural Adhesive (a more dense epoxy).

V-Wrap 770 Epoxy Adhesive
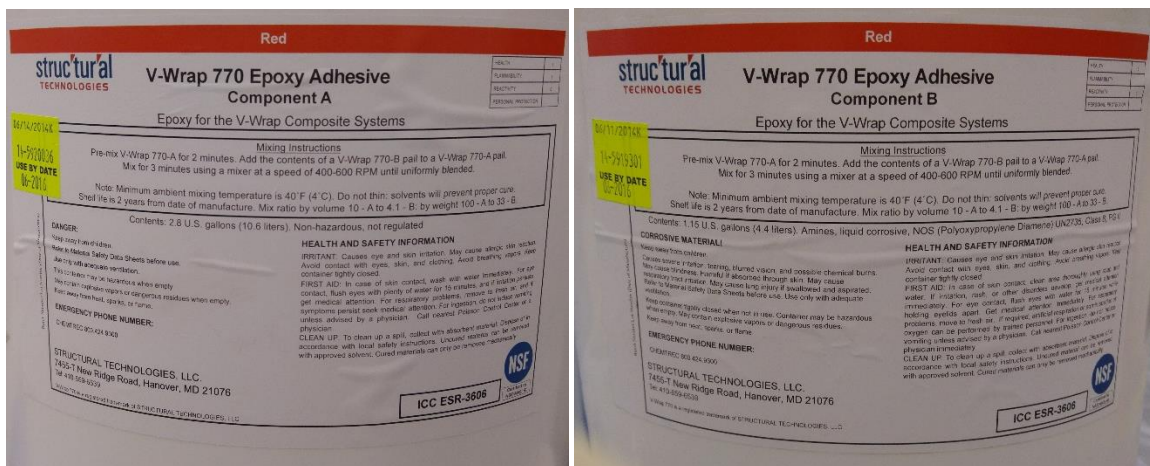
Figure 2.18 - V-Wrap 770 Epoxy properties

As shown in Figure 2.18, V-Wrap 770 is a two-part epoxy for high strength composite bonding applications. V-Wrap 770 matrix material is combined with V-Wrap carbon and glass fabrics to provide a wet-layup composite for strengthening of structural members. It is formulated to provide high elongation to optimize properties of the V-Wrap composite systems. It provides a quite long working time for application, with no offensive odor. V-Wrap 770 may be thickened with fumed silica to produce a tack coat/putty or a finishing coat, added to thicken the resin. The maximum ratio by volume is 1.5 of fumed silica to 1 part of resin. This epoxy has an approximate "open time" of 45 minutes. The "open time" is the portion of the cure time, after mixing, that the resin/hardener mixture remains a liquid and is still workable and suitable for the application.

Tensile Strength (ASTM D638):	8,800psi (60.7 MPa)
Tensile Modulus (ASTM D638):	400,000 psi (2,760 MPa)
Elongation at Break (ASTM D638):	4.4%
Flexural Strength (ASTM D790):	13,780 psi (95 MPa)
Flexural Modulus (ASTM D790):	380,000 psi (2,620 MPa)
Compressive Strength (ASTM D695):	12,450 psi (85.8 MPa)
Compressive Modulus (ASTM D695):	387,000 psi (2,670 MPa)
Tg (ASTM D4065):	180°F (82°C)
Density:	
Mixed Product	9.17 lbs/gal (1.11 kg/L)
Part A	9.7 lbs/gal (1.16 kg/L)
Part B	7.9 lbs/gal (0.95 kg/L)
VOC Content (ASTM D2369):	0% VOC

The curing period time of the V-Wrap 770 is about 4 days at ambient temperature.

Fortress Epoxy

Fortress 4000 is a toughened, high temperature use structural epoxy adhesive designed for the bonding of carbon or glass fibers to itself and many dissimilar materials. It is a two-phase (toughened) epoxy resin produced using an elastomer with a flexible epoxy resin backbone for maximum stress and fatigue resistance. 4000 bonds with an immediate high tack consistency, and offers a quick cure when used at ambient temperatures ranging from 60˚F (15˚C) to 95˚F (35˚C). The working life at 77˚F (25˚C) is 60 minutes (working time increases with lower ambient temperatures), with full cures occurring between 12 – 14 hours depending on cure temperature. The heat deflection temperature of Fortress 4000 is around105º C (220°F). The material mixes at 100:35 by weight (resin to hardener). The convenient color-coded components form a uniform color when properly mixed.

Fortress 4000 is highly recommended as a "tack coat" for applying epoxy resin saturated reinforcement materials to a vertical and overhead substrate such as concrete, or steel in the areas of seismic retrofit and structural upgrades.

Recommended curing of fortress 4000 adhesive:

• Gel at ambient + 8 hours at 50ºC

• Gel at ambient + 6 hours at 70ºC

• Gel at ambient + 7 days at ambient

Fortress Material	4000 Resin	w/4000 Hardener
Density at 25°C	1.1 – 1.2 g/cm³ (9.7 – 9.8 lbs)	1.03 – 1.04 g/cm³ (8.65 – 8.75 lbs)
Viscosity	Thixotropic Gel	Thixotropic Gel
Color	Yellow	Blue
Color Mixed	-	Green
Mix Ratio by Weight	100	35
Working Life, 1000 grams at 77°F	-	55 – 60 minutes
Initial Cure Time	-	6 – 8 hours
Shore D Hardness	-	87
Heat Deflection Temperature	-	105°C (220°F)
Tensile Lap-Shear (DIN EN 1465)	-	10.5 MPa
Peeling Resistance (DIN 53282)	-	2.3 N/mm (minimum)

N.B: Because of the longer curing period of 7 days at an ambient temperature of the Fortress 4000, the specimens were tested after a week from the FRP sheet and anchors' installation.

Figure 2.19 - Fortress™ 4000 resin epoxy in action

Figure 2.19 shows the Fortress 4000 epoxy provided with the specific epoxy gun working with compressed air.

2.3 FABRICATION OF THE SPECIMENS

2.3.1 Concrete sandblasting

It is widely accepted that surface roughness influences bond capacity, increasing the bond once the FRP is applied on the concrete. Although most design guidelines include qualitative recommendations on surface preparation, these recommendations are rather vague. For example, ACI 440, TR 55 and CNR-DT 200 recommend the preparation of concrete surface by grinding to ensure a certain roughness degree. However, the guidelines provide no clear indication of the effect of surface roughness on bond capacity. Also, the removing the smoothness concrete paste helps to recreate an old concrete surface (usually the sandblast is required for old concretes to renew it). Figure 2.20 shows the operation of sandblasting, while Figure 2.21 shows all the specimens sandblasted and ready for the next operation: the anchors hole drilling.

Figure 2.20 - Operation of sandblasting

Figure 2.21 – Specimens sandblasted

The most effective reference tool for determining concrete surface profiles is the molded rubber comparator chips, available from the International Concrete Repair Institute (ICRI). These samples replicate ten grades of surface roughness and are designed for direct visual and tactile comparison to the concrete surface in question.

There is no definitive text description for the ten grades: the comparator is the standard. However, ICRI does tell us how much surface profile is sufficient for various types of coatings and overlays. For the specific case of this research, after the surfaces were grinded, the specimens were visually inspected and compared with the benchmark guidelines for the concrete surface profile (CSP) developed by the International Concrete Repair Institute. It was found a CSP level equal to 3 (Fig. 2.22).
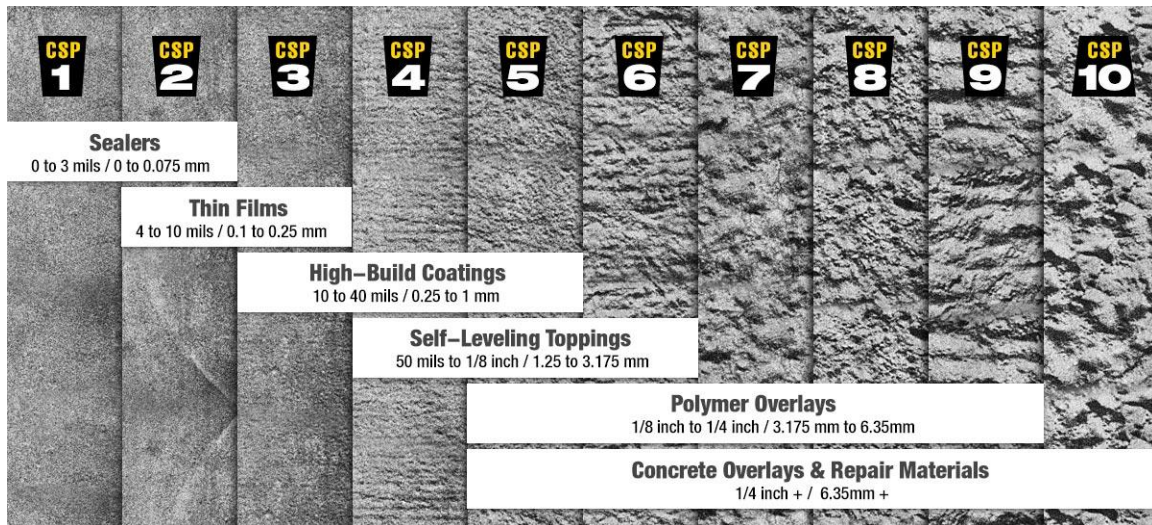
Figure 2.22 – Grades of surface roughness, ICRI

2.3.2 Surface and anchors' hole preparation

For the first test, 14 specimens were prepared, while for the second the specimens to prepare were 20. The preparation of those took place in different time, but the procedure adopted was the same. For the first test run the dimensions of the specimens were 356 mm x 305 mm x 203 mm (14"x 12"x 8"), while for the test 2 the dimensions of the samples were 356 mm x 254 mm x 254 mm (14"x 10"x 10").

Firstly, the surface on the external edge, in which the FRP sheet will be installed, was rounded with a grinder, in order to avoid the problem of spalling and a sudden load reduction on the FRP sheet during testing (Brena and McGuirk, 2013). After the grinding, the specimens were dived for the category of anchor installed.

- Each specimen that would have a flat staple anchored was drilled in the center of the upper surface using a special grinder with a blade of the same diameter of the rounded part of the anchor legs.

Figure 2.23 - Special grinder for the flat staples

The Figure 2.23 shows the specific grinder used for drill the striped holes in the blocks.

Figure 2.24 – Specimens grinded

In Figure 2.24 we can see the blocks grinded. After this procedure, the dust was blown up from the striped holes using an air compressor to clean perfectly the inside where the anchors will be inserted.

Finally, a duct tape (along with a length of 3 inches) was installed on the external edge already grinded, in order to avoid bonding between the FRP sheet and the concrete surface.

- Each specimen with a round staple anchored, instead, was drilled by the sides of the upper surface of the specimens using a Hilti hammer driller. The exact positions of the holes for the round staples in shown in the following Figure 2.25 (marked as red circles).
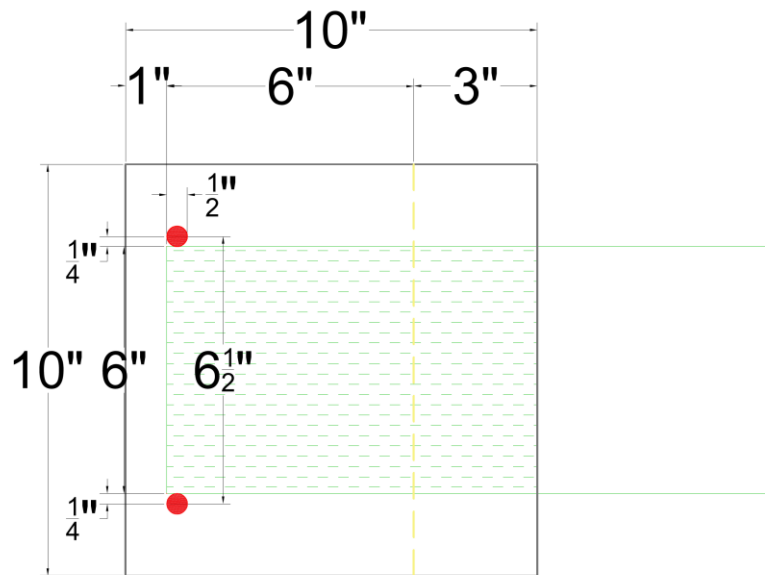
Figure 2.25 – Holes position for the round staples specimens

Again, the dust was blown up from the holes and the duct tape was installed on the external edges.

2.4 CFRP PREPARATION

2.4.1 Dry and Wet CFRP Installation

Once test specimens have been prepared for FRP bonding, CFRP sheets, and CFRP anchors were prepared for installation. CFRP sheets were cut from V-Wrap C200 H material to the dimensions listed below.

Quantity and dimensions of FRP materials:

1. CFRP flexural sheet: 1 per specimen

    - 100 in. X 6 in. - For the flat staple anchors.
    - 112 in. X 6 in. For the round staple anchors.

2. CFRP sandwich: 1 per specimen

    - 6 in. x 6 in. - for the flat staple anchors.
    - 18 in. x 6 in. for the round staple anchors.

Note: The length of the FRP sheet (and also the dimensions of the eps foam blocks) was computed based on the dimensions of the hydraulic jack, of the load cell and of the plates used to perform the test

Anchor patches (called generally "sandwiches") are installed above the anchor and usually allow better force transfer from the CFRP sheet to the anchor, improving the resistance of the system on the side in which they are installed. This patch is oriented with fibers in the same direction of the fibers of the flexural sheet.

2.4.1.1 Installation Procedure

2.4.1.1.1 Specimen substrate cleaning

In order to allow a good bonding between the FRP sheet and the concrete surface, the latter had to be cleaned. In order to do that, an air compressor and a brush were used to remove all the particle of sand resulting from the sandblasting.

2.4.1.1.2 Primer application

Below the procedure to obtain the primer that was applied on the concrete surface in order to bond the CFRP strengthening system is explained. First of all, the epoxy resin (part A) and the curing agent (part B) were mixed together with the mixing ratio reported in the manufacturer's instructions of 100:33 by weight. The two parts were completely

mixed together until a smooth, uniform streak-free consistency was reached (see Figure 2.26). Then, fume silica was added to the bucket in order to make the epoxy thicker. The fumed silica was added as a mixing ratio by volume of 1:1 to the primer (see Figure 2.27). Again, once a uniform consistency was obtained, the thickened epoxy (the primer mixed with the fumed silica) was applied using a spatula, in order to fill all the concrete cavities and little holes.

Figure 2.26 – Mixing of the epoxy resin with the curing agent

Figure 2.27 – Mixing of the primer and the fumed silica

2.4.1.2 FRP impregnation and application – Dry FRP_Old installation

The FRP sheet was disposed over a previously cover clean table and only 6 in. of fibers were impregnated at each end, while the remaining part was kept dry. In this way, only

the 6-inches fibers at the ends were rolled, in order to obtain a uniform impregnation. The lamina was applied to the concrete substrate within 45 minutes from the primer application and the fiber impregnation. It is important to underline that it took 45 minutes because this is the "open time" (also called working time or wet lay-up time) and it is the portion of the cure time, after mixing, that the resin/hardener mixture remains a liquid and is still workable and suitable for the application.

Then, the fibers were laid down on the concrete surface and then rolled again to avoid the formation of air bubbles in between the FRP sheet and the substrate. Some tape was applied over the sheet in the unbounded part in order to keep it straight and avoid any movement during the curing period. The exact position of the FRP sheet was beforehand marked with a marker, in order to be precise during the installation.

After the installation of the FRP sheets, the specimens were left to cure in the laboratory at room temperature of 23 ± 1 °C and relative humidity of 60 ± 5 % for some hours.

2.4.1.3 FRP impregnation and application – Wet FRP New installation using EPS foam shapes

For the wet installation, it has been developed the following working plan:

Firstly, 10 EPS (expanded polystyrene) foam shapes were assembled (see appendix for more details).

The dimensions of the EPS foam shapes were computed based on the dimensions of the steel support, of the hydraulic jack, of the load cell and of the plates used to perform the test.

Figure 2.28 – Installation of a Mylar sheet over the EPS foam shapes

The EPS foam shape was previously covered with a Mylar sheet of dimensions 8 in. x 106 in (Figure 2.28), in order to prevent the adhesion of the impregnated lamina on the EPS shape surface, during the curing period. The EPS shape was also taped on the concrete block in order to prevent them from any movement and keep the FRP impregnated in perfect position during the same curing period

It is important that the mylar sheet can extend over the concrete surface, covering in this way the 3 in. of the unbonded part, already marked and taped with an adhesive tape.

Then, in order to apply the FRP, again they were disposed over a previously cover clean table and they were impregnated for their entire length.

Figure 2.29 – Impregnation of the fibers

The Figure 2.29 shows the impregnation process of the fibers.

After that, each lamina was carefully placed on the EPS foam shape and rolled all over the EPS shape surface and the concrete substrate at the ends, to avoid the formation of air bubbles along with all the entire length.

The lamina was applied to the concrete substrate within the same "open time" of 45 minutes from the primer application and the fiber impregnation.
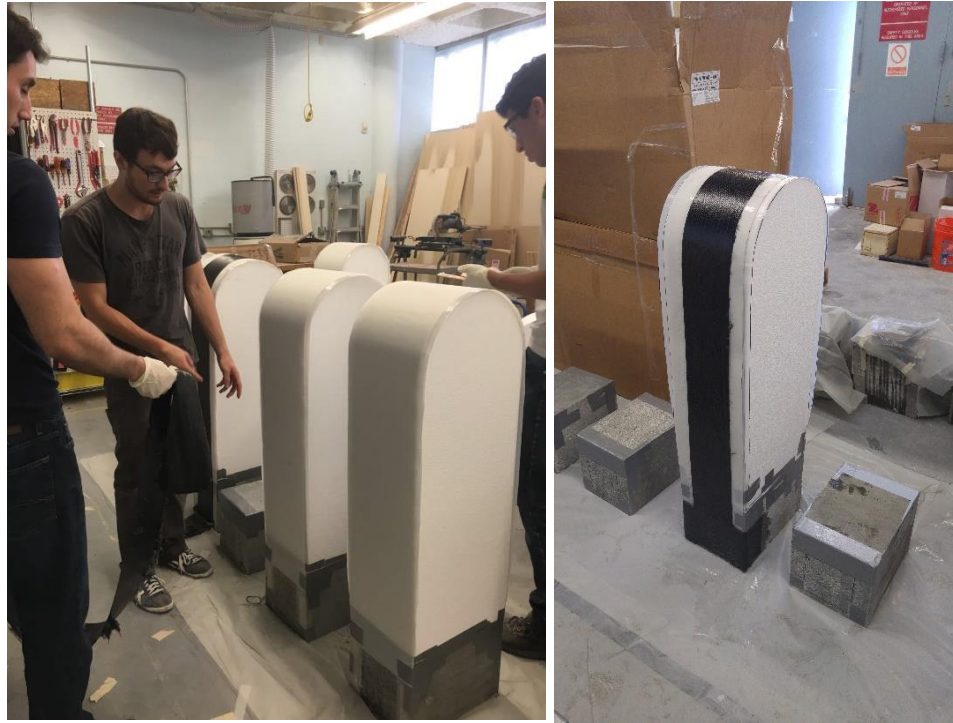
Figure 2.30 – Application of the impregnated fibers on the specimens (on the left) and final product of a benchmark (on the right)

The Figure 2.30 shows the application of the impregnated fibers on the specimens (on the left) and final product of a benchmark (on the right).

Note: the length of the bonded FRP sheet was computed based on the expression of the Optimal Bond Length, which is the minimum bonded length that ensures the transmission of the bonding forces (CNR-DT200). For the tests, a bonded length greater that the optimal one was taken. The computation of the optimal bond length is shown in chapter 2.1.1

Test 1 was performed using the old installation with the dry FRP, while test 2 was performed using the new installation with the wet FRP.

2.4.2 Anchors' installation

2.4.2.1 Flat Staple

An anchor was installed on both sides of the specimens. The length of the bonded FRP sheet was the same as in the benchmark (100 in.), in order to be able to compare the results and compute the enhance. The procedure of installation was the following:

Once the impregnated CFRP sheet was positioned, the pre-mixed epoxy was poured into the stripe holes with a specific epoxy gun, designed for this work.

Figure 2.31 – Installation of the staple anchors, with the proper epoxy gun

With the same technique, an epoxy layer was poured also on the legs and on the under part of the anchor, on the surface into direct contact with the FRP lamina. After that, the anchor was inserted and squeezed into the stripe holes, on the exact position previously marked laterally on the concrete.

The picture in Figure 2.31 shows the use of the epoxy gun to fill the stripe holes.

2.4.2.2 Round Staple

The anchors were installed on both sides of the specimens, following the procedure used for the flat staple anchors . In this case, the length of the bonded FRP sheet was 112 in., because of the operating principle of this type of anchor. In fact, on both sides, the ends of the FRP lamina were wrapped around the anchors and the 12 remaining inches (on both sides) were used to cover the entire bond length of 6 in. per side.

Figure 2.32 – Round staple installation

The picture in Figure 2.32 illustrates the operation of inserting the round staple anchor on the holes, leaving other 6 in. of FRP lamina to wrap around the anchor in order to cover the bond length.

Also for this case, an epoxy layer was poured into the holes, on the legs and on the under part of the round staple anchor

Figure 2.33 – Double round staple configuration

Figure 2.33 presents a specimen equipped with the double round staple configuration, in which, at the very end, the anchor is covered by the lamina wrapped around, while at 3 inches from it, another round staple in installed.

2.5 Dry and Wet CFRP Differences

Since, there is a need for a standardized bond test that is reliable, repeatable, easy to perform and able to represent the stress state that is observed in the real field applications in the best possible way, researchers are still nowadays focusing on find a proper shear test that can represent the real stress state observed in the real field.

Installing the specimens with the EPS foam shape, in the wet FRP configuration, guarantees two main factors:

1. Firstly, it represents exactly the real application when the system acts in situ. An interrupted strip of wet CFRP acts as a continuum system.
2. Also, impregnating the carbon fibers with a resin epoxy allows the latter to behave as a matrix, which means to keep the fibers straight, transferring the stresses to them, avoiding intensifications or different stresses distribution along all the CFRP strip.

In addition, the V-Wrap C200 H CFRP sheet reaches better material properties as previously shown in the chapter 2.2.2, in terms of ultimate strength and modulus of elasticity, when impregnated.

2.5 TESTING

2.5.1 Instrumentation

The strain gauges (abbreviated SG) are used to read the transversal strain distribution in the FRP sheet. Depending on the type of anchor provided on each specimen, they can give interesting parameters of what is happening in terms of internal forces in front and behind the anchor.
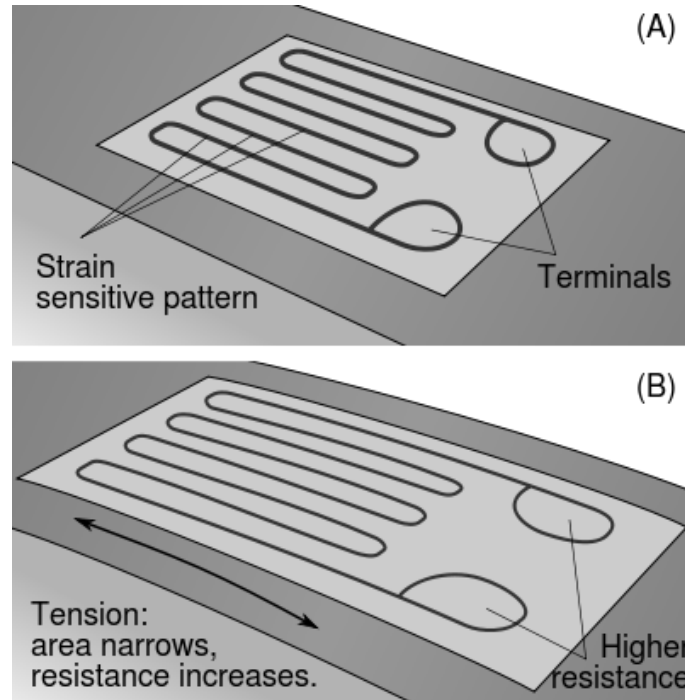
Figure 2.34 - Stain gauges

The gauge (Figure 2.34) is attached to the specimens thanks to a suitable adhesive and as the CFRP sheet is deformed, the foil is deformed, causing its electrical resistance to change. This resistance change is then related to the strain by the quantity known as the gauge factor. All those information (electrical resistance, gauge factor, and gauge length) are carefully updated each time in the data acquisition system, which records the strains.

Electrical strain gauges of 6 mm length were used to instrument the specimens. They were placed on the surface of the FRP sheets, as the following sketch in Figure 2.35.
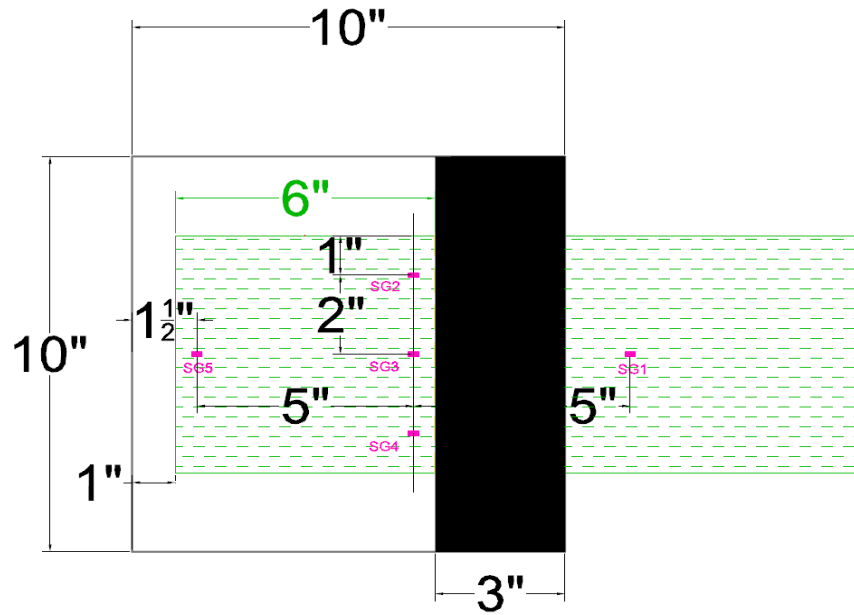
Figure 2.35 – Strain gauges' positions on the specimens

The position of the strain gauges was decided depending on different parameters. Firstly, it is interesting to read the transverse strains (perpendicular to the fibers direction of the FRP sheet). For this reason, the SG2, SG3, and SG4 are positioned with a distance of 2 inches between each other (with a margin of 1 inch for the lateral ones, SG2 and SG4). In this way, it is possible to understand for each specimen if the applied load is centered.

Then, another series of three SG, identified as the SG1, SG3 and SG5 are fundamental to read the parallel strains. In fact, positioned in the centerline, those SG are located 5 inches of distance between each other, able to read three main different positions.

SG1 is positioned on the unbonded part; SG3 is positioned just before the anchor, while the SG5 is installed behind the anchor.

For all the specimens the SG were placed in the same position, while in some of them no SG were placed, and in some others, some SG were dismissed. For better understand the reason and the interpretation of the strains' results check the test results' chapter n. 4.

2.5.2 Test set-up

In the double shear test performed, the debonding force over the instrumented side of the block was evaluated as half of the applied peak load P. The following figures (Figure 2.36 and Figure 2.37) illustrates the approximated distribution of the loads in this test and the final set up of the test.
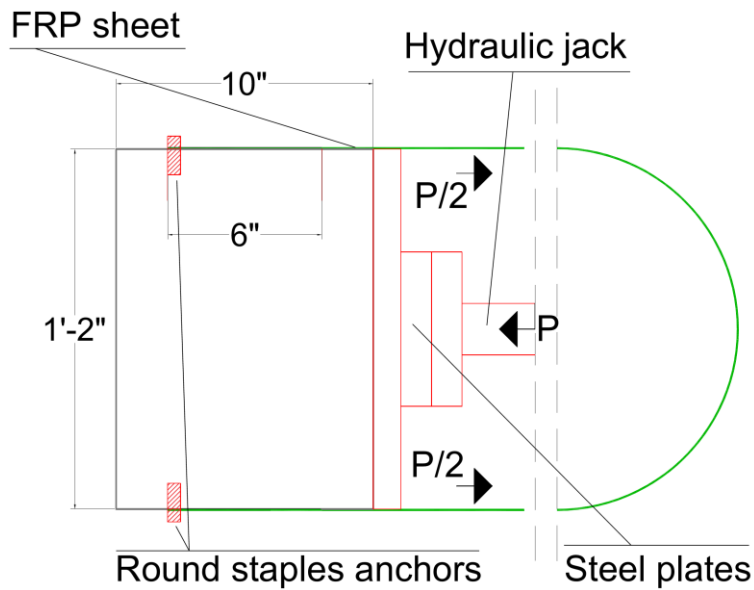
Figure 2.36 – Distribution of the loads in the double shear test performed
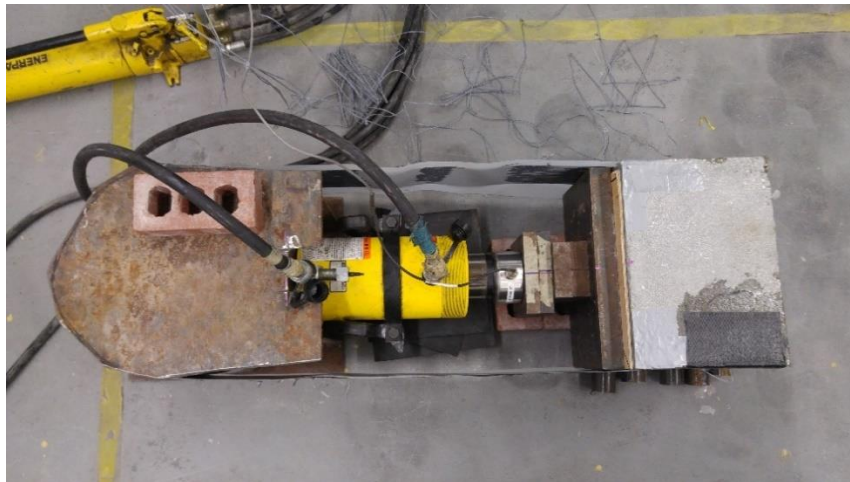
Figure 2.37 – Set up of test 2

The double shear test was performed with the following test set-up procedure:

Firstly, the instrumentation (SG and Load Cell) were connected to the DAQ. After that, they were both calibrated as the following:

- Strain gauges info: 5mm length, 120 ± 0.5 Ω resistance, 2.11% gauge factor.
- Load cell info: up to 50 kips (= 222 KN) of applied load.

The DAQ started recording the data from the very begging of the applied load, that was increased by load control at a rate of 0.3-0.4 KN/s. The load was then applied until the failure of the system occurred.

Figure 2.38 - Setting up of the test – positioning of the steel plates and setting up of the hydraulic jack

3. TEST RESULTS

The specimens were tested to examine the performance of the two types of anchors, the flat staple, and the round staple anchors, in order to understand the improvements in terms of distribution of strains, stresses, peak loads and efficiencies given by installing a certain type of anchor. This chapter is divided into three main sections according to the main studies developed in this research.

The first section presents a full analysis of the results obtained from the flat staple anchorage system. Also, this section will compare the results given by a previous testing method used for the double shear test, in which the unbonded part of the CFRP wrapped around the steel support is dry.

The second section is dedicated to the results deduced from testing the round staple anchorage system. Here the test was conducted only with the new installation methodology (wet CFRP). In fact, after initial testing using the new installation (wet CFRP), this methodology revealed a significant success, which brought to test the following specimens (the round staples) only through this new installation.

The third section is a description of the failure modes observed in each single test.

3.1 FLAT STAPLES

As already described in the previous chapters, two different tests' series were run for the flat staples anchorage type.

3.1.1 Test 1 – Dry CRFP testing

The results from the test 1 refer to the results get from the dry CFRP configuration. In this first test 14 specimens were tested as:

- N° 2 benchmarks
- N° 3 3W_2D configuration (it states for 3 inches width and 2 inches depth)
- N° 3 3W_1D configuration
- N° 3 1,5W_2D configuration
- N° 3 1,5W_1D configuration

N.B: the W as capital letter means width, and the D as a capital letter refers to the depth of the anchor (in this way, for example, the "3W_2D configuration" it states for a 3 inches width and 2 inches depth anchor type. From now on, only this technical nomenclature will be used.

The following table (Table 3.1) summarizes the results in terms of peak loads, increases of the load (in percentage) with respect to the benchmark, rupture side, measured strains in the CFRP sheet and failure modes. The Peak Load P represents the maximum load applied by the hydraulic jack during the tests.

Table 3.1 - Summary test 1

Shear test n.1 (DRY CFRP)

	Specimen ID	Anchor's dimensions	P [KN]	P/2 [KN]	Increase in Peak Load [%]	Rupture Side	Rupture Type	Strains in percentage at peak load				
								SG1 [%]	SG2 [%]	SG3 [%]	SG4 [%]	SG5 [%]
BENCHMARKS	T1_BM_001	No anchor	45,80	22,90	34,53%		G	0,610	0,374	0,382	0,399	0,001
	T1_BM_002	No anchor	22,29	11,15	-34,53%		G	0,000	0,000	0,000	0,000	0,000
	Average		34,05	17,02	**0,00%**			0,000	0,000	0,000	0,000	0,000
	Standard deviation		11,76	5,88								
	C.V. [%]		34,53	34,53								
	T1_FS_3W_2D_001	3"W - 2"D	32,33	16,16	-5,06%	Left (instrumented side)	G	0,662	0,274	0,422	0,402	0,002
	T1_FS_3W_2D_002	3"W - 2"D	88,04	44,02	158,57%	Left (instrumented side)	G/C	1,007	0,722	0,684	0,670	0,006
	T1_FS_3W_2D_003	3"W - 2"D	61,16	30,58	79,62%	Left (instrumented side)	G					
	Average		60,51	30,25	**158,57%**			0,835	0,498	0,553	0,536	0,004
	Standard deviation		22,75	11,37								
	C.V. [%]		37,60	37,60								
	T1_FS_3W_1D_001	3"W - 1"D	67,11	33,56	97,11%	Left (instrumented side)	G	0,837	0,272	0,667	0,657	0,001
	T1_FS_3W_1D_002	3"W - 1"D	83,55	41,78	145,40%	Left (instrumented side)	G/C	0,815	0,498	0,464	0,170	0,003
	T1_FS_3W_1D_003	3"W - 1"D	67,31	33,65	97,68%	Right (not instrumented side)	G	0,815	0,373	0,620	0,448	0,000
	Average		72,66	36,33	**145,40%**			0,823	0,381	0,584	0,425	0,001
	Standard deviation		7,71	3,85								
	C.V. [%]		10,60	10,60								
FLAT STAPLES	T1_FS_1,5W_2D_001	1,5"W - 2"D	61,60	30,80	80,91%	Right (not instrumented side)	G	0,782	0,206	0,320	0,605	0,003
	T1_FS_1,5W_2D_002	1,5"W - 2"D	34,25	17,12	0,59%	Left (instrumented side)	G					
	T1_FS_1,5W_2D_003	1,5"W - 2"D	86,35	43,18	153,62%	Left (instrumented side)	G/C	0,880	0,529	0,268	0,315	0,004
	Average		60,73	30,37	**153,62%**			0,831	0,367	0,294	0,460	0,004
	Standard deviation		21,28	10,64								
	C.V. [%]		35,04	35,04								
	T1_FS_1,5W_1D_001	1,5"W - 1"D	59,67	29,83	75,25%	Right (not instrumented side)	G	0,853	1,314	0,594	0,463	0,003
	T1_FS_1,5W_1D_002	1,5"W - 1"D	86,41	43,20	153,78%	Left (instrumented side)	G/C	0,788	0,513	0,377	0,893	0,014
	T1_FS_1,5W_1D_003	1,5"W - 1"D	64,89	32,44	90,57%	Right (not instrumented side)	G	1,014	0,6365	0,4983	0,6522	0,000
	Average		70,32	35,16	**153,78%**			0,885	0,821	0,490	0,669	0,006
	Standard deviation		11,57	5,79								
	C.V. [%]		16,46	16,46								

It is very important to remind that, for all the tests run for this research, the side without strain gauges was strengthened with another FRP sheet over the anchor, covering in this way all the bonded area, in order to make each specimen fail on the other side provided with the instrumentation of the strain gauges. For this reason, in table 3.1, there is also a column "rupture side" which explain if the rupture occurred on the expected left side (the instrumented one) or on the reinforced side (on the right side, the one not instrumented). From this table, we can also easily understand that most of the test were useless. That is because the rupture did not occur on the bonded part, where the anchor was installed, but on the dry CFRP, outside the bond area at a relatively low-stress level compared with the tensile strength of the CFRP itself. This might be caused by four main reasons:

- Different stresses distribution on the dry CFRP, caused by the not perfectly centered applied load, that brought to a rip in the most stressed fiber, causing the cracking start. It is important to remind that in the dry CFRP, as soon as a little crack occur, this immediately propagate toward the closest dry fibers, leading to the crack of the entire CFRP sheet.
- The unevenness of adhesive on CFRP sheet out of the bond area, leading to uneven stress distribution in the CFRP fibers.
- The application of the epoxy resin on CFRP sheet out of the bond area, leading again to uneven stress distribution in the CFRP fibers.
- The low unbounded area furnished on the concrete surface (only 1 inch), which could have caused again an uneven stress distribution in the CFRP fibers, just out of the bonded area where most of the ruptures occurred.

For all these reasons, the results of this first test are overall senseless. Only 4 specimens highlighted in green (table 3.1) failed as soon as the debonding initiated. Unfortunately, even if a correlation between different depths could have been obtained from those 4 specimens, that would not make any sense because of the very low peak load they reached if compared to the successful test 2. Also, by reading the strains, we can easily understand why the strain gauge number 1 was the most stressed since this is the strain located exactly where the rupture occurred. In this way, we will not get in the depth of this first test, but we will analyze the results of the second test, in which, thanks to the new installation provided, all the specimens succeeded, providing reasonable results and very interesting data analysis.

3.1.2 Test 2 – Wet CRFP testing

The results from the test 2 refer to the results obtained from the dry CFRP installing method. In this second and successful test, 12 specimens were tested as it follows:

- N° 3 benchmarks
- N° 3 3W_1D configuration (it states for 3 inches width and 2 inches depth)
- N° 3 2W_1D configuration
- N° 3 1W_1D configuration

The following table (Table 3.2) summarizes the results obtained from the test 2.

Table 3.2 - Summary test 2, flat staples

	Specimen ID	Anchor's dimensions	P/2 [KN]	Increase in Peak Load [%]	Rupture Side	Rupture Type	Strains in % at peak load					Increase in % of strains at the peak load				
							SG1 [%]	SG2 [%]	SG3 [%]	SG4 [%]	SG5 [%]	SG1 [%]	SG2 [%]	SG3 [%]	SG4 [%]	SG5 [%]
BENCHMARKS	T2_BM_001	No anchor	29,01	-19,68%	Left (instrum.side)	A	0,340	0,276	0,302	0,530	0,021	0,00%	-18,61%	-22,86%	9,16%	59,99%
	T2_BM_002	No anchor	37,88	4,91%	Right (not instrum. side)	A	x	0,402	0,482	0,441	0,005	x	18,61%	22,86%	-9,16%	-59,99%
	T2_BM_003	No anchor	41,45	14,77%	Right(not instrum. side)	A	x	x	x	x	x	x	x	x	x	x
	Average		36,11				0,340	0,339	0,392	0,485	0,013	0,00%	0,00%	0,00%	0,00%	0,00%
	Standard deviation		4,44	0,00%			0,000	0,063	0,090	0,044	0,008					
	C.V. [%]		12,29				0,000	0,186	22,863	9,164	59,988					
FLAT STAPLES	T2_FS_3W_001	3"W - 1"D	55,37	53,34%	Left (instrum. side)	C	0,196	0,134	0,524	1,298	0,411	-42,33%	-60,32%	33,61%	167,54%	3015,60%
	T2_FS_3W_002	3"W - 1"D	62,26	72,41%	Left (instrum. side)	F	0,459	0,148	0,481	0,729	0,038	34,93%	-56,43%	22,71%	50,25%	190,41%
	T2_FS_3W_003	3"W - 1"D	81,62	126,01%	Right (not instrum. side)	F	0,414	0,197	x	0,374	x	21,47%	-41,80%	x	-22,94%	x
	Average		66,42				0,356	0,160	0,502	0,800	0,225	4,69%	-52,85%	28,16%	64,95%	1603,00%
	Standard deviation		11,11	83,92%												
	C.V. [%]		16,73													
	T2_FS_2W_001	2"W - 1"D	54,78	51,69%	Left (instrum. side)	B	0,293	0,878	0,654	0,584	0,082	-14,04%	159,47%	66,88%	20,30%	524,79%
	T2_FS_2W_002	2"W - 1"D	66,98	85,49%	Left (instrum. side)	C/F	0,245	0,379	0,677	0,559	x	-27,97%	11,96%	72,65%	15,23%	x
	T2_FS_2W_003	2"W - 1"D	64,88	79,65%	Left (instrum. side)	C/F	x	x	x	x	x	x	x	x	x	x
	Average		62,21				0,269	0,629	0,665	0,571	0,082	-21,00%	85,72%	69,76%	17,76%	524,79%
	Standard deviation		5,33	72,28%												
	C.V. [%]		8,56													
	T2_FS_1W_001	1"W - 1"D	57,18	58,34%	Left (instrum. side)	C	0,115	0,513	0,399	0,405	0,049	-66,36%	51,64%	1,74%	-16,46%	268,50%
	T2_FS_1W_002	1"W - 1"D	55,69	54,21%	Left (instrum.side)	C	0,331	0,204	0,545	0,966	x	-2,79%	-39,85%	39,04%	99,24%	x
	T2_FS_1W_003	1"W - 1"D	59,17	63,84%	Left (instrum.side)	C	x	x	x	x	x	x	x	x	x	x
	Average		57,35				0,223	0,358	0,472	0,686	0,049	-34,58%	5,89%	20,39%	41,39%	268,50%
	Standard deviation		1,42	58,80%												
	C.V. [%]		2,48													

As shown in the table above (Table 3.2), the average peak load gradually increased from the specimens without anchors (T2_BM) to the specimens with anchors, depending on the type of anchor installed and the configuration adopted. While characterizing the anchor resistance in terms of load, we must refer to the load identified as $\frac{P}{2}$ because this represents the load applied to one side.
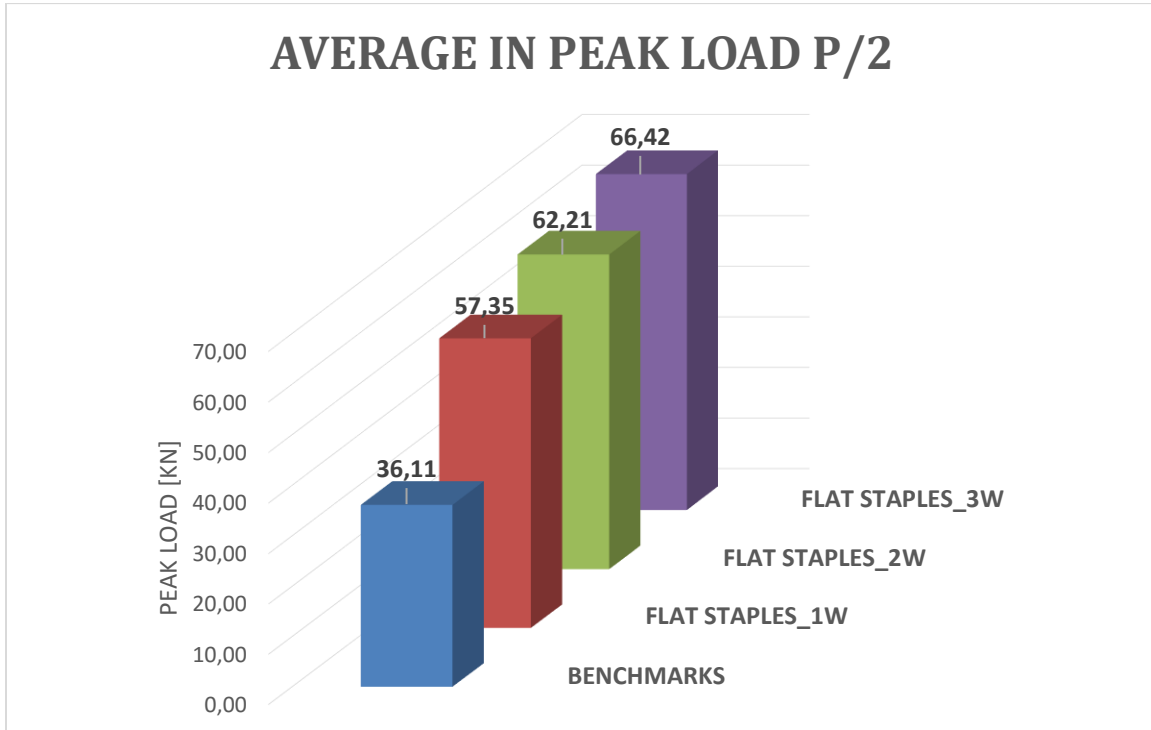

Figure 3.1 - Peak loads' average of the flat staples specimens referring to the benchmarks

The previous Figure 3.1 represents the average in terms of peak loads reached by the specimens.

Herein it is interesting here to compare the theoretical peak load calculated (thanks to the CNR formulas) which is 38,53 KN, with the average of the peak load obtained from the experimental results, which is 36,11 KN. This good correspondence between the theoretical peak load and the real peak load is crucial to give reliability to the results obtained from the test 2.
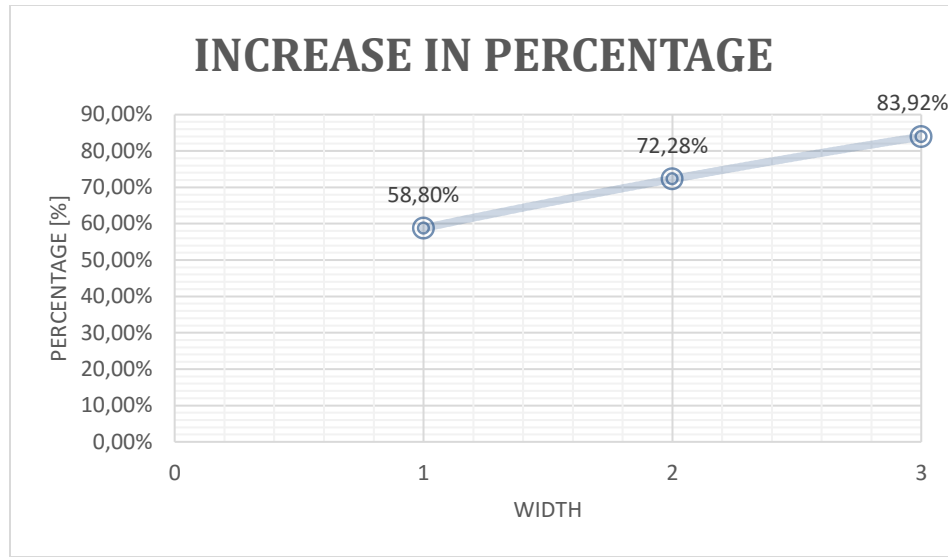
Figure 3.2 - Increase in percentage of the peak loads' average of the flat staples specimens

In Figure 3.2 is shown the increase in percentage reached by the average of the types of anchor system installed. It is interesting to notice that the increase it is not linear, but logarithmic. This is an important fact that should be considered while choosing the best configuration, as it will be explained in the appropriate chapter 4.2.

3.1.2.1 Strain gauges readings

Benchmarks

A typical strain distribution along the bonded length of the CFRP material is shown in Figure 3.3 and 3.4
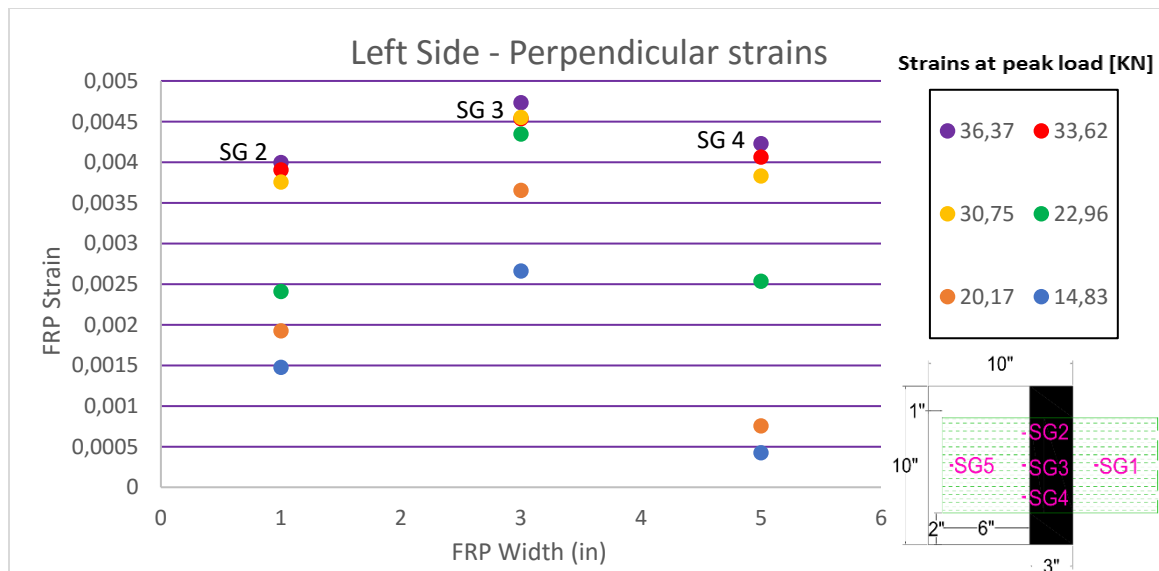

Figure 3.3 - Perpendicular strain distribution of a benchmark
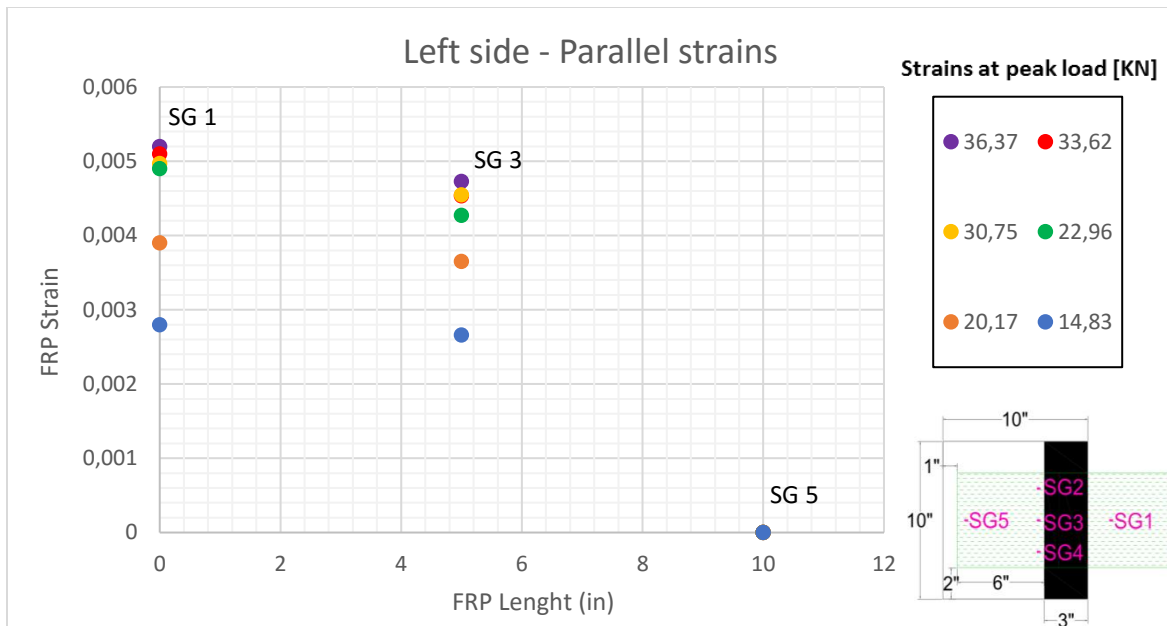
Figure 3.4 - Parallel strain distribution of a benchmark

Figure 3.3 and Figure 3.4 above refer to a benchmark sample, the one with no anchor installed.

Figure 3.3 shows the trend of the perpendicular strain, the ones longitudinal to the CFRP fibers' axis.

In particular, the x-axis represents the width of the CFRP sheet in inches. In this way, all the points settled at 1 inch identify the readings from the SG2, all the points settled at 3 inches are the readings taken from the SG3 and the points on the 5th inch represent the readings taken from the SG4.

The following Figure 3.5 illustrates the location of the strain gauges, with the relative distance between all of them.

Figure 3.5 - Strain gauges position

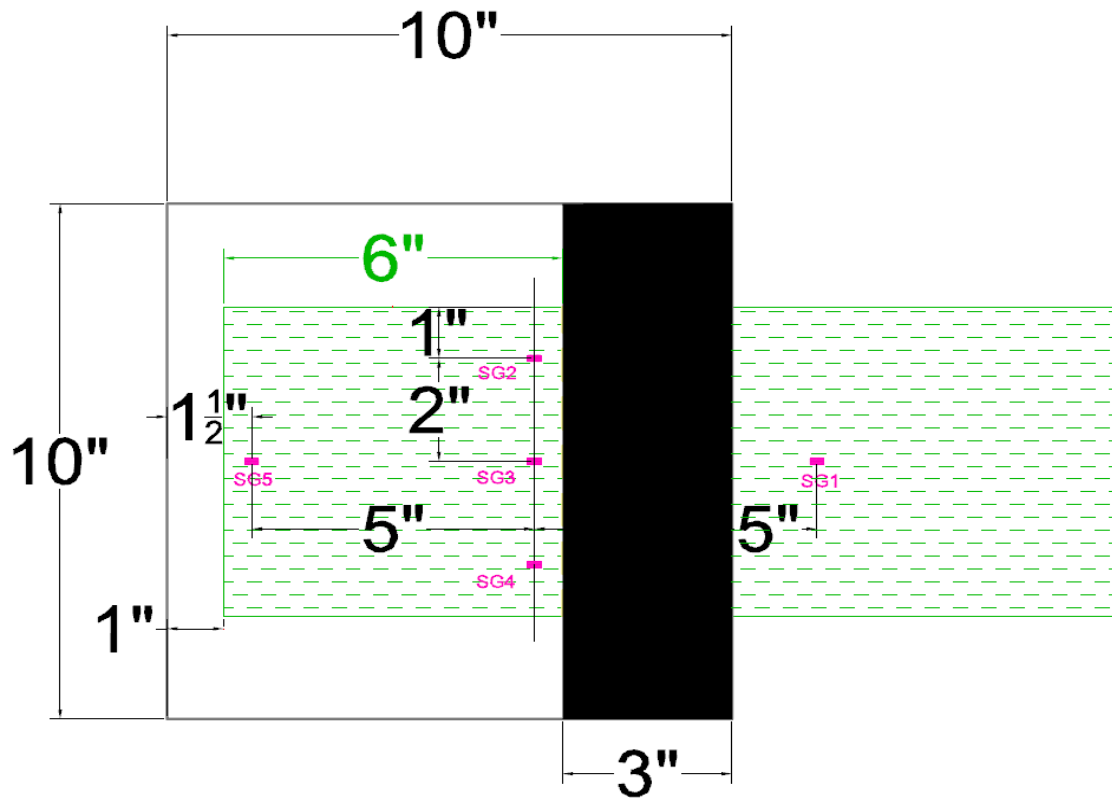Again, from the reading of the strain gauges in Figure 3.3, it is interesting to notice how for this benchmark the applied load was well distributed along the entire length of the CFRP sheet. Indeed, the ending curves (30,75 KN, 33,62 KN, and 36,37 KN) assume a flat trend, while the SG2 and SG4 read more or less the same strains' value.

That typical trend is mean of a good and well-distributed applied load (from the hydraulic jack) all along the 6" width of the CFRP.

The Figure 3.4, instead, represents the strains' distribution on the fibers' axis, and the points along the 0-inch width represent the SG1, while the points on the 5th inch are the readings from the SG3, and finally the readings at the 10th inch are the ones registered by the SG5. Here, it is interesting to underline how the strains' read by the SG1 and are a little more high from the ones' read by the SG3. This is most due to the fact that, since no anchor where installed in this sample, the progressive behavior of the debonding crack initiated from the loaded end (readings of the SG1) with high strains' values, propagating all through the bonded length to the points where the strain diminishes significantly, at the free ends.

FLAT STAPLE 2W_1D_001

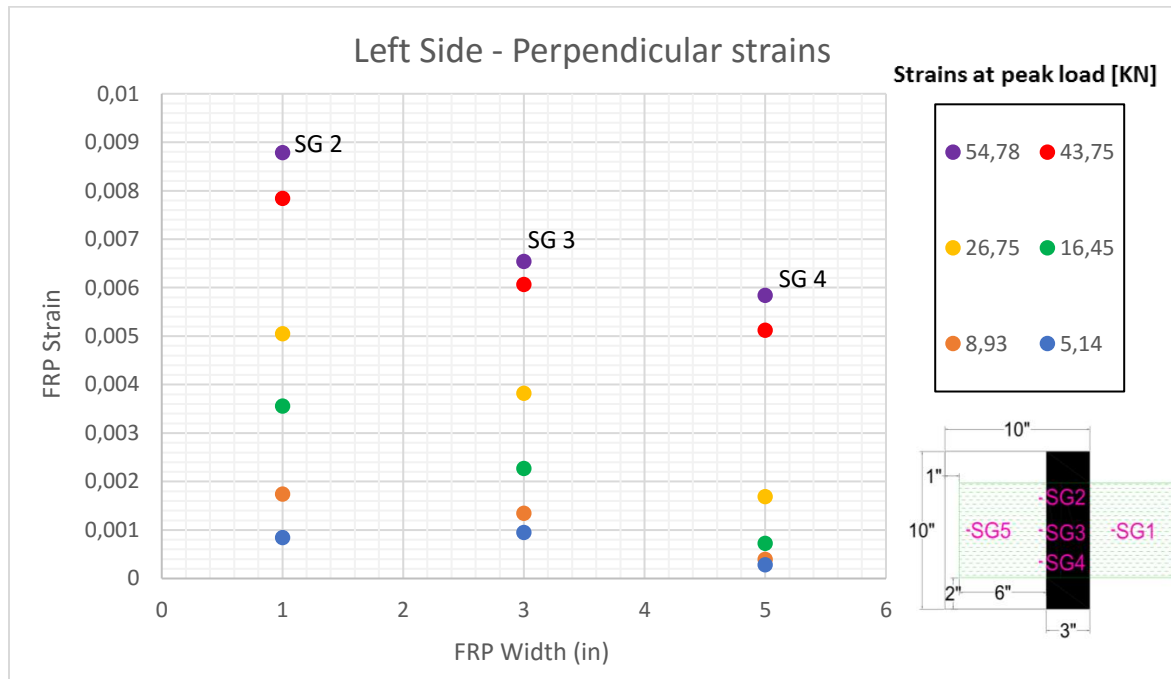Below, the strains' results of the flat staple 2W_1D_001 are shown.

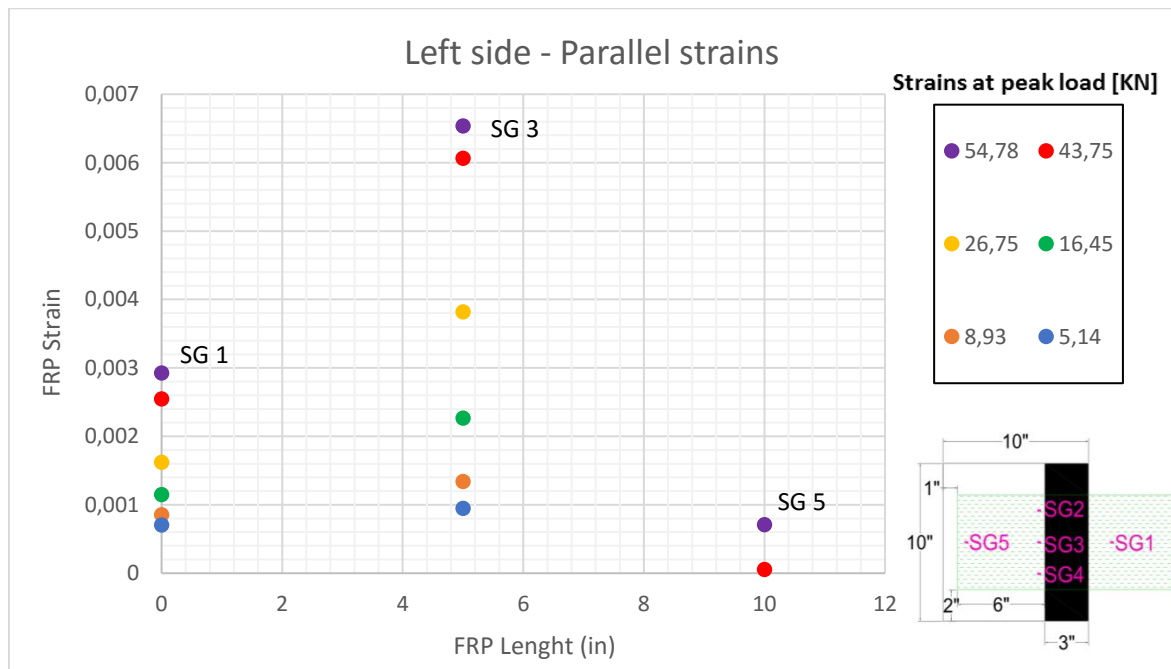Figure 3.6 - Perpendicular strain distribution of the T2_FS_2W_1D_001

Figure 3.7 - Parallel strain distribution of the T2_FS_2W_1D_001

From these two images, it is possible to notice two main differences between the benchmark.

- Firstly, the strain gauges SG2, 3 and 4 recorded higher values than the ones read from the benchmark. The SG2, 3 and 4 are considered the most important, due to the fact that are placed in the in front of the anchor. This region is of particular interest being the sheet fibers directly engaged by the anchor. The recorded values are the greatest ones in terms of deformation and they may be considered as the bond capacity of the system.

- Secondly, the Figure 3.7 clearly shows how the SG3 read a higher value compared to the SG1, contrarily from what the benchmark displayed. Again, this is a proof of the effective anchor work

- Thirdly, as the crack system occurred, the SG5, recorded a sudden alteration, leaping immediately to high values of strain. Here is shown only the strain recorded at the very peak load, but after that, it is important to say that the value increased by 1%. This fact has been noticed in every specimen that was provided with an anchor system.
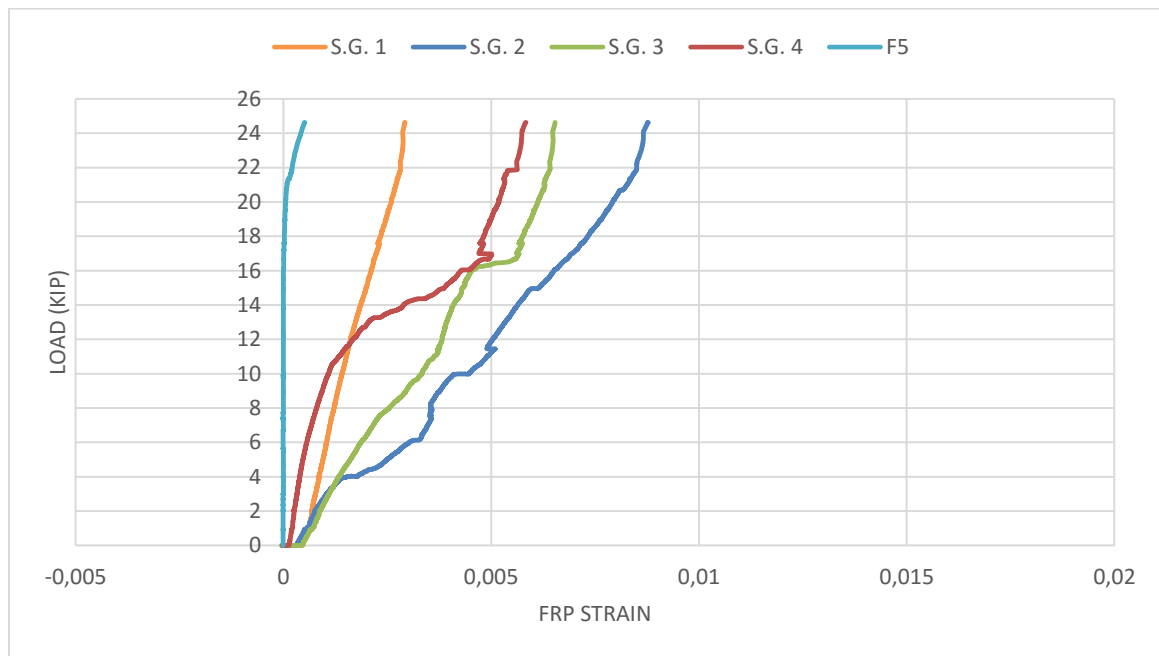

Figure 3.8 - Load - strain curve of the T2_FS_2W_1D_001
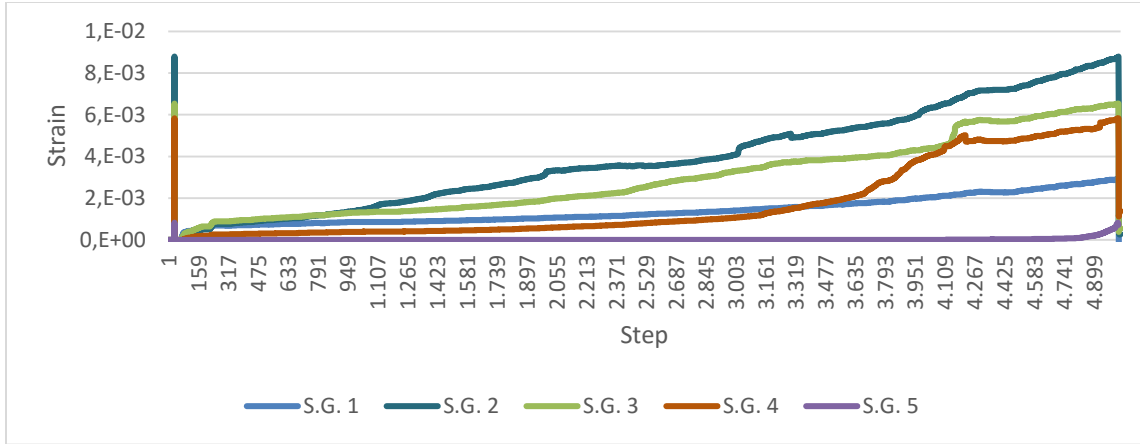
Figure 3.9 - Load - time curve of the T2_FS_2W_1D_001

The strain readings taken at different locations along the bond length (SG2, SG3, SG4, SG5) and the unbonded length (SG1) show the progressive behavior of the debonding crack, which initiated at the loaded end (readings of the SG2, SG3, SG4) and propagated towards the free end, behind the anchor as the reading of the SG5. Figure 3.8 wants to show how, as the interfacial crack propagates through the monitored locations, it is evident the sudden change in the stiffness of the load, identified with a change in the trend of the stress-strain curve of the affected strain gauges. Figure 3.9 shows, instead, the variation of the strain/time. In that figure, the numbers identify ad step represents the rows of the data read by the DAQ (data acquisition system).

FLAT STAPLE 3W_1D_002

Below, the strains' results of the flat staple 3W_1D_002 are shown.

Figure 3.10 - Perpendicular strain distribution of the T2_FS_3W_1D_002

87
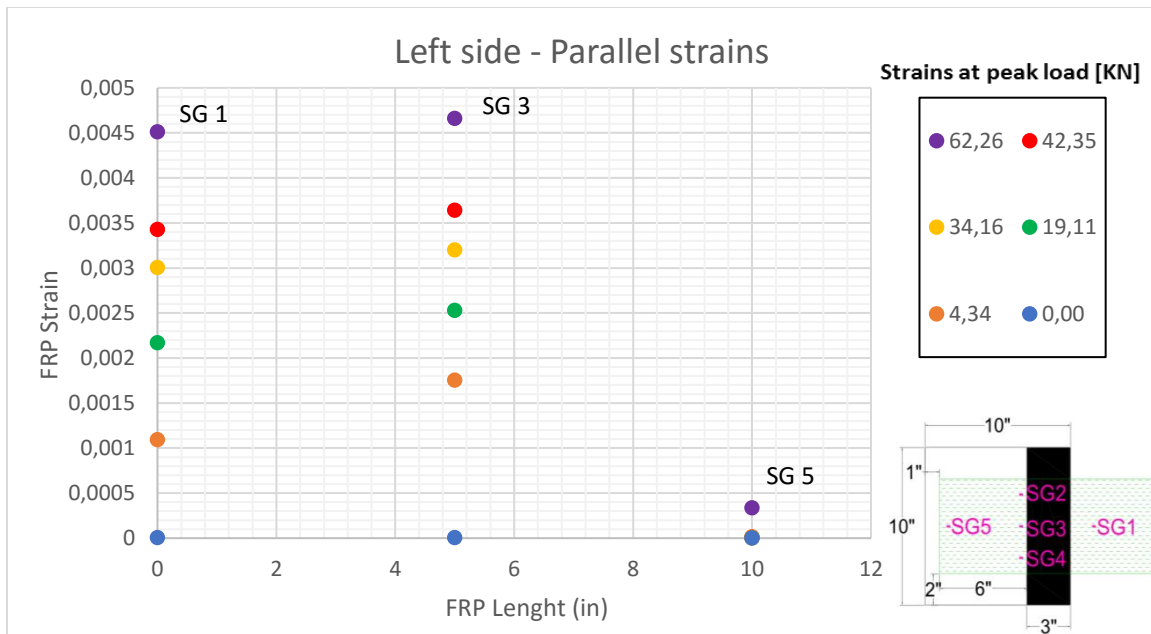
Figure 3.11 - Parallel strain distribution of the T2_FS_3W_1D_002

This case it is introduced to underline an important fact that was observed.

From the readings of SG 2, 3 and 4 in Figure 3.11, it is clearly possible to see that the strains are very bad-distributed. In fact, an important aspect of the double shear test that has to be underlined is related with its set up: the results obtained from the tests were found to be highly dependent on the alignment of the system. Perfect alignment was very difficult to ensure and different degrees of load eccentricity were observed. Moreover, the specimens were found to be very sensitive to the handling operations. This has to be noticed especially from the first test run. With the test 2, even if the load was not completely centered and the system not perfectly aligned, this problematic seems to have been overcome.

Here in Figure 3.12 it is proposed the same case but with the old installation, from the test n.1:
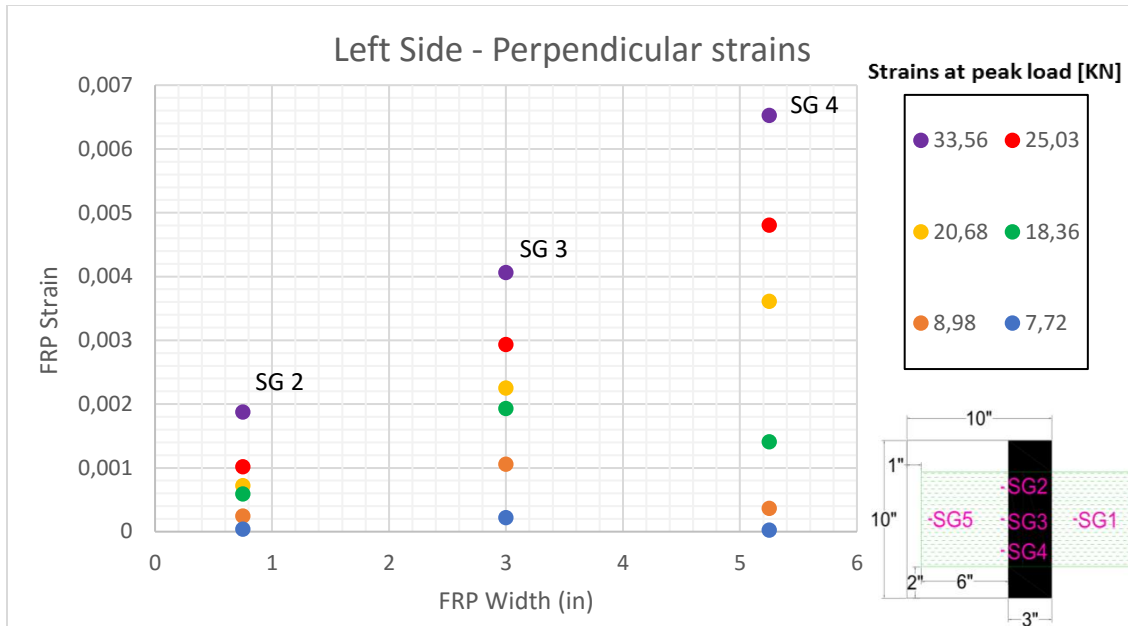
Figure 3.12 - Perpendicular strain distribution of the T1_FS_3W_1D_001

Immediately, we notice how the different distribution of strains made the system's collapse for the test n.1, while the test n. 2, even the bad distribution of strains, was successful. This reason is due to the fact that the new installation provides the entire CFRP sheets acting as a matrix, as better explained in the previous chapter 2.5.3. The Graph in Figure 3.12 refers to the specimen T1_FS_3W_1D_001 (referred to the test's results in table 3.1).

FLAT STAPLE 1W_1D_001

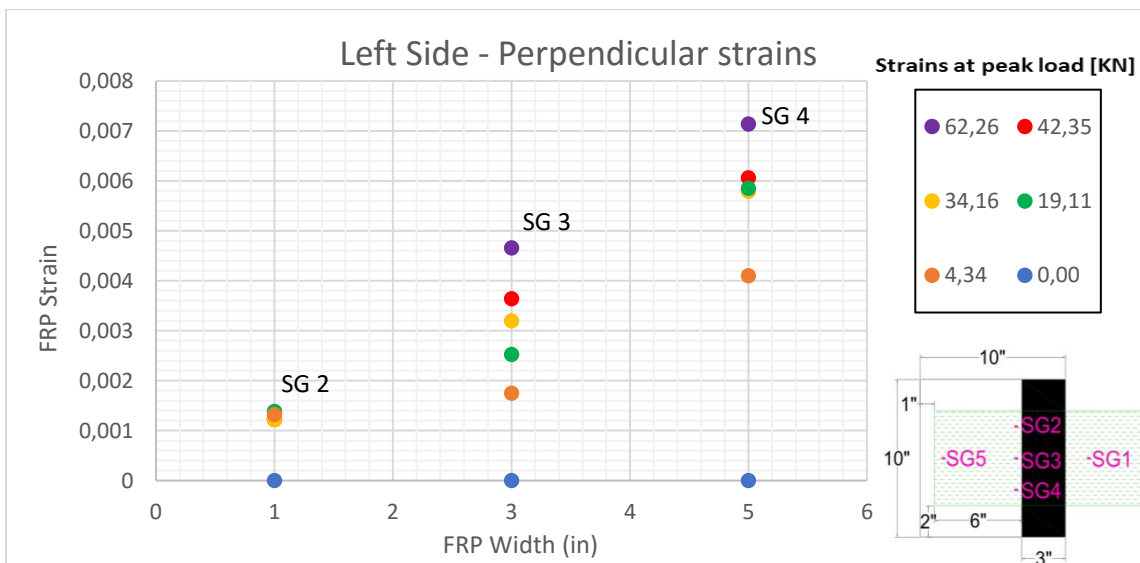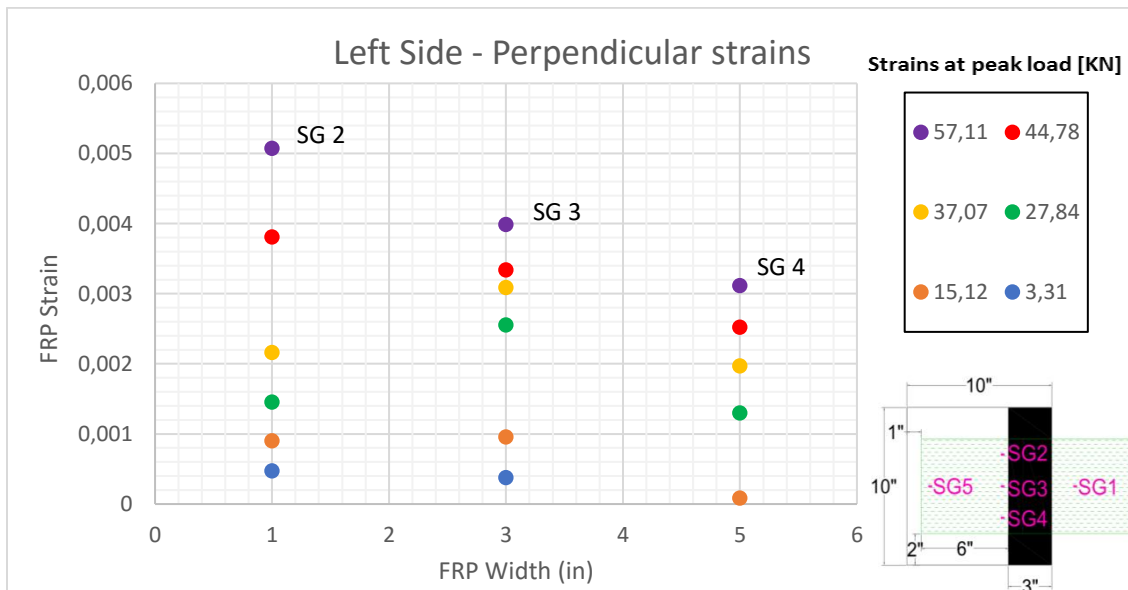*Figure 3.13 - Perpendicular strain distribution of the T2_FS_1W_1D_001*
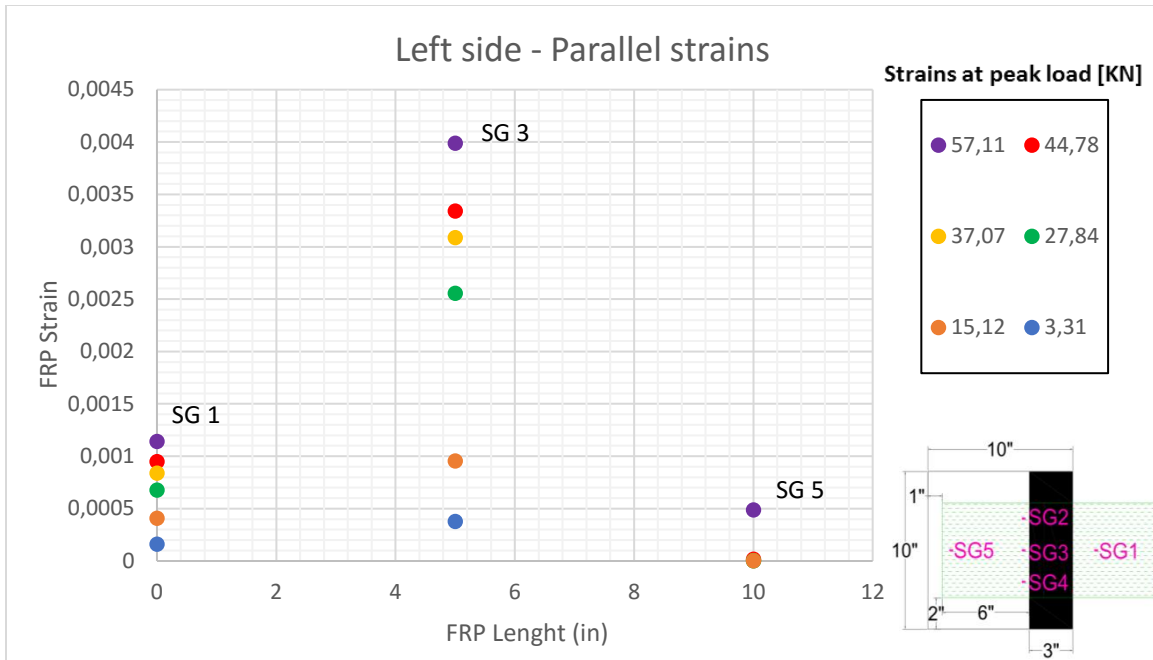
Figure 3.14 - Parallel strain distribution of the T2_FS_1W_1D_001

Below, in Figure 3.15 the graphs referred to the average's readings of strain gauges n.1 and n.3 are plotted.
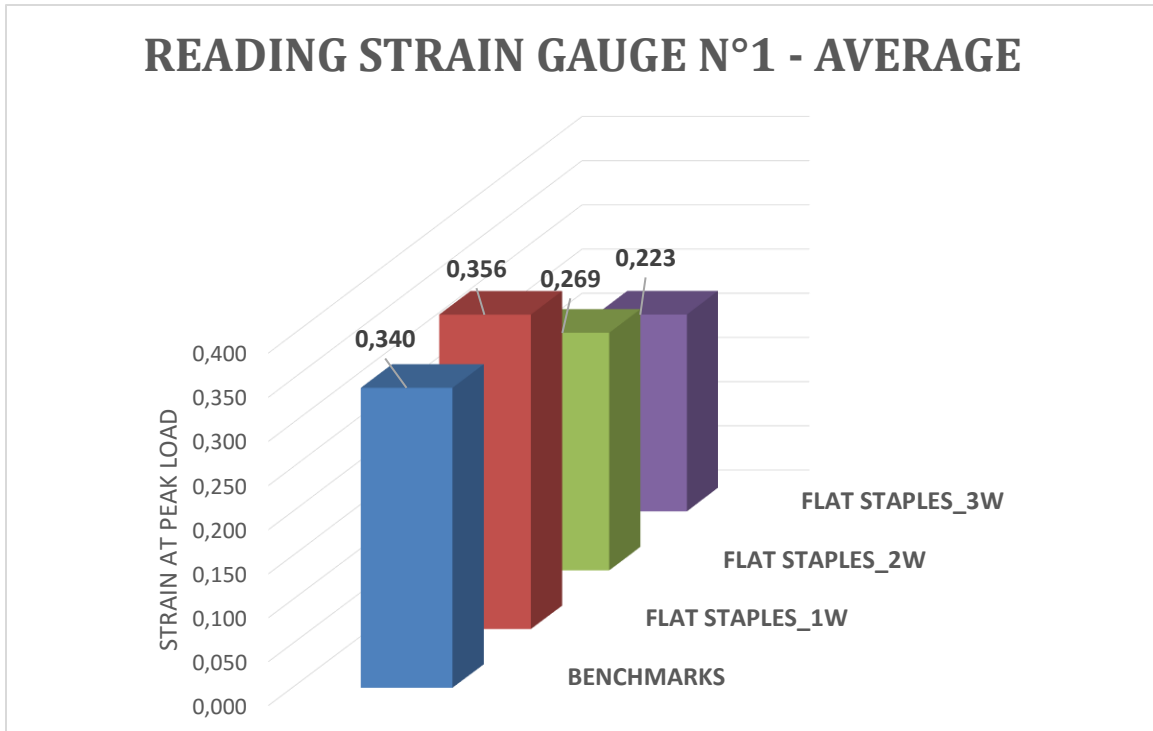
Figure 3.15 - Average values of the strain gauges n°1
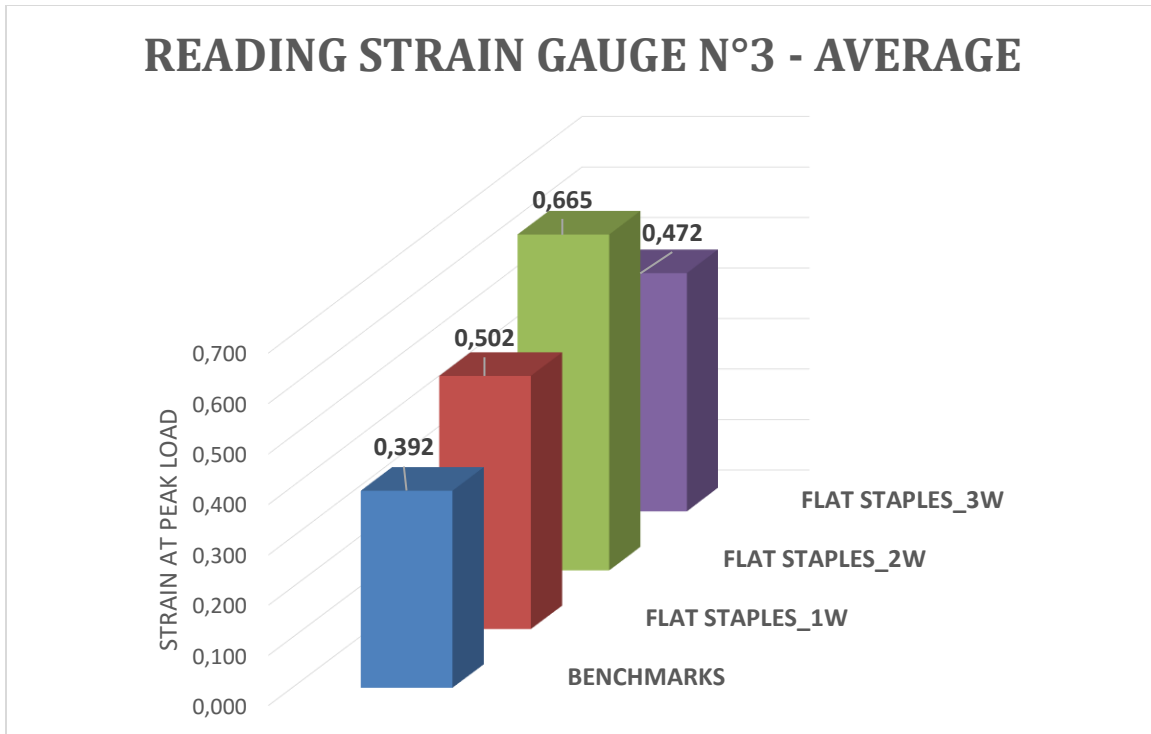
Figure 3.16 - Average values of the strain gauges n°3

Again, there is consistency between al the results deducted and all the claims previously made are here collected in terms of average between all the samples run.

3.2 ROUND STAPLES

3.2.1 Test 2 – Wet CRFP testing

The round staples anchors were run with the wet CFRP installation. 9 more specimens here were tested as:

- N° 3 RS_2D configuration (it states for 3 inches width and 2 inches depth)
- N° 3 RS_1D configuration
- N° 3 DRS_1D configuration

The same benchmarks, which were run for the characterization of the flat staple anchors, were used.

N.B: the RS as capital letters means Round Staple, DRS means Double Round Staple and the D as a capital letter refers to the depth of the anchor (in this way, for example, the "DRS_1D configuration" it states for a 1-inch depth in double round staple configuration. From now on, only this technical nomenclature will be used.

Again, the following table 3.3 summarizes the results in terms of peak loads, increases of the load and strains with respect to the benchmark, rupture side, measured strain in the FRP sheets and failure modes.

Also, In this table 3.3, the first two results, which are referred to the 2-depth round staple configuration, has been crossed, since they were just a first prototype of the round staples anchors, while tests from the third one on are the experimental anchors in the new improved form.

Table 3.3 - Summary test 2, round staples

Shear test n.2 (WET FRP)

	Specimen ID	Anchor's dimensions	P/2 [KN]	Increase in Peak Load [%]	Rupture Side	Rupture Type	Strains in % at peak load					Increase in % of strains at the peak load				
							SG1 [%]	SG2 [%]	SG3 [%]	SG4 [%]	SG5 [%]	SG1 [%]	SG2 [%]	SG3 [%]	SG4 [%]	SG5 [%]
ROUND STAPLES	RS_2D_001	2"D_OLD	30,75	14,86%	Left (instrum. side)	D	0,241	0,317	0,517	0,600	0,013	-29,11%	-6,44%	31,95%	23,64%	-2,95%
	RS_2D_002	2"D_OLD	36,49	1,95%	Left (instrum. side)	C/D	0,339	0,223	0,070	0,064	0,550	-0,50%	-34,00%	-82,04%	-86,78%	4067,28%
	RS_2D_003	2"D_NEW	49,13	36,06%	Left (instrum. side)	D	0,104	x	0,191	0,304	x	-69,39%	x	-51,37%	-37,28%	x
	Average		49,13				0,228	0,270	0,259	0,323	0,281	-33,00%	-20,22%	-33,82%	-33,48%	2032,17%
	Standard deviation		0,00	36,06%												
	C.V. [%]		0,00													
	RS_1D_001	1"D_NEW	46,34	28,31%	Right (not instrum. side)	E	0,218	0,140	0,295	0,120	x	-36,05%	-58,58%	-24,85%	-75,24%	x
	RS_1D_002	1"D_NEW	59,20	63,94%	Left (instrum. side)	E	0,242	0,089	x	0,081	x	-28,82%	-73,62%	x	-83,40%	x
	RS_1D_003	1"D_NEW	52,31	44,86%	Right (not instrum. side)	D	0,333	0,085	0,219	0,397	x	-2,20%	-74,80%	-44,19%	-18,07%	x
	Average		52,62				0,264	0,105	0,257	0,199	x	-22,36%	-69,00%	-34,52%	-58,90%	x
	Standard deviation		5,26	45,70%												
	C.V. [%]		9,99													
	DRS_1D_001	1"D_NEW	65,13	80,35%	Left (instrum. side)	C	0,519	x	0,178	x	0,085	52,44%	x	-54,53%	x	544,50%
	DRS_1D_002	1"D_NEW	68,88	90,73%	Left (instrum. side)	C/F	0,376	x	0,258	x	0,065	10,37%	x	-34,29%	x	395,89%
	DRS_1D_003	1"D_NEW	62,84	74,02%	Left (instrum. side)	E	x	x	x	x	x		x	x	x	
	Average		65,61				0,447	x	0,218	x	0,075	31,40%	x	-44,41%	x	470,20%
	Standard deviation		2,49	81,70%												
	C.V. [%]		3,79													

The following results refer to the RS_2D_001.

Figure 3.17 - Perpendicular strain distribution of the RS_2D_001
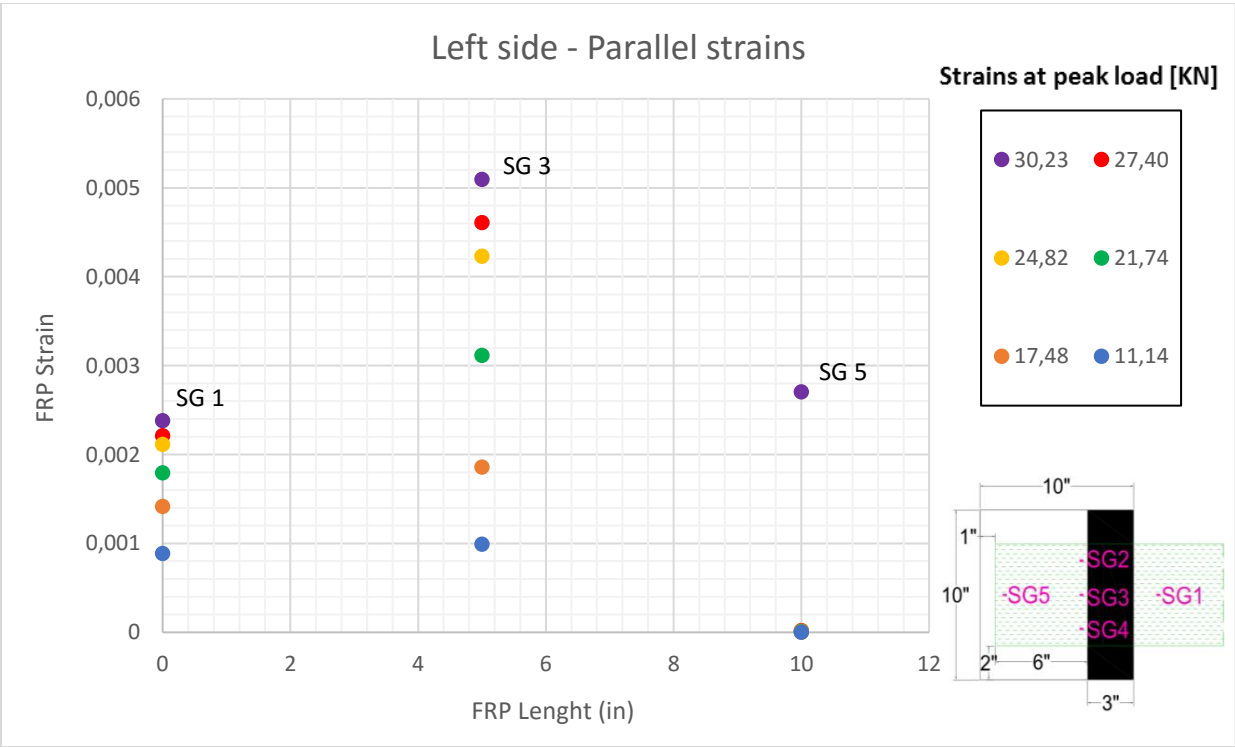
Figure 3.18 - Parallel strain distribution of the RS_2D_001

For this specimen, it is important to underline that the SG 2, 3 and 4, were positioned on the flexural sheet below the anchor. In fact, these strains show the same trend and behavior of to the ones installed on the flat staple anchors (previously shown in Figure 3.10).

The following Figure 3.19 represents the strains' reading of the RS_1D_001. In this case, the SG 2, 3 and 4 were installed on the flexural sheet above the anchor, in the wrapped part around the anchor that it covers entirely the latter.
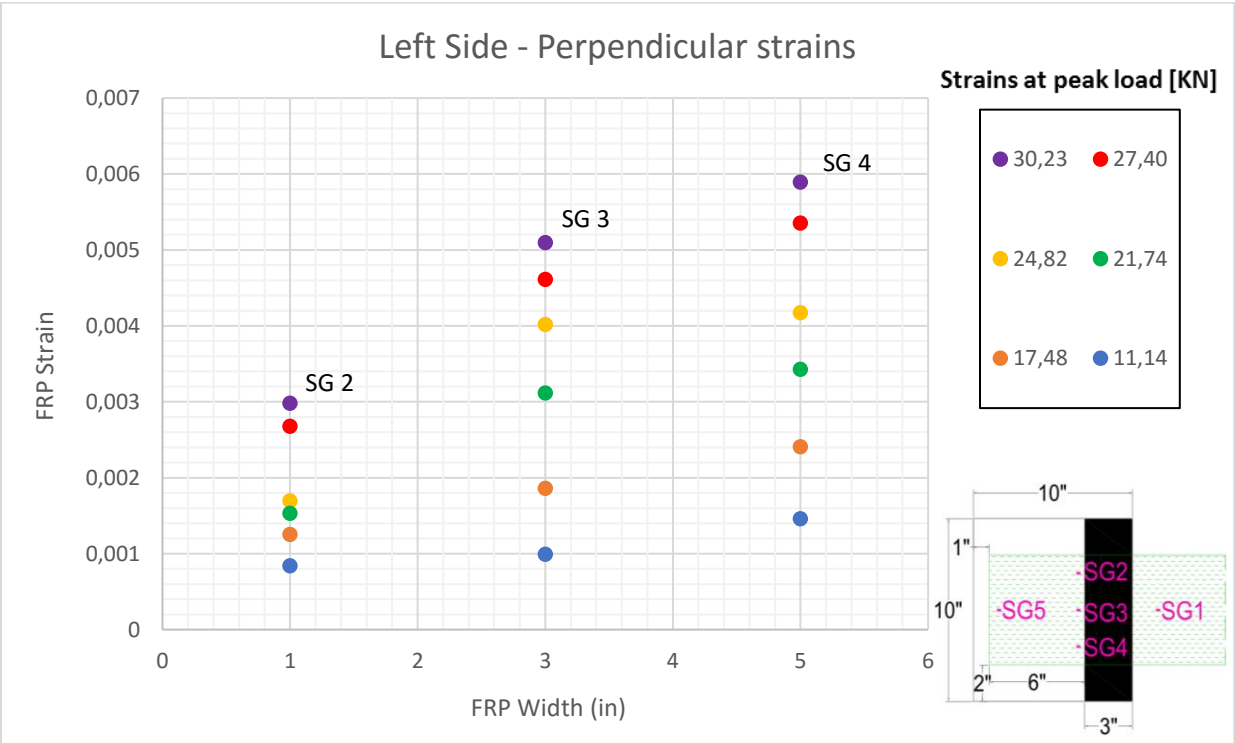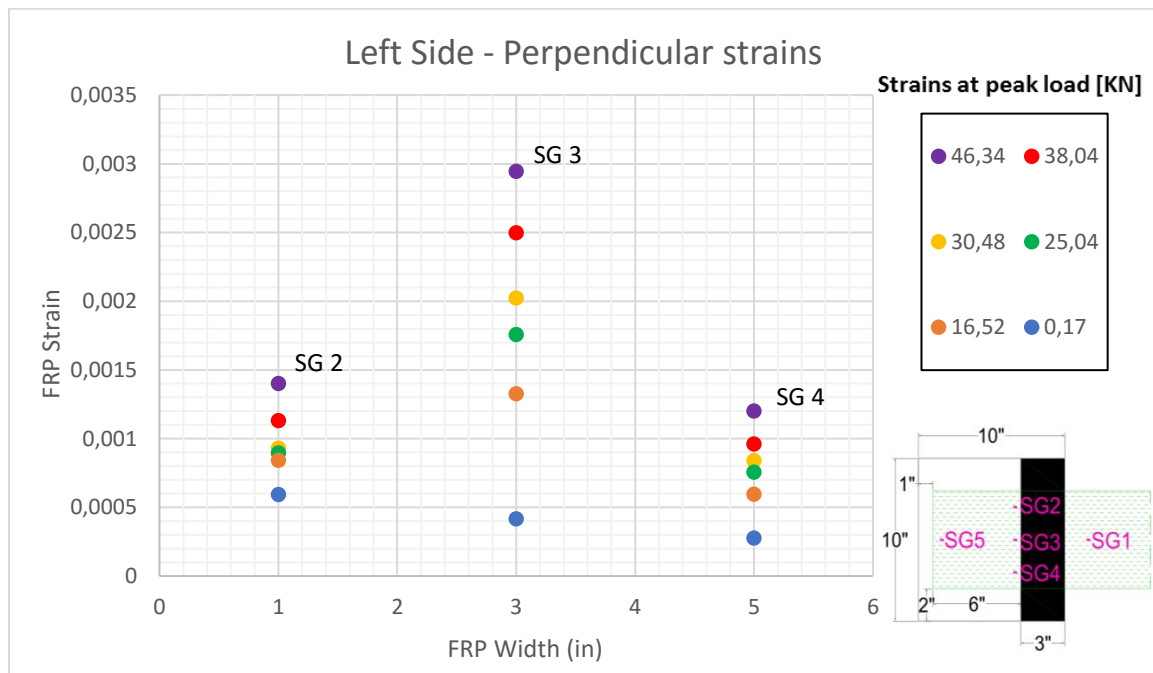

Figure 3.19 - Perpendicular strain distribution of the RS_2D_001

95
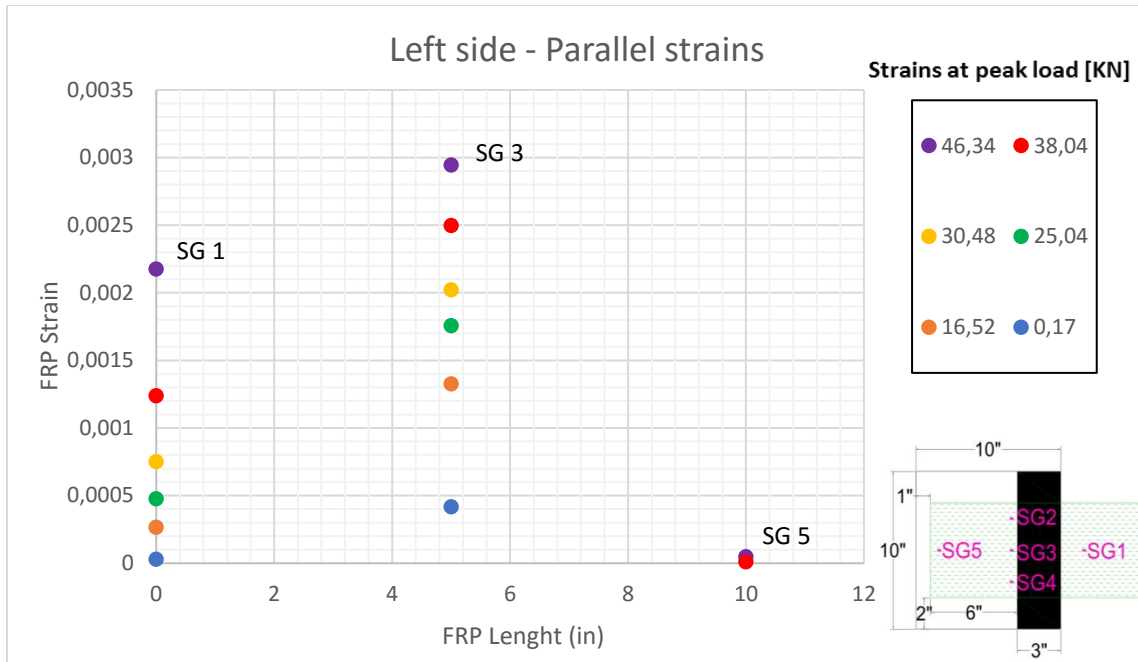
Figure 3.20 - Parallel strain distribution of the RS_2D_001

In this case, it is interesting to notice how, in general, the trend is always the same, but the strains are much smaller as compared to the previous ones. In fact, the strain peak here is at 0,3%, while usually, it reaches values around 0,7 - 0,8%. This is because we double the nominal cross-sectional area from 152,4 mm^2 to 304,8 mm^2. In fact, increasing the cross-sectional area of the CFRP, the strains decrease as the following formula:

$$\frac{Force}{E \cdot A} = \varepsilon$$

Where the Force (peak load) and the modulus of elasticity E remain constant.

It is important to underline how the 2-inches depth configuration does not produce any good improvement if related to the 1-inch depth. Also, as explained better later in chapter 5.1, it has been stated that 1-inch depth is the best configuration (concrete cover).
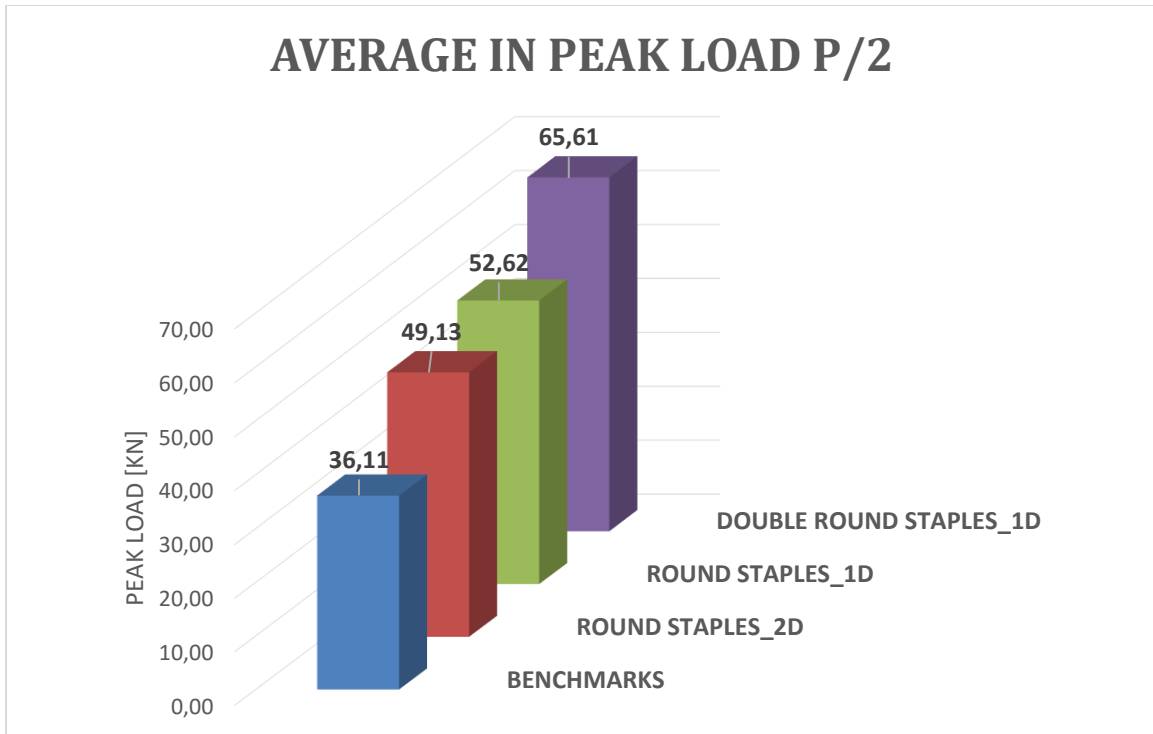
Figure 3.21 - Peak loads' average of the round staples specimens
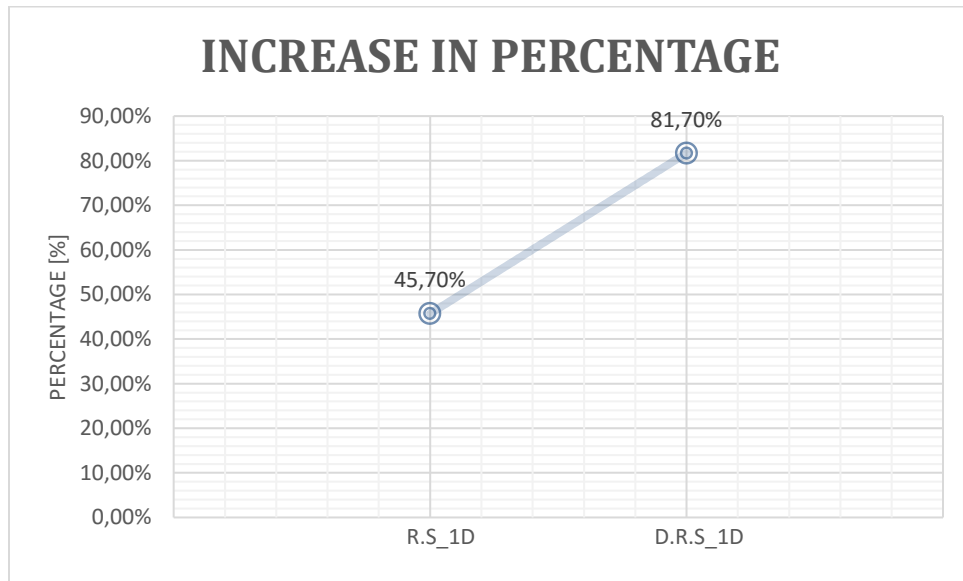
Figure 3.22 Increase in percentage of the peak loads' average of the round staples specimens

Since from Figure 3.21, it seems strange how the 2 inches depth configuration could be less than the 1-inch depth. It is important to say that in the 2 inches depth only one specimen was run with the new round staple system. As it shown in table 3.3 this only result is not sufficient to prove any rule and also this only result could be part of a minimum in a series of more specimens hypothetically run. In fact, the minimum value of

the 1-inch depth is 46,34, which is less than 49,13. This is just a hypothesis, but it is enough to understand that also in this case, on increasing the depth, we don't reach any consistent and remarkable improvement.

3.3 FAILURE MODES ANALYSIS

During the tests, six main failure modes were observed.

This section wants to describe each type of rupture, analyzing case by case the reason, giving an interpretation and a potential understanding of what each failure means.

Below the main failure modes are summarized as letters:

    A. Rupture as delamination of the CFRP sheet
    B. Slippage of the CFRP sheet beneath the anchor, without their ruptures
    C. Slippage of the CFRP sheet beneath the anchor, with the rupture of the CFRP sheet
    D. Rupture of the anchor with the delamination of the CFRP
    E. Rupture of the concrete substrate and rupture of the anchor
    F. Rupture of the concrete substrate without the rupture of the anchor
    G. Rupture of the CFRP sheet outside the bond area

Failure A - Rupture as delamination of the CFRP sheet

Figure 3.23 – Failure mode A

Only the benchmarks presented this type of failure. That is due to the fact that of the absence of an anchorage system. The failure mode A is a rupture by debonding of the CFRP sheet at the adhesive-to-concrete interface. Debonding initiated at the loaded end of the CFRP sheet and it brought propagated to the unloaded end.

The debonding caused the removal of the epoxy layer from the substrate and also a thin layer of concrete was noticed on the detached FRP sheet area.

Figure 3.23 shows the typical type A failure.

Failure B - Slippage of the CFRP sheet beneath the anchor, without their ruptures

Figure 3.24 - Failure mode B

This type of failure is a particular one: It happened as a debonding of the CFRP sheet at the adhesive-to-concrete interface, followed literally by a slippage of the CFRP sheet beneath the anchor, as to mean an insufficient adhesive-to-concrete and anchor-to-CFRP interface. In fact, this failure mode is due to an insufficient quantitative of primer spread on the concrete surface first, and under the anchor area secondly.

Anyway, this failure mode is still ideal for determining the sufficiency of the anchor, since the strains across the width of the sheet monitored showed a good stress distribution with high values of the same (check Figure 3.6).

This failure mode was observed in only one anchored specimen. The above Figure 3.24 represents the failure mode B.

Failure C - Slippage of the CFRP sheet beneath the anchor, with the rupture of the CFRP sheet

Figure 3.25 - Failure mode C

With the use of anchors, a CFRP sheet rupture failure reveals that the sheet has developed its full strength. The failure mode C is ideal for determining the sufficiency of the anchors and develop guidelines for anchor design. This rupture indicates the maximum tensile strength reached by the FRP-anchorage system, with a good anchor resistance.

However, there may be cases in which a sheet rupture does not indicate the development of full strength of the system. This can be understood by the strains reading. A good level of strains (usually values around a minimum of 0.6%, 0.7%) indicate the development of full strength of the system.

Figure 3.25, 3.26 represent the failure mode C. The rupture of the fibers took place until the surface beneath the anchor, that appeared still anchored to the concrete surface after the failure.
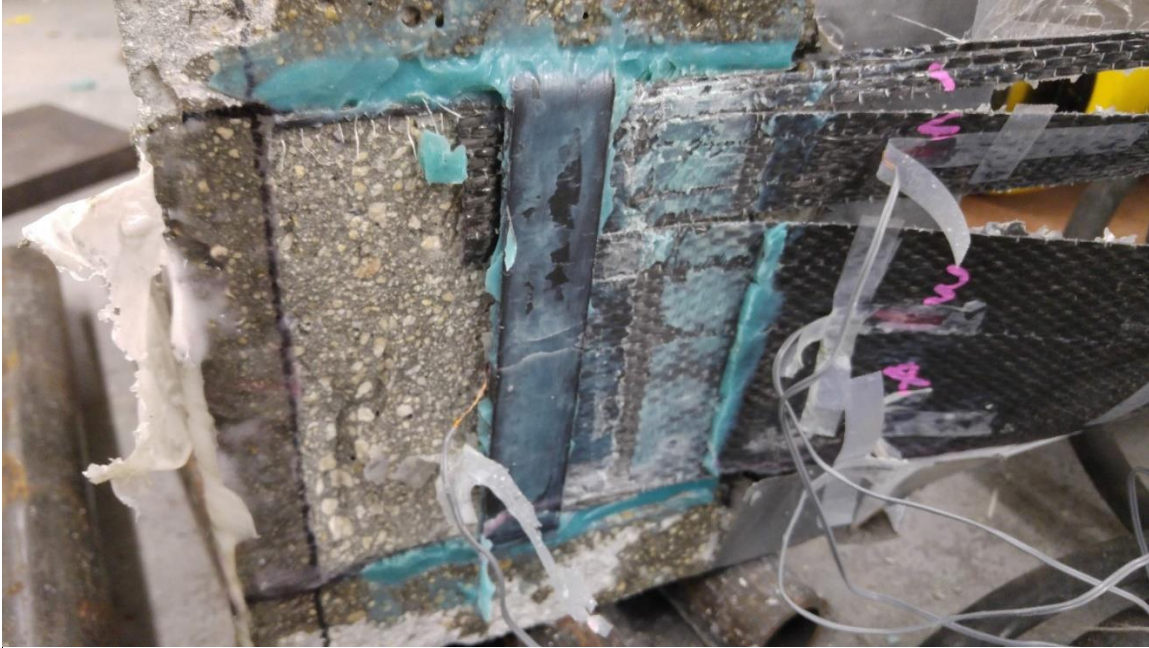
Figure 3.26 - Failure mode C (2)

After the propagation of the debonding cracks toward the anchor region, the enhanced strength of the anchored system was reached thanks to the remaining length of the bonded FRP sheet and the restraint provided by the anchor. The debonding started in the adhesive-to-concrete interface and the layer of primer was totally removed from the concrete surface at the end of the test.

Failure D - Rupture of the anchor with the delamination of the CFRP

The failure of the anchor indicates that anchors do not have sufficient capacity to develop the full strength of the CFRP sheet and is generally an undesirable failure mode. From previous studies, it has been stated that anchor failures depend on several factors as the size of the anchor, the force transfer mechanism between the sheet and anchor (bend radius and CFRP patches), and finally the adherence to installation procedures.

This type of failure was observed only for the round staple anchor, In particular, for the anchors that showed a greater embedded depth (2-inches depth). Especially, for all of them, the rupture happened on the bend radius, on the rounded corner side where the fibers were to change direction from the vertical to the horizontal plane.

The Figure 3.27 shows the failure mode D.
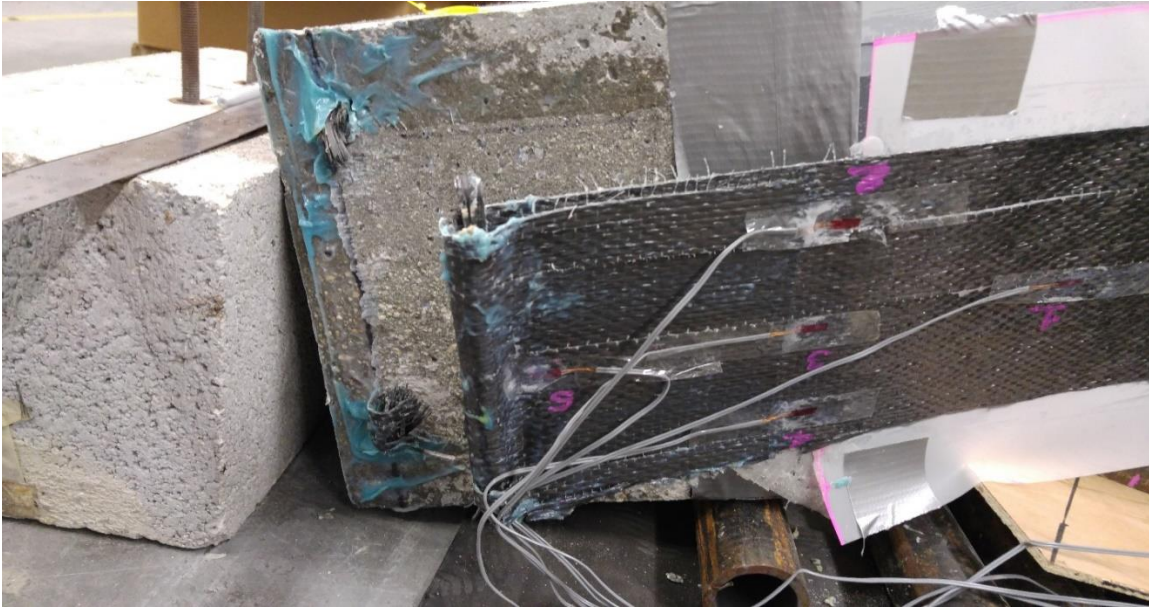
Figure 3.27 - Failure mode D

Failure E - Rupture of the anchor followed by the rupture of the concrete substrate

Again, the failure mode E was observed only in the specimens that were anchored with the round staple anchorage system. In this case, the rupture of the concrete always initiated first at one end, where the leg of the round staple was embedded; after this, immediately the opposite leg of the anchor took the entire stress, breaking again the anchor along the bend radius. Figure 3.28 shows the failure mode E

Figure 3.28 - Failure mode E

Failure F - Rupture of the concrete substrate without the rupture of the anchor

Figure 3.29 - Failure mode F

The failure mode F was observed only in the specimens that were anchored with the flat staple anchorage system. In this case, the failure was due entirely to the rupture of the concrete substrate, as shown in the pictures (see Figure 3.29). Since the maximum shear capacity of the non-reinforced concrete was reached, the anchor was still performing well, assuming that it could have been achieved a higher load.

This rupture was fully observed in two of the 3-inches flat staple anchors and partially in two of the 2-inches flat staple anchors.

Failure G - Rupture of the CFRP sheet outside the bond area

The failure mode G was observed only in the specimens that were run for the test 1, with the old installation. This is the worst type of rupture because unfortunately, we can not obtain any interesting data from them.

The rupture did not occur on the bonded part, where the anchor was installed, but on the dry CFRP outside the bond area at a relatively low-stress level compared with the tensile strength of the CFRP itself. Figure 3.30 shows the failure mode G. This type of rupture, as already explained in the previous chapter 3.1, is due to problems correlated with the

installation process and the alignment of the system. In fact, the perfect alignment with the installation used for the test 1 was very hard to ensure and the specimens were found to be very sensitive to the handling operations.

Figure 3.30 - Failure mode G

3.4 AIR BUBBLES INSPECTION METHOD

One of the primary importance while installing CFRP external reinforcement is guarantee a good concrete-sheet adherence, in order to fully develop the system's strength.

Besides the mechanical behavior of the system, the durability issues coming along an improper installation are the most critical aspect, making inspections become essential in real-case applications.

Among the standard inspection method, as knocking on the sheet's surface with a hammer, or hand touching the surface with a hand in order to identify eventual voids, are the most commonly employed on the field, those are clearly insufficient and non-systematic solutions, even the advantages of being inexpensive and easily performable. Here, a slightly more expensive and onerous solution is proposed, coming with the advantage of guaranteeing a systematic inspection of the installation and allowing an easy detection and documentation of the eventual voids. Using a thermal camera and a heat-gun, after a uniform and accurate heating of the fiber sheet, the inspection is performed.

104

The voids will appear sensibly warmer than the surrounding properly-bonded zones. The solution well-suits research purposes as well, allowing to properly define the defect pattern and look for a direct relation with the experienced failure mode.

The solution well-suits research purposes as well, allowing to properly define the defect pattern and look for a direct relation with the experienced failure mode. The same solution was being exploited in the context of an already existing thesis (Rossini, 2016)
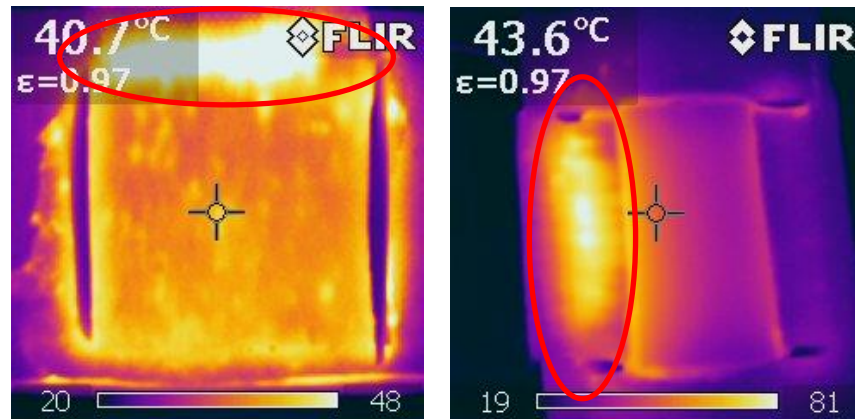
Figure 3.31 – Thermal camera inspecting specimens from test 1

Figure 3.31 refers to specimens from the test 1. The picture on the left shows a benchmark while the picture on the right refers to an anchored specimen. Clearly, it is possible to notice the air bubbles as white spots with different thermal values (warmer than the rest of the surface). From this thermal images it is possible to confirm the assumptions made in the chapter 3.1.1 about the useless results obtained from test 1: the unevenness of adhesive, caused from air bubbles, on CFRP sheet on the edge of the bond area, leading to uneven stress distribution in the CFRP fibers.
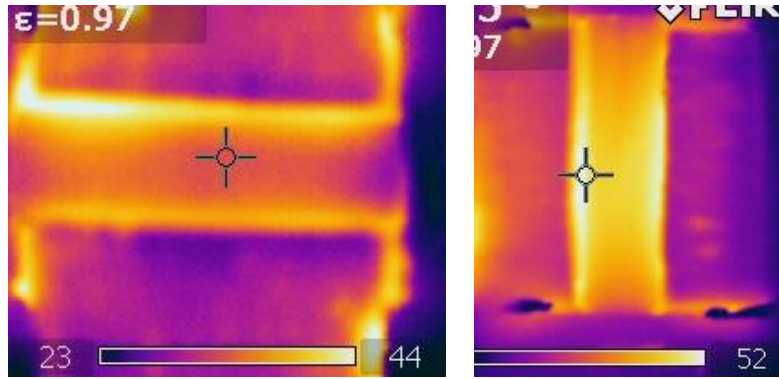
Figure 3.32 - Thermal camera inspecting anchored specimens from test 2

Figure 3.32 refers instead to some of the specimens run for the second test. Here it is possible to notice how the thermal camera revealed a better uniform surface.

What has not be developed in this thesis, but would be interesting to do for future investigations, is to find a correlation between the content of voids (in terms of a percentage parameter of the concrete-sheet adherence) and the mechanical behavior of the system (in terms of peak loads and failure modes of the samples).

4. COMPARISONS

4.1 STAPLES VS SPIKE ANCHORS

In this section, a brief comparison between the performance of the staple anchors and the spike anchor system is provided in terms of peak load, strains distribution, and type of rupture.

4.1.1 Peak load interpretation

Table 4.1 - Summary anchors peak loads

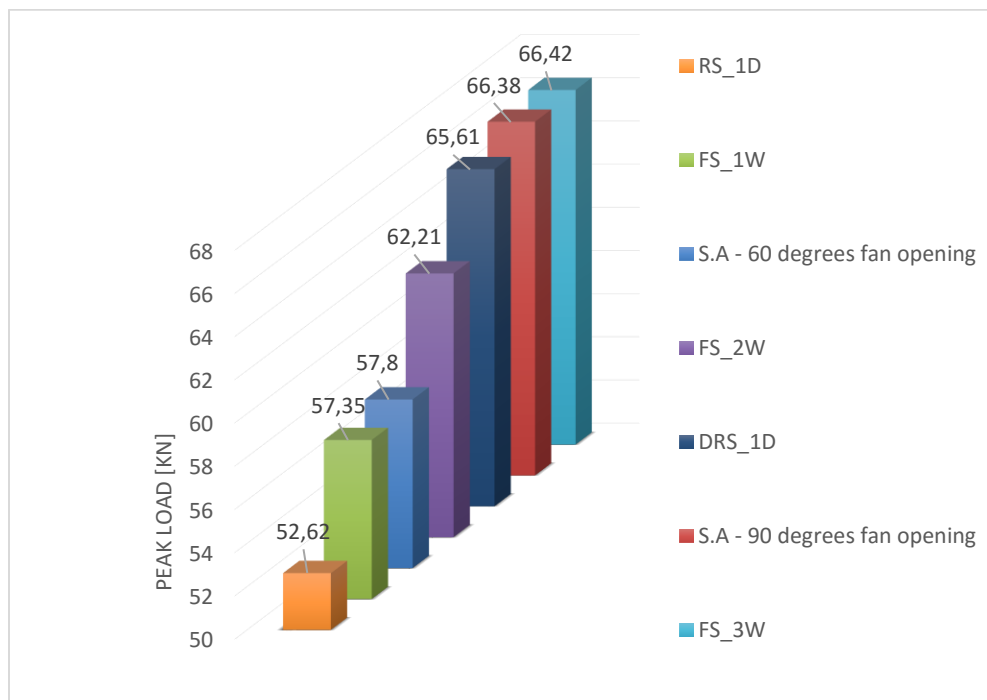| Anchor's type	Anchor's Configuration	Peak Load [KN]
Spike anchors	60 degrees fan opening	57,8
	90 degrees fan opening	66,38
Flat staple anchors	1 in. width – 1 in. depth	57,35
	2 in. width - 1 in. depth	62,21
	3 in. width - 1 in. depth	66,42
Round staple anchors	Single conf. - 1 in. depth	52,62
	Double conf. - 1 in. depth	65,61

Figure 4.1 - Comparisons staples-spikes peak loads in ascending order

Table 4.1 and Figure 4.1 present a comparison in terms of peak load between the spike anchors type and the staple anchorage system.

It is possible to clearly see how, for the flat staple anchorage system, the 1-inch width configuration perfectly resembles the 60 degrees fan opening, while the 3-inches width can be compared to the 90 degrees fan opening spike anchor (in terms of peak load). The 2-inches width, instead, it situates in between the two type, getting close mostly to the 3-inches configuration. This is due to the fact that each configuration presents a difference in terms of covered area. Obviously, the peak load increases at the increase of that covered area, which is the only variable between all the specimens.

Regarding the round staples, it is possible to notice a huge difference between the single configuration and the double configuration; in fact, the latter leads to an improvement of about 24,7% from the single round staple configuration. That is due to the fact that the double round staples seem to have a better splitting and bending control, giving to the 1st anchor located at the edge (the one in which the FRP laminate is wrapped around) the only task to resist and contrast the stresses. In this way, the 2nd extra anchor, positioned 3 inches far from the first one, besides taking part of the stresses, it controls mostly the stresses redistributing them better for the 1st anchor. Finally, another important reason for the big improvement is due to the fact that the effective contact area, in the case of the double round staple anchor configuration, it is doubled.

4.1.2 Strain interpretation

Since the covered surface is greater than the one covered by the spikes, without any doubts the staples anchor distribute better the stresses. In fact, for the spike anchors, the strains were concentrated in front of the anchor (and that covered area was not along the entire FRP sheet width). Our anchors, instead, they distribute better the strains over the entire area of the FRP, since they literally cover all the entire FRP laminate width fixed, in this study, at 6 inches. For this reason, in some cases, the spikes used to break only by the outside edges, while the staple anchors present other ruptures' types, as already discussed in chapter 3.3. Figures 4.2 and 4.3 show respectively the strain distributions along the 60 and 90 degrees configuration of the spike anchors.
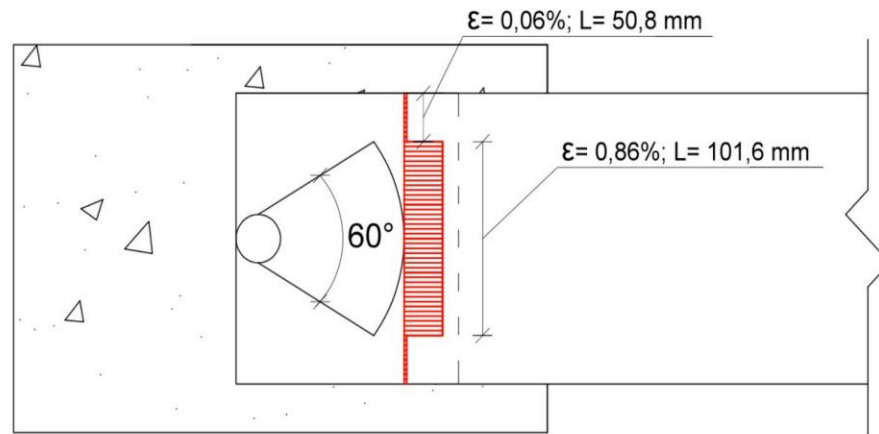
Figure 4.2 - Strain distribution along the 60 degrees fan opening configuration of the spike anchorage system
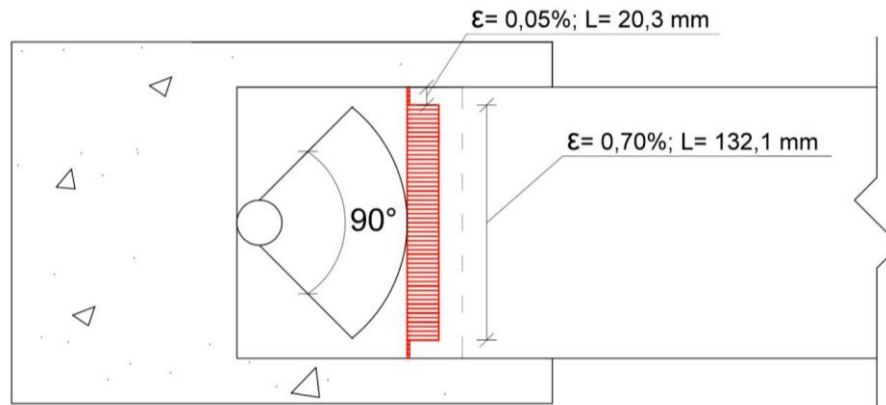
Figure 4.3 - Strain distribution along the 90 degrees fan opening configuration of the spike anchorage system

Based on the data obtained from the test of the spikes anchors, run by Berneschi in 2015, the maximum value of strain was measured in front of the anchor in both the two specimens. In the case of 60° configuration specimens, this was greater than that measured in the 90° configuration specimens. Moreover, the strain recorded near the edge of the sheets (area not covered by the anchor) was always less than 0.1%. Based on this result, strain fields that develop in the FRP sheet appear to be not uniform in the transverse direction. For this reason, strains plotted longitudinally along the FRP sheet centerline are not representative of distributions near the edge of sheets and should be not taken as a design value. It is evidence that only sheet regions located within the anchor splay develop high stresses and strains. Due to the observations written above, a stress distribution model was supposed. It has the typical Gaussian distribution shape,

symmetric with respect to the tension load. The following sketch in Figure 4.4 illustrates the supposed strain distribution.
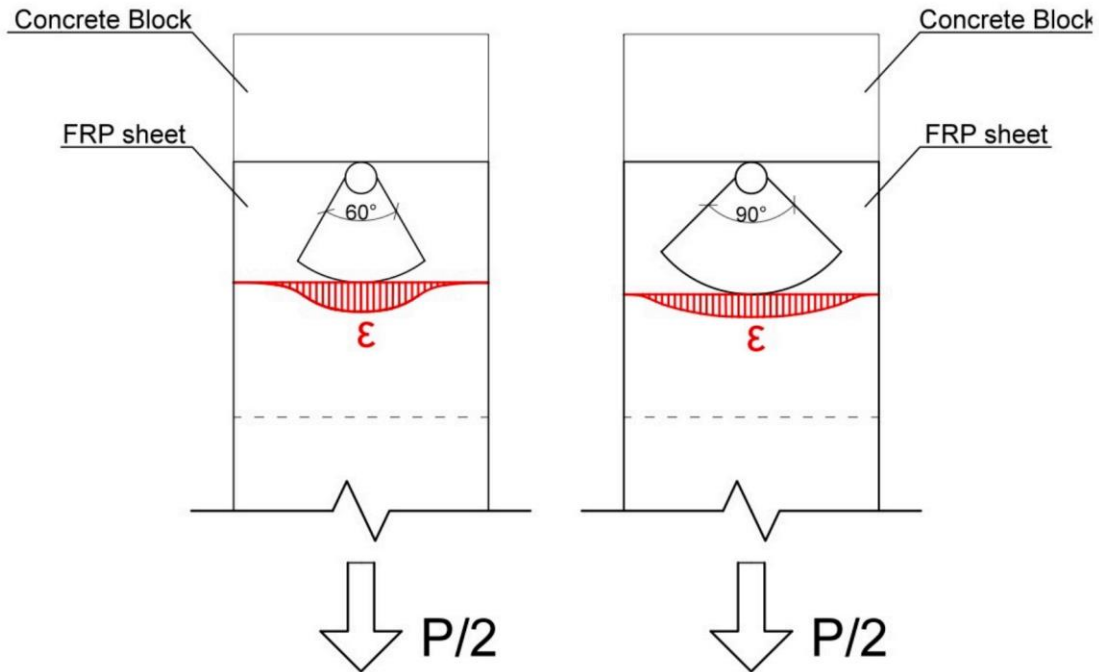
Figure 4.4 - Strain distribution model on the spike anchors (Berneschi, 2015)

4.1.2.1 Flat Staples
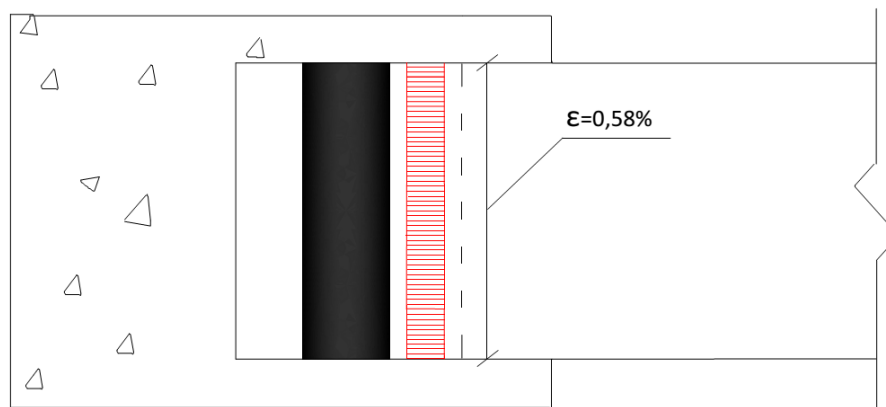
Figure 4.5 - Strain distribution along the 2-width flat staples

Figure 4.5 shows the typical strain distribution along the flat staples. The case shown in Figure 4.5 is the one referred to the 2-width, with an average between the SG2, SG3 and SG4 (the strain gauges positioned just in front of the anchors) of $\varepsilon = 0,58\%$.
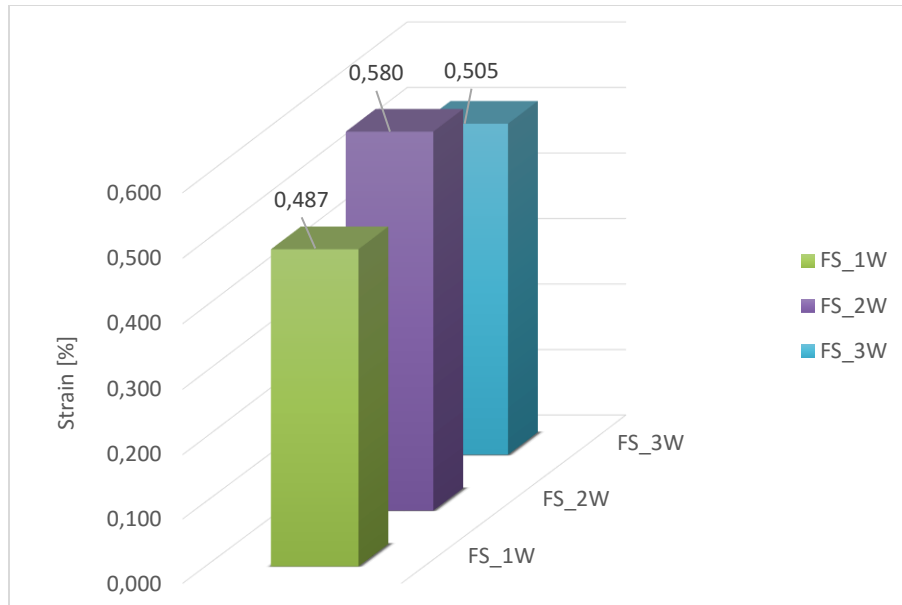
Figure 4.6 - Average of the strain distribution in front of the flat staple anchors for each configuration

Figure 4.6 shows the average of the SG2, SG3 and SG4 for the flat staples. We can observe a growth between the FS_1W and the FS_2W, while the FS_3W assumes a value which in between the previous ones. In this way, we can clearly identify the 2-width anchor as the one that is strong enough to develop the full capacity of the sheet.

4.1.2.2 Round staples
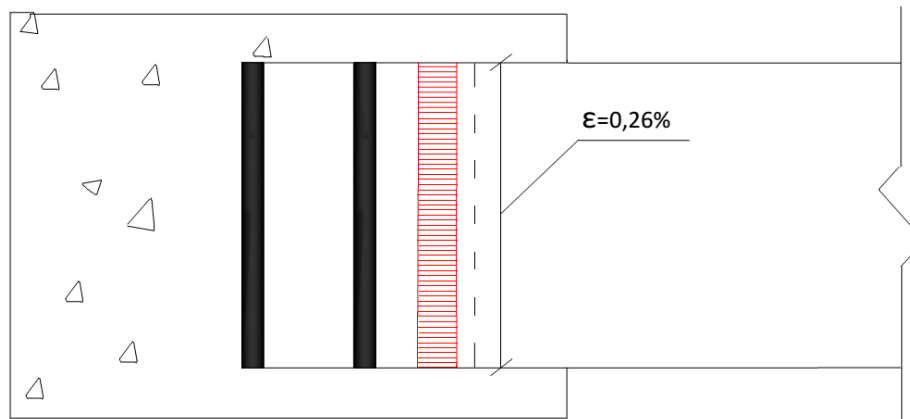
Figure 4.7 - Strain distribution along the double round staple anchorage system

The same applies to the strain distribution read from the round staples. As already explained, it is important to remind that in this case the strain gauges were installed on the second layer of the FRP sheet, wrapped around the first layer that is bonded to the concrete substrate. Figure 4.7 shows the strain distribution in front of the anchorage

system for the double round staple configuration with an average value of about $\varepsilon = 0,26\%$.
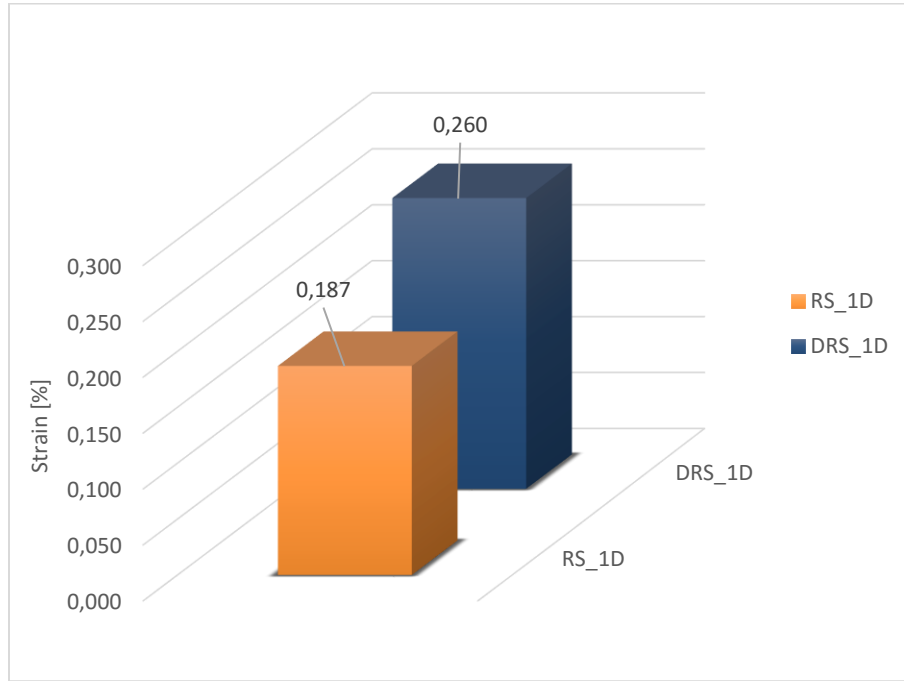
Figure 4.8 - Average of the strain distribution in front of the round staple anchors for each configuration

Again, Figure 4.8 illustrates the average of the strain gauges located in front of the anchors for the round staples. In this case, the increase is in ascending order from the RS_1D to the DRS_1D. Again, since the latter presents higher values of strains recorded, the double round staple configuration represents the case in which the anchors are strong enough to develop the full capacity of the sheet.

4.1.2.3 Theoretical peak load derived from the measured strains

Below, it is presented a correlation that connects the measured strains with the theoretical peak load. In fact, for each specimen, it can be calculated a theoretical peak load just by correlating the measured strains with the modulus of elasticity and the nominal area of the FRP laminate. The results refer only to the best-discovered configurations of flat and round staple anchors (see chapter 4.2).

$$\sigma = E \cdot \varepsilon$$

$$\frac{P}{2}_{th} = \sigma \cdot A$$

σ is the nominal stress in the FRP sheet

E is the modulus of elasticity refereed to the wet FRP sheet and equal to 77,04

A is the nominal area of the FRP sheet: $A = 152,4\ mm^2$

$\frac{P}{2}_{th}$ is the theoretical peak load calculated from the strains read at the peak load

In this way for the two best configurations identified, we have that the theoretical peak load is:

$$\frac{P}{2}_{th} = 68,10\ KN$$

for the 2-width flat staple, while for the double round staple the theoretical peak load is:

$$\frac{P}{2}_{th} = 61,05\ KN$$

	E	ε	A	P/2th	P/2	ΔP
	[Gpa]	[%]	[mm²]	[KN]	[KN]	[%]
Benchmark	77,04	0,4	152,4	46,96	36,11	30%
FS_2W	77,04	0,58	152,4	68,10	62,21	9%
DRS_1D	77,04	0,26	304,8	61,05	65,61	-7%

4.1.3 Types of failure modes

In this section, we discuss the failure modes in the anchored specimens provided with the spike anchors and with the staple anchors.

Regarding the spike anchors, three main type of ruptures were observed:

1. Adhesive-to-concrete interface debonding followed by rupture of the FRP sheet around the anchor
2. Adhesive-to-concrete interface debonding followed by slippage of the FRP sheet under the anchor
3. Failure at the concrete substrate

In the failure mode 1, the rupture of the fibers took place and started around the fan (on the uncovered area) that appeared still bonded to the FRP sheet after the failure, as shown in Figure 4.9

Figure 4.9 - Failure mode 1, spike anchors

This first rupture mode was observed in the 60 degrees fan opening, where the covered area by the fan was smaller than the one covered by the 90 degrees configuration.

Rupture mode 2 was observed, instead, in the 90 degrees fan opening, where the initial debonding was in the adhesive-to-concrete interface and the primer was completely removed from the concrete surface. The final failure of the system was due to the slippage of the FRP sheet under the anchor. In this case, delamination between the fan and the FRP sheet was observed.

Also, the failure mode 3, which is the failure of the concrete substrate, is typical of the 90 degrees fan opening.

Regarding the flat staples, as already analyzed in chapter 3.3, five different types of rupture were observed in the anchored specimens:

- B. Slippage of the CFRP sheet beneath the anchor, without their ruptures
- C. Slippage of the CFRP sheet beneath the anchor, with the rupture of the CFRP sheet
- D. Rupture of the anchor with the delamination of the CFRP
- E. Rupture of the concrete substrate and rupture of the anchor
- F. Rupture of the concrete substrate without the rupture of the anchor

While failure modes B and C are typical of the staple anchorage system, the failure modes E and F can be correlated to the failure mode 3 observed in the spike anchors. At this point some considerations should be made:

Generally, a CFRP sheet rupture failure (failure mode 1 and 2 for the spikes and C for the staples) indicates that the sheet has developed its full strength. This failure mode is ideal for determining the sufficiency of the anchors and obtaining guidelines for anchor design, and for this reason, is the desired failure mode. On the other hand, an anchor failure (failure mode D) indicates that anchors do not have enough capacity to develop the full strength of the CFRP laminate, representing an undesirable failure mode. In addition, failure modes E, F (for the staples) and 3 (for the spikes) show that the anchorage system-CFRP sheet is stronger than the concrete used to test the specimens.

4.2 RECOMMENDATION ON PRELIMINARY DESIGN PREVISIONS

Based on:

- Dispersion of the results (a low COV observed mainly in the 2-inches flat staple anchorage system).
- Type of rupture (the ideal failure mode is the failure mode C, which represents the full strength developed by the CFRP laminate).
- Strains interpretation (highest values of the strains are obviously preferred).
- Peak load significantly high.

We can say that the best configurations are:

- ➢ The 2-inches width, 1-inch depth anchor, for the flat staple anchorage system.
- ➢ The double round staple configuration, with 1-inch depth, for the round staple anchorage system.

In fact, only these two anchorage systems respect all the points previously explained in details. Regarding the flat staple anchorage system, it is important to underline that even if the 3-inches configuration reaches a higher value of peak load, that was too much. In fact, the 3-inches width anchor presented a break of the concrete (that was even a high strength concrete with around 59MPa of f'_c concrete compressive strength). The 2-inches width anchor, instead, presented a delamination with the rupture of the FRP, without the break of the anchor (in two cases that kind of rupture was combined with the rupture of the concrete substrate, which it pushes the 2-inches anchor to the limit of the usage). In this way, we can say that the 2-inches width anchor is strong enough, in order to achieve the full capacity of the FRP laminate.

Regarding the comparisons with the spikes anchors, the 2-inches anchor outclasses the 60 degrees fan opening in terms of peak load, strain interpretation and type of rupture (as shown in chapter 4). The 3-inches anchor performs a little better than the 90 degrees fan opening spike anchor, mostly in terms of strains. In fact, the big disadvantage of the spike anchors is that of not distribute the stresses evenly all along the FRP width. Regarding the round staples, the double round staple configuration is the preferred one. In fact, with an ideal rupture type and a uniform strain distribution, it reaches a high value of peak loads (in between the 2-inches and the 3-inches flat staple anchors).

Finally, from the results obtained in this research, tests on beams should be done, using the following set-up:

- One anchor 2-inches width, 1-inch depth on each end, on a 6" FRP sheet width.
- A double round staple configuration, 1-inch depth on each end, always on a 6" FRP sheet – width.

Note: It would be good to use the same width of the FRP sheet used in all the shear test (6" width).

5.   CONCLUSIONS

5.1 COMMENTS

The research presented in this thesis represents an initial study of the interaction between the staple anchors and FRP laminates. Since the anchors are more subjected to shear forces rather than pullout forces, an experimental campaign through shear tests has been developed in order to fully understand the behavior of this anchorage system. This thesis determined the anchors' effectiveness through an innovative double shear test meant to be reliable, repeatable, easy to perform and able to represent the stress state that is observed in the real field applications. In fact, the new installation adopted for the test 2 revealed firstly a consistency of all the results obtained, by the interpretation of the rupture types and the relatively low values of COV between specimens with the same anchorage system installed. In addition, this innovative double shear test represents exactly the real application when the system acts in situ as an interrupted strip of wet CFRP (as a continuum), installed for the retrofit of old concrete structures. Thirdly, impregnating the carbon fibers with a resin epoxy allows the latter to behave as a matrix, which means to keep the fibers straight, transferring the stresses to them, avoiding intensifications or different stresses distribution along all the CFRP strip. From these three main reasons, this new set up of the test has proved to be a very big improvement in terms of characteristics and results obtained with the past methodology used in the laboratory of the University of Miami.

In this way, from the main test (test 2) run it has been obtained a full understanding of the improvement on the global strengthening system by modifying different parameters of this anchor system. From the results obtained from this test, it came up the 2-inches width, 1-inch depth anchor, as the best configuration for the flat staple anchorage system and the double round staple configuration, with 1-inch depth, for the round staple anchorage system. It is important to remark that in test 2 the depth for all the anchorage system was always fixed at 1-inch. In fact, we suppose the 1'' depth as a sufficient and an ideal depth for a main reason: the rebars interaction. Since most of the worldwide regulations give some minimum requirements for the concrete cover (see table 4.1), a 1'' depth, while anchoring an FRP reinforcement, would not be a problem of interact and damage the internal reinforcement of a slab.

Table 5.1 - Summary of the most common concrete cover requirement

Country	Concrete Code	Range of Concrete Cover (mm)
UK	BS:8110	25-50
EU	EN 1992 (EC2)	diameter +10 - 55
USA	ACI:318	40-50
Australia	AS:3600	15-78

Finally, this thesis compared the staple anchorage system with one of the most CFRP anchorage system used nowadays: the spikes anchors. Comparing the results obtained from the two different anchorage systems in terms of peak load, strain interpretation and type of failure modes we can say that the 2-inches and 3-inches staple anchors can be totally comparable with the 60 and 90 degrees fan opening spike anchors, even outclassing them from some point of view (see chapter 4.1).

6. BIBLIOGRAPHY

- AASHTO-2012 "Guide Specification for Design of Bonded FRP Systems for Repair and Strengthening of Concrete Bridge Elements". American Association of State Highway and Transportation Officials (AASHTO) 2012.Washington, DC.
- AC125-2012 "Acceptance criteria for concrete and reinforced and unreinforced masonry strengthening using externally bonded fiber reinforced polymer (FRP) composite systems". International Code Council Evaluation Service. June 2012.
- ACI 318-11 "Appendix D – Anchoring to Concrete" Reported by ACi Committee.
- ACI 355.4-11 "Qualification of Post-Installed Adhesive Anchors in Concrete and Commentary". Reported by ACi Committee 440.
- ACI Committee 440. "Guide for the design and construction of externally bonded FRP systems for strengthening concrete structures". ACI 440.2 R-08. Farmington Hills (MI): American Concrete Institute; 2008. p.76.
- ACI Committee 440. "Guide for the design and construction of structural concrete reinforced with FRP bars". ACI 440.1 R-06. Farmington Hills (MI): American Concrete Institute; 2006. ACS. "National historic chemical landmarks-Bacon's breakthrough". Washington (DC); 2007.
- ASTM C31/C31M - 12 "Standard Practice for Making and Curing Concrete Test Specimens in the Field". American Society for Testing and Materials (ASTM) 2012.
- ASTM C39/C39M - 14 "Standard Test Method for Compressive Strength of Cylindrical Concrete Specimens". American Society for Testing and Materials 162 (ASTM) 2014.
- ASTM C143/143M – 12 "Standard Test Method for Slump of Hydraulic-Cement Concrete". American Society for Testing and Materials (ASTM) 2012.
- ASTM D3039/D3039M - 08 "Standard Tests Method for Tensile Properties of Polymer Matrix Composite Materials". American Society for Testing and Materials (ASTM) 2008.
- ASTM E4 – 13 "Standard Practice for Force Verification of Testing Machines". American Society for Testing and Materials (ASTM) 2013.
- ASTM E83 – 10a "Standard Practice for Verification and Classification of Extensometer Systems". American Society for Testing and Materials (ASTM) 2010. ASTM E178 – 08 "Standard Practice for Dealing With Outlying Observations". American Society for Testing and Materials (ASTM) 2008.
- ASTM E488/E488M – 10 "Standard Test Methods for Strength of Anchor in Concrete Elements". American Society for Testing and Materials (ASTM) 2010
- Berneschi A. "Enhancing the use of externally bonded FRP laminates with FRP anchor spikes", 2015. Master's Thesis. Milano, Italy: Politecnico di Milano.
- Brena S.F. and McGuirk G.N. "Advanced on the behavior characterization of FRPanchored carbon fiber-reinforced polymer sheets used to strengthen concrete elements", International Journal of Concrete Structures and Materials, March 2013, Vol.7, No.1.

- Carozzi F.G., Colombi P., Montalbano A. and Poggi C. "Utilizzo di connettori per l'incremento della forza di distacco del rinforzo in FRP di strutture in muratura o calcestruzzo". 2° Convegno Nazionale Assocompositi, Torino 29-31 Maggio 2012.
- Carozzi F.G., Colombi P., Poggi C. "Calibration of end-debonding strength model for FRP-reinforced masonry". Elvisier Ltd, 2014
- Chen J.F., Teng J.G., "Anchorage strength models for FRP and steel plates bonded to concrete". J Struct Eng ASCE 2001. pp.127-784-791.
- CNR (National Research Council). "Guide for the design and construction of externally bonded FRP systems for strengthening existing structures". Rome, Italy: Advisory Committee on Technical Recommendation for Construction of National Research Council; 2004. pp. 154.
- CNR-Advisory Committee on Technical Recommendations for Construction. "Guide for the Design and Construction of Externally Bonded FRP Systems for Strengthening Existing Structures". Materials, RC and PC structures, masonry structures. CNR-DT 200 R1/2013. Roma – 10 Ottobre 2013.
- F.C. Campbell, ASM International, "Structural Composite Materials" (2010)
- Grelle S.V. and Sneed L.H., "Review of anchorage system for externally bonded FRP laminates". Internation journal of concrete structures and materials, March 2017, Vol.7, No.1, pp. 17-33. IStructE. "Interim guidance on the design of reinforced concrete structures using fibre composite reinforcement". London: Institution of Structural Engineers; 1999. pp. 116.
- Manoochehr Zoghi, The international handbook of FRP composites in civil engineering (2013)
- Nanni A., Rizkalla S., Bakis C.E., et al. "Characterization of GFRP ribbed rod used for reinforced concrete construction". Proceedings of the international composites exhibition (ICE-98). Nashville (TN); 1998. pp.16A/1-6.
- Nanni A. "Composite: Coming on Strong", Concrete Constuction, Vol.44, 199, p.120
- Nanni A. "Composites: coming on Conc Constr". 1999. 44(1): pp. 120-124.
- Nanni A. "Concrete repair with externally bonded FRP reinforcement". Concr Int 1995. 17(6): pp.22-26.
- Prota A., Tan K., Nanni A., et al. "Performance of shallow reinforced concrete beams 166 with externally bonded steel-reinforced polymer". ACI Struct J; 2006. 103(2): pp.163- 170.
- Rossini M., "FRP Anchors for External Reinforcement of Concrete Structural Elements", 2016. Master's Thesis. Milano, Italy: Politecnico di Milano.
- Serbescu A., Guadagnini M., Pilakoutas K. "Standardised double-shear test for determining bond of the FRP to concrete and corresponding model development" Elsevier Ltd, 2013.
- Smith ST, Teng JG. "FRP-strengthened RC beams-I: review of debonding strength models". Eng Struct 2002;24(4):385-395. Taljsten B. "Strengthening of beams by plate bonding". ASCE-J Mater Civil Eng; 1997. 9(4): pp.206-212.

- Tamura T. "FiBRA, fiber-reinforced-plastic (FRP) reinforcement for concrete structures: properties and applications". In: Nanni A., editor. developments in civil engineering. Volume 42. Amsterdam: Elsevier; 1993. pp. 291-303].
- Teng J. G. Smith S. T. Yao J. and Chean J. F. "Intermediate Crack Induced Debonding in RC Beams and Slabs",Construction and Building Materials, 2001, V. 17, No. 6-7 pp 447-462.
- Teng J.G. et al. "RP composites in civil engineering". Hong Kong: Elsevier; 2001.
- Teng J.G., Chen J.F., Smith ST, et al. "FRP strengthened RC structures". Chichester: John Wiley & Sons Ltd; 2002. pp. 11–101.
- Wang H. H. Test of Glass Fiber Reinforced Polymer (GFRP) Anchors, 2013
- Zhang H.W. and Smith S.T. "Influence of FRP anchor fan configuration and dowel angle on anchoring FRP plates". Elsevier Ltd., 2011.

ONLINE BIBLIOGRAPHY

- http://www.plasticseurope.org/what-is-plastic/types-of-plastics-11148/epoxy-resins/applications.aspx *(04/04/2016)*
- https://en.wikipedia.org/wiki/Epoxy *(05/24/2016)*
- https://en.wikipedia.org/wiki/Carbon_fibers *(06/21/2016)*
- http://www.matter.org.uk/matscicdrom/manual/co.html *(06/16/2016)*
- http://igestek.com/en/what-is-a-composite/ *(04/2/2016)*
- http://www.veckfasteners.com/composite-advantages/ *04/14/2016)*
- http://civil-engg-world.blogspot.com/2011/04/numerical-relationship-between.html *(07/08/2016)*
- https://en.wikipedia.org/wiki/Concrete_slump_test *(08/11/2016)*
- https://en.wikipedia.org/wiki/Strain_gauge *(06/01/2016)*
- https://en.wikipedia.org/wiki/Concrete_cover *(07/01/2016)*
- https://westsystem.com *(05/27/2016)*
- https://adhesives.org *(05/27/2016)*
- http://blastjournal.com/concrete-surface-preparation-a-primer-3/ *(07/11/2016)*

7.   APPENDICES

Appendix A: Conversion of Units table

Unit	Divisions	SI Equivalent
UNIT FOR LENGTH		
1 inch (in)		25.4 mm
1 foot (ft)	12 in	0.305 m
1 yard (yd)	3 ft (36 in)	0.914 m
1 mile (mi)	1760 yd (5280 ft)	1.609 km
UNIT FOR AREA		
1 square inch (in^2)		645.16 mm^2
1 square foot (ft^2)	144 in^2	0.093 m^2
1 acre (ac)	43560 ft^2	4046.873 m^2
UNIT FOR VOLUME		
1 cubic inch (in^3)		16.387 mm^3
1 cubic foot (ft^3)	1728 in^3	0.028 m^3
1 gallon (gal US)		0.004 m^3
UNIT FOR MASS		
1 ounce (oz)		28.350 g
1 pound (lb)	16 oz	453.592 g
UNIT FOR FORCE		
1 pound force (lbf)		4.448 N
1 kip force (kipf)	1000 lbf	4448.222 N
UNIT FOR DENSITY		
1 pounds per cubic foot (lb/ft^3)		16.018 kg/ m^3
UNIT FOR SPEED		
1 mile per hour (mph)		1.609 km/h
UNIT FOR MOMENT		
1 inch-pound force (in lbf)		0.113 Nm
1 foot-pound force (ft lbf)	12 in lbf	1.356 Nm
UNIT FOR PRESSURE		
1 pound per square inch (psi)		6894.757 Pa
UNIT FOR PRESSURE		
1 degree Fahrenheit (ºF)		ºF = 9/5ºC + 32

Appendix B: Test 2 Setup

10 eps foam shapes were provided as the following sketch in Fig 7.1.
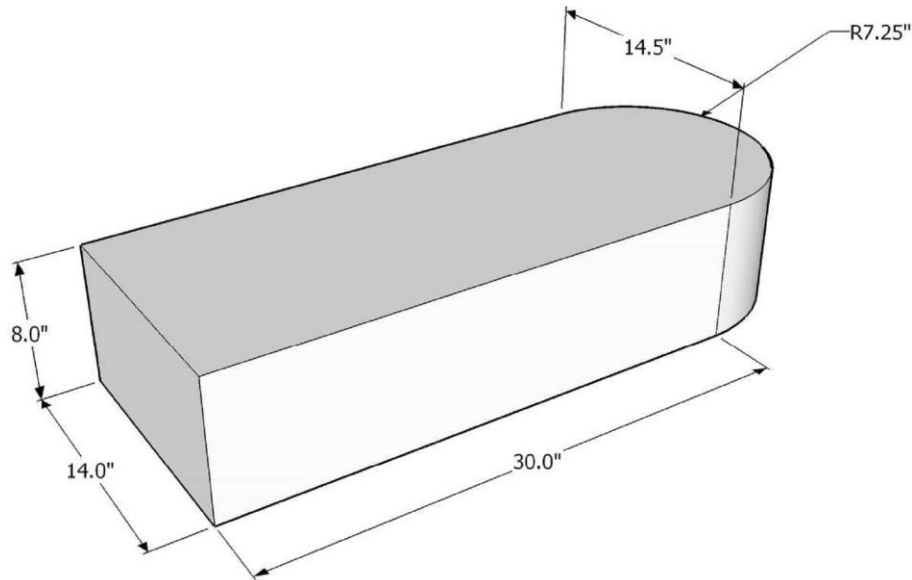
Figure 7.1 – 3D view of the Eps foam shape

The dimensions of the eps foam block were computed based on the dimensions of the steel support, of the hydraulic jack, of the load cell and of the plates used to perform the test.

A steel support was specifically provided in order to compute the double shear test.

The steel support provided was composed of the following 3 different components (welded together):

- Section C10x25, length 13''.
- Section HSS 14''x0.500', length 10''.
- Plate 15''x18''.

Since, during the set-up of the test, the CFRP sheet wrapped around the steel plate was entirely impregnated and cured (stiffened), the upper plate of the steel support provided had to be cut, in order to fit the CFRP laminate previously cured on the EPS foam shape designed.

Figure 7.2 and 7.3 show the section and the front view of the steel plate assembled, with the highlighting (in red) of the cut part.
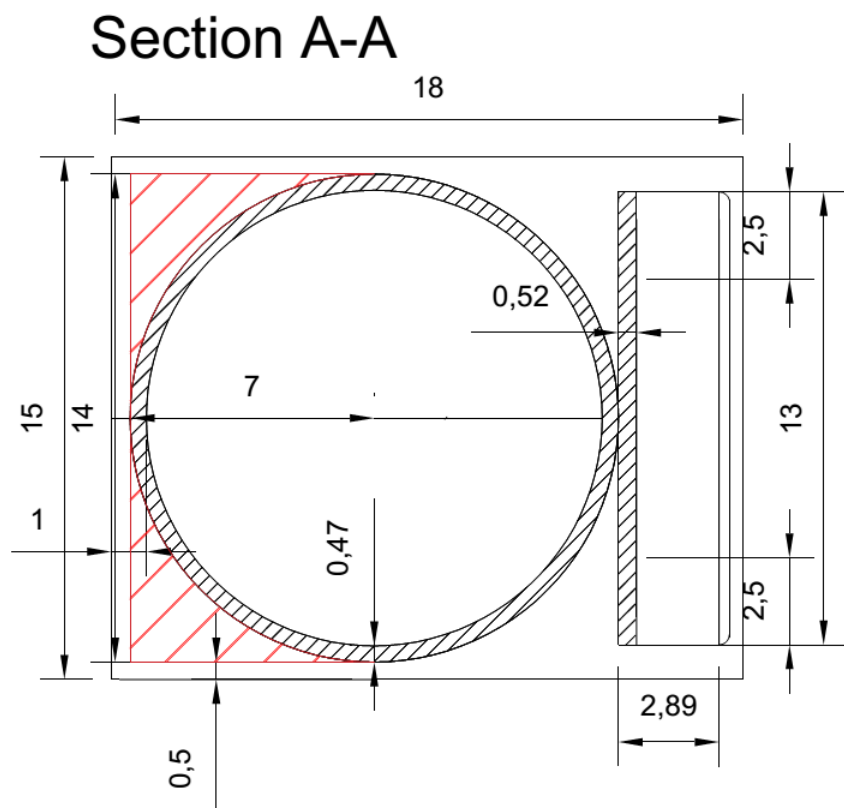
Section A-A

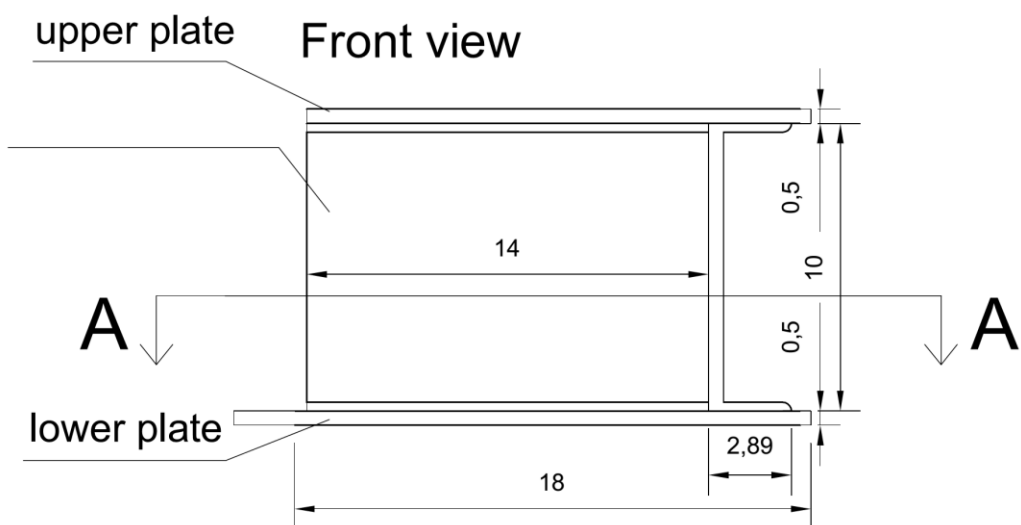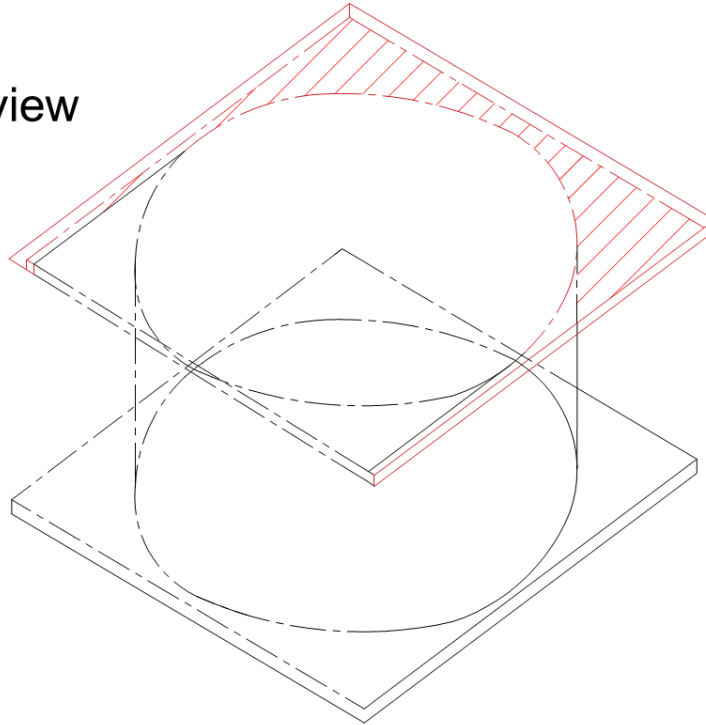*Figure 7.2 – Section of the steel support*

Front view

Figure 7.3 – Front view of the steel support

Figure 7.4 and 7.5 show respectively, the cutting operation of the upper steel plate and the 3D view of the steel plate.

Figure 7.4 – Steel plate cutting operation

Figure 7.5 – 3D view of the steel plate